# The nature of the Cadillac – Larder Lake Fault: Implications for gold mineralization along the Kerr-Addison-Cheminis segment

by

Nadia St-Jean

A thesis submitted in partial
Fulfillment of the requirements for
the degree of
Master of Science (MSc) in Earth Sciences

The Faculty of Graduate Studies
Laurentian University
Sudbury, Ontario, Canada

**THESIS DEFENCE COMMITTEE/COMITÉ DE SOUTENANCE DE THÈSE**
**Laurentian Université/Université Laurentienne**
Faculty of Graduate Studies/Faculté des études supérieures

| | |
|---|---|
| Title of Thesis<br>Titre de la thèse | The nature of the Cadillac – Larder Lake Fault: Implications for gold mineralization along the Kerr-Addison-Cheminis segment |
| Name of Candidate<br>Nom du candidat | St. Jean, Nadia |
| Degree<br>Diplôme | Master of Science |
| Department/Program<br>Département/Programme | Geology |
| Date of Defence<br>Date de la soutenance | May 29, 2020 |

**APPROVED/APPROUVÉ**

Thesis Examiners/Examinateurs de thèse:

Dr. Bruno Lafrance
(Co-Supervisor/Co-directeur(trice) de thèse)

Dr. Ross Sherlock
(Co-Supervisor/Co-directeur(trice) de thèse)

Dr. Kate Rubingh
(Committee member/Membre du comité)

Dr. Andrew Wurst
(External Examiner/Examinateur externe)

Approved for the Faculty of Graduate Studies
Approuvé pour la Faculté des études supérieures
Dr. David Lesbarrères
Monsieur David Lesbarrères
Dean, Faculty of Graduate Studies
Doyen, Faculté des études supérieures

**ACCESSIBILITY CLAUSE AND PERMISSION TO USE**

## ACCESSIBILITY CLAUSE AND PERMISSION TO USE

# Abstract

The Cadillac-Larder Lake Fault (CLLF) is a major fault system that controls the location of gold deposits in the southern Abitibi greenstone belt. Over a distance of 250 km from Matachewan in Ontario to Val d'Or in Quebec, it marks the contact between mafic-ultramafic volcanic rocks of the Piché/Larder Lake group and younger metasedimentary rocks of the Hearst, Timiskaming and Cadillac sedimentary assemblages. In the Larder Lake area, the contact between sedimentary rocks of the Timiskaming assemblage to the north and volcanic rocks of the Larder Lake group to the south defines the CLLF. This contact is typically sheared and deformed by two generations of folds but locally, in areas of low strain, an unconformity is preserved, expressed by a pebbly sandstone which youngs away from the underlying ultramafic rocks and contains detrital clasts of the ultramafic rocks. The sandstone stratigraphically overlies older volcanic rocks of the Larder Lake group suggesting that the unconformable contact between the Timiskaming assemblage and Larder Lake group is a primary feature that was later structurally modified. The structural history of the CLLF and surrounding rocks began prior to the deposition of the Timiskaming assemblage with the juxtaposition of the Larder Lake and Blake River groups during an early thrusting and imbricating $D_1$ deformation event. Both the Larder Lake group and the Timiskaming assemblage were then deformed during a $D_2$ deformation / mineralizing event, which produced regional $F_2$ folds, a regional $S_2$ cleavage, and ductile shearing along the contact between the Larder Lake group and the Timiskaming assemblage. Reactivation of this contact during and post the $D_2$ event localized the distribution of gold deposits and formed the present day manifestation of the CLLF.

# Keywords

Cadillac – Larder Lake Fault, Kerr-Addison, Larder Lake, structural geology, gold mineralization, contact relationship, Timiskaming.

# Co-Authorship Statement

This manuscript has multiple authors; this section outlines the contributions made by the co-authors and the candidate in pursuit of this Masters of Science Degree:

1. This thesis was developed by Dr. Bruno Lafrance and Dr. Ross Sherlock with input from the candidate. These two co-authors visited the field sites throughout the duration of the project and provided input prior to, during and following the collection of field data.

2. Field mapping and sample collection was completed by the candidate with the assistance of Leslie Hunt during the 2017 and 2018 field season (May to August). The area studied from Virginiatown, Ontario to Cheminis, Ontario is approximately 10 km in length in which 5 locations were mapped in detail at scales ranging from 1:10 to 1:10,000.

3. Forty two (2) field samples were collected by the candidate for Whole Rock Geochemistry. Twenty six (26) samples were collected by the candidate for gold and base metal concentrations. The samples were cut and prepared by the candidate at the Willet Green Miller Centre and sent to ALS Laboratories in Sudbury, Ontario where they were crushed and pulverized before analysis. Three (3) standard samples were included to conduct QA/QC review of analytical results. In addition, forty (40) samples were collected for petrography, which were prepared and cut by the candidate before being polished by Willard Desjardins at Laurentian University.

4. All interpretations in this thesis and all first drafts were completed by the candidate and reviewed by the co-authors.

# Acknowledgments

As a mature student returning to graduate studies after working in the industry for 5 years, I am immensely grateful to have been a part of Metal Earth and to be surrounded by expert geologists in their respective fields. I took a break from the mining industry to sharpen my knowledge about geology and have had the opportunity to study alongside some amazing scientists. My main objective in pursuing a Master's degree was to study in detail more advanced concepts and topics and I have been able to accomplish this goal thanks to the graduate program offered by Laurentian University, which was manifested in the teachings of the amazing professors within the Geology department. I would like to give thanks for the guidance, input and constructive criticism given to me by my professors and also my fellow students.

I would also like to thank the exploration team from Gold Candle Ltd., in particular, Jacqueline Blackwell and Tim Stubley. The exploration team welcomed me with open arms and the company granted me access to new and old diamond drill core that I was able to study and extrapolate for this study. I would like to thank them for many geological discussions and input which were highly beneficial to this study.

Most importantly, I have an enormous amount of gratitude for my supervisors, Bruno Lafrance and Ross Sherlock. Between the two of them and I, this thesis has managed to manifest itself as a well-balanced argument about a conflicting topic that I have had the pleasure of dissecting. I have benefitted immensely from their extensive knowledge about structural geology, ore deposits, alteration, mapping and the Abitibi district, but also from their mentorship and patience for a student not familiar with the academic process. It has been an honor to be able to work with them.

Of course, I also have to thank my mom, who, despite not having any idea what I do, is unconditionally loving and supportive of my career and success.

# Table of Contents

# List of Tables

# List of Figures

# Chapter 1: Introduction to the Thesis

## 1.1 Research Problem

Although it has been known for almost a century that the Cadillac-Larder Lake Fault (CLLF) exerts a primary control on the distribution of gold deposits in the southern Abitibi subprovince, many questions remain on its early history. The CLLF is a major, 250 km long, stratigraphic break between older metavolcanic rocks to the south and younger metasedimentary rocks to the north (Poulsen, 2017). This study focuses on a 12 km segment of the CLLF between Larder Lake, Ontario, to the Quebec border, including the Kerr-Addison gold deposit, which is one of the largest gold deposits found to date along this deformation zone. Although the CLLF has been mapped historically as the northern contact between the younger Timiskaming sedimentary rocks and the older metavolcanic Larder Lake group, and recognized as a major structural boundary, a number of key questions related to the nature of the structure and contact remain to be answered. The geological relationship between these two assemblages, which is critical to understanding the early history of the CLLF, is addressed in the thesis.

## 1.2 Objectives of the Thesis

This thesis is a structural-stratigraphic study that focuses on the Larder Lake to Kearns segment of the CLLF. The latter is located along the contact between the Timiskaming assemblage and the Larder Lake group. The main objective of the study is to resolve the nature of this contact and its deformation history. To fulfill this objective:

1. Well-exposed sections across the CLLF were mapped in detail at scales of 1:10 to 1:10,000;

2. Samples were collected for petrography and whole rock geochemistry to characterize units along and in close proximity to the CLLF;

3. Drill holes across the CLLF were logged and sampled;

4. Strongly strained and weakly deformed sections across the CLLF were compared and interpreted in terms of the regional structural and geological history of the area.

## 1.3 Structure of the Thesis

This thesis consists of two chapters. Chapter 1 presents the objectives of the thesis and the research problem addressed by the thesis. Chapter 2 is a manuscript written for submission to a scientific journal and entitled *The nature of the Cadillac – Larder Lake Fault: Implications for gold mineralization along the Kerr-Addison-Cheminis segment.* Co-authors on this manuscript are:

- Lafrance, B., Mineral Exploration Research Centre, Harquail School of Earth Sciences, Laurentian University, 935 Ramsey Lake Road, Sudbury, Ontario, P3E 2C6, Canada.

- Sherlock, R., Mineral Exploration Research Centre, Harquail School of Earth Sciences, Laurentian University, 935 Ramsey Lake Road, Sudbury, Ontario, P3E 2C6, Canada.

Additional information on geochemical data is presented in Appendix A.

# Chapter 2: The nature of the Cadillac – Larder Lake Fault: Implications for gold mineralization along the Kerr-Addison-Cheminis segment

## 2.1 Introduction

The Cadillac-Larder Lake Fault (CLLF) is one of two broadly east-trending, metal-endowed, regional faults in the southern Abitibi subprovince of the Archean Superior craton. The CLLF can be traced over a distance of 250 km from Matachewan, Ontario, to Val d'Or, Quebec (Figure 1). Historically termed a "break", it marks a major stratigraphic discontinuity between metasedimentary assemblages and older metavolcanic successions. It is typically expressed as a 10-500 m wide zone of high strain associated with strong planar and linear fabrics, extensive iron and magnesium carbonate alteration, quartz-carbonate veining and gold mineralization (Thomson, 1941; Ludden et al., 1986; Sibson et al., 1988; Card et al., 1989; Wilkinson et al., 1999; Poulsen et al., 2000; Robert, 2001).

The CLLF is a major transcrustal fault that focused hydrothermal fluids and controls the distribution of gold deposits along its strike length. Previous work has focused on the kinematic history of highly strained segments of the fault (Wilkinson et al., 1999; Ispolatov et al., 2008; Zhang et al., 2014; Lafrance, 2015; Bedeaux et al., 2017). In contrast, this study focuses on low strain segments of the fault in the Larder Lake area to determine the early history of the fault. This study suggests that the contact between the Larder Lake group and the Timiskaming assemblage, which marks the CLLF, predates the $D_2$ deformation event. Textural and structural evidence suggests that the original contact between the older Larder Lake group and the Timiskaming assemblage was a stratigraphic unconformity that was reactivated and deformed during a $D_2$

deformation event, which also controlled the emplacement of gold-bearing veins in hydrothermally altered mafic and ultramafic rocks of the Larder Lake group.

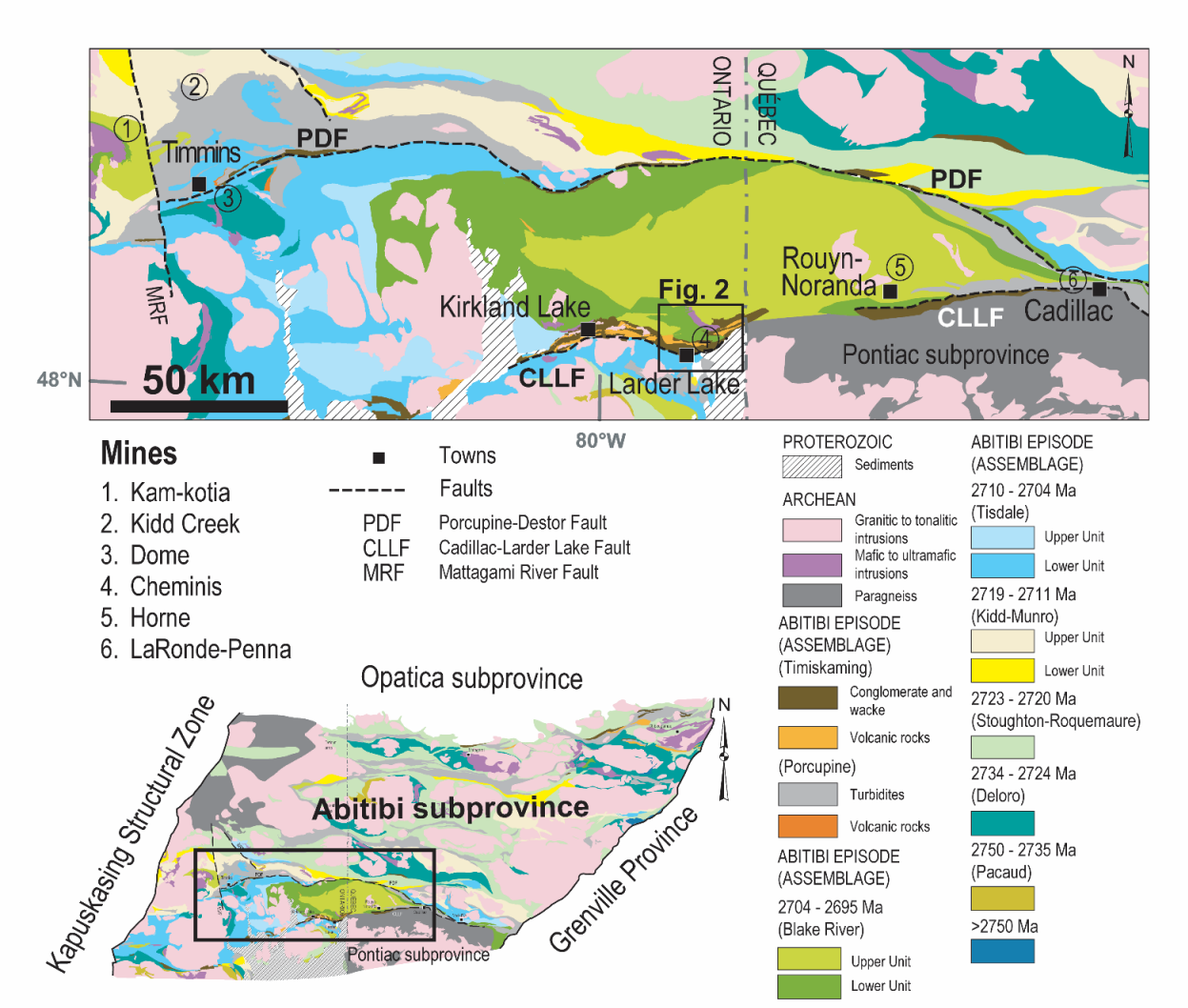


**Figure 1**. Regional geology map of the Abitibi subprovince, modified after Thurston et al., 2008. Inset map showing the two major structural features, the Porcupine-Destor Fault (PDF) and CLLF, in the southern Abitibi subprovince. Outlined in black is the study area shown in Figure 2.

## 2.1.1 Regional Geology

The southern Abitibi subprovince (Figure 1) comprises six major volcanic assemblages, including from oldest to youngest: Pacaud (2750–2735 Ma), Deloro (2730–2724 Ma), Stoughton-

Roquemaure (2723–2720 Ma), Kidd-Munro (2719–2711 Ma), Tisdale (2710–2704 Ma), and Blake River (2704–2696 Ma) (Ayer et al., 2005). Of these assemblages, two are present in the Larder Lake area: the Blake River and Tisdale. The lower part only of the Tisdale assemblage is present and is locally named the Larder Lake group. The Blake River group consists dominantly of tholeiitic mafic volcanic and felsic volcanic units while the Larder Lake group is characterized by komatiitic ultramafic and tholeiitic mafic volcanic rocks. Although not recognized in the Larder Lake area, the lower Tisdale assemblage locally contains units of calc-alkaline felsic volcanic rocks and banded iron formation (Ayer et al., 2005). These volcanic assemblages were intruded by calc-alkaline to alkaline composite stocks, ranging in age from ca. 2695 Ma to 2660 Ma, and were unconformably overlain by Porcupine turbidite-dominated sedimentary successions (2690–2685 Ma) and Timiskaming-type clastic-dominated sedimentary successions (<2677 – 2670 Ma) (Hyde, 1980; Corfu, et al., 1991; Mueller et al., 1994; Ayer et al., 2002, 2005; Davis, 2002; Thurston, et al., 2008).

Timiskaming sedimentary successions are spatially associated with major trans-lithospheric crustal fault zones, including the CLLF and the Porcupine Destor fault (PDF), which control the distribution of gold deposits in the southern Abitibi subprovince (Card et al., 1989; Hodgson and Hamilton, 1989; Thurston and Chivers, 1990; Mueller, 1991; Mueller and Donaldson, 1992; Poulsen et al., 2000). The PDF and CLLF have produced more than 88.9 Moz Au and 105.4 Moz Au, respectively (Monecke et al., 2017). The Timiskaming sedimentary rocks have been described in detail by Hyde (1980), who divided the assemblage into 12 sedimentary and volcanic facies. In general, the Timiskaming succession is comprised of trachytic to phonolitic volcanic rocks intercalated with a wide range of sedimentary rocks varying from conglomerate, sandstone and

siltstone to chert and banded iron formation (Hyde, 1980). Both non-marine and marine facies are present. The non-marine facies is interpreted to be deposited in alluvial-fluvial to aeolian dune settings and defined mainly based on cross-stratification, fining upward graded beds, the presence of conglomerates and the lenticular nature of bedding. The marine facies consists dominantly of turbiditic sequences including banded iron formation, sandy turbidite and lesser conglomerate (Hyde, 1980).

In Ontario, the CLLF lies entirely within the Abitibi subprovince whereas in Quebec it marks the contact between the Abitibi and the Pontiac subprovinces. The Pontiac subprovince lies immediately south of the Abitibi subprovince and consist of turbidites with lesser conglomerates, mafic to ultramafic volcanic units, and plutons (Camiré et al., 1993; Davis, 2002; Perrouty et al., 2017). It is bracketed in age from ca. 2685 Ma, the dates of the youngest sedimentary detrital zircons, to ca. 2682 Ma, the crystallization age of the crosscutting Fournière pluton (Davis, 2002). In the Larder Lake area, the CLLF separates older volcanic units of the Larder Lake group (*ca*. 2705 Ma; Corfu et al., 1989) from the Timiskaming assemblage (<2677 – 2670 Ma; Ayer et al., 2005), which also unconformably overlies the Blake River group to the north (2704–2696 Ma; Ayer et al., 2005). The volcanic and sedimentary units of the Timiskaming assemblage separate the Larder Lake group and Blake River groups (Figure 2) and also include syenitic, granitic, dioritic to granodioritic intrusive rocks (2677-2670 Ma; Thomson, 1941; Frarey and Krogh, 1986; Corfu et al., 1991, 1989; Corfu and Noble, 1992; Ayer et al., 2002, 2005; Thurston et al., 2008).

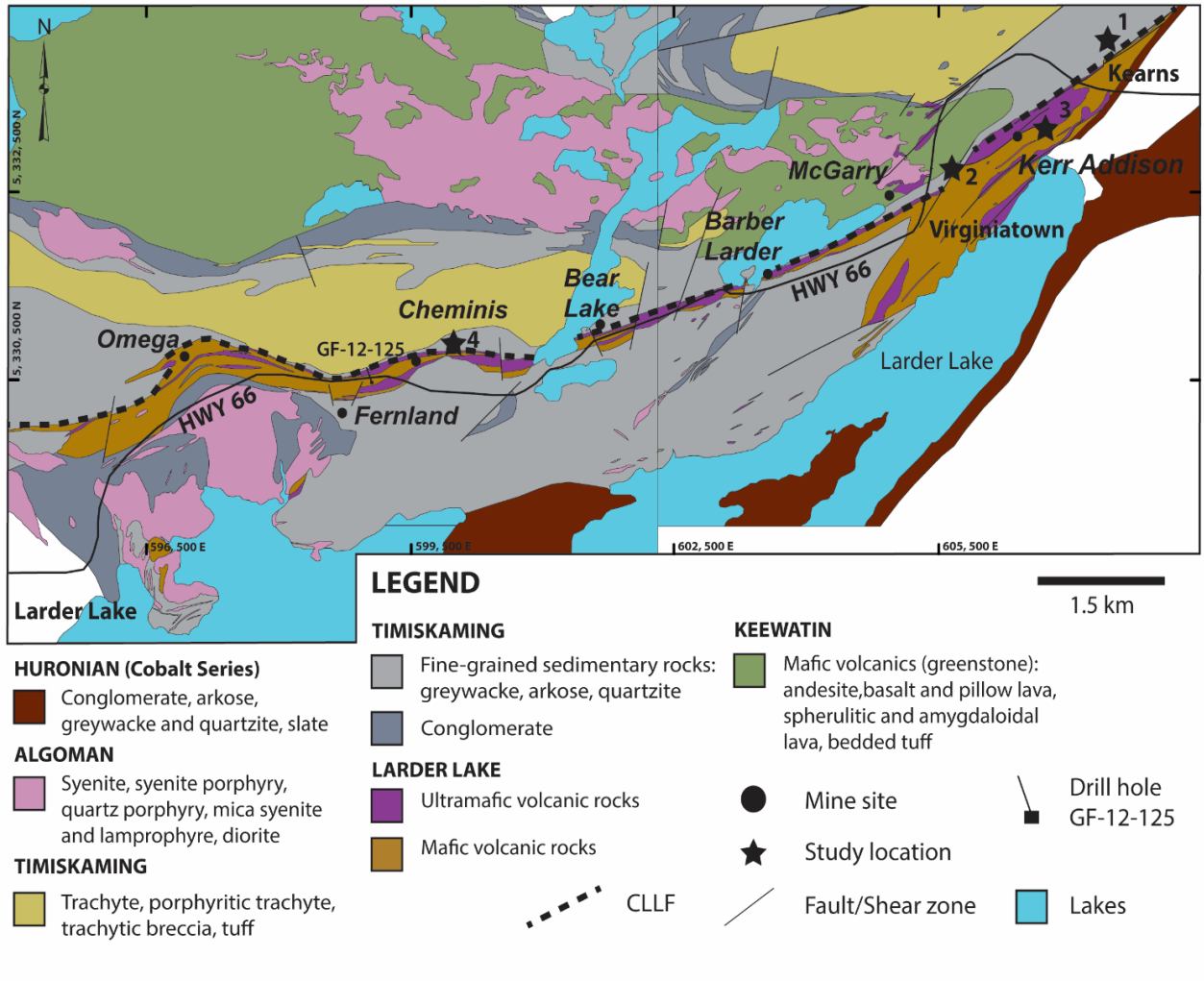


**Figure 2**. Regional geologic map of the Larder Lake area (adapted from Thomson 1941, Map No. 50a and 50b) Universal Transverse Mercator (UTM) co-ordinates provided using North American Datum 1983 (NAD83) in Zone 17N. Study locations are identified as 1-4 where the CLLF and the contact between the Timiskaming assemblage and Larder Lake group were mapped in detail.

## 2.1.2 Previous Work in the Larder Lake area

Wilson (1912) subdivided the rocks of the Larder Lake area into the Keewatin group and younger Pontiac schists. The Keewatin group included greenschist facies, mafic to intermediate, volcanic rocks, and what was interpreted at the time to be a chrome mica-rich dolomite of the Larder Lake and Blake River groups, as well as the slates and banded iron formation of the Timiskaming assemblage. Wilson (1912) suggested that the chrome mica-rich dolomite was an ideal host for

gold mineralization because it had been hydrothermally altered and was cut by "*innumerable anastomosing and intersecting*" quartz and quartz-carbonate veins. The Pontiac schists are best exposed in the province of Quebec. They are described as a unit distinctly separate from the Keewatin group and characterized by a very fine-grained mica schist of sedimentary origin composed dominantly of biotite and quartz. Wilson (1912) was unable to determine the contact relationship between the two assemblages.

Thomson (1941) later separated the Timiskaming sedimentary rocks from the Keewatin mafic volcanic rocks but retained volcanic rocks of the Larder Lake group as part of the Timiskaming assemblage. These observations were based on the consistent south-younging graded turbiditic sandstone of the Timiskaming rocks on both sides of the sliver of Larder Lake volcanic rocks exposed from the town of Larder Lake to 10-15 km west of the Ontario-Quebec border. Thomson (1941) interpreted the contacts between the Timiskaming and Larder Lake groups as primary and conformable.

Hyde (1980) completed the first comprehensive study of the Timiskaming rocks and divided them into a non-marine facies of conglomerates and sandstone and a marine facies of laminated siltstone, mudstone, sandstone, and turbidite deposits. The former were interpreted to have been deposited as alluvial fan and braided river deposits from uplifted and eroded volcanic and plutonic terranes whereas the latter were interpreted to have been transported and deposited as submarine fan deposits on the narrow marine shelf bordering the Abitibi subprovince (Hyde 1980). Although not part of this work, the Timiskaming sedimentary rocks are associated with an alkalic volcanic sequence of trachyte, phonolite and calc-alkaline volcanic rocks (north of the CLLF, Figure 2)

(Cooke & Moorhouse, 1969; Hyde, 1980). The volcanic units are interpreted as penecontemporaneous with the sedimentary rocks because they are intercalated with the conglomerates and marine turbidites. In addition, clasts of trachyte are locally found within the conglomerate (Thomson, 1941). These Timiskaming volcanic rocks consist of both coherent flows and, to a larger extent, volcaniclastic rocks of intermediate composition, and are considered the volcanic equivalents of the late Timiskaming plutons and stocks (Thomson, 1941; Cooke & Moorhouse, 1969; Hyde, 1980).

Jensen (1985) separated the sedimentary rocks of the Timiskaming assemblage located north of the CLLF from those located south of the fault (Figure 2). The latter were considered as a separate unit due to a lack of red jasperoid clasts and trachyte clasts, and as such were included as part of the older Larder Lake group (Jensen, 1978a, 1978b, 1979, 1980, 1985). Based on the presence of spinifex textures, the dolomite or carbonate rocks described by Wilson (1912), Thomson (1941) and others, were re-interpreted by Jensen (1985) as carbonate-altered komatiites based on a new understanding of the emplacement of effusive ultramafic rocks in the late 70s and 80s (Jensen, 1974, 1985; Tihor and Crocket, 1977).

Jackson and Fyon (1991) introduced the term Hearst assemblage to represent the sedimentary rocks located south of the CLLF. The Hearst assemblage lacks alkalic volcanic rocks and is dominated by turbidite units locally interbedded with iron formation and polymictic conglomerate. This formation has yielded zircons from northern Skead township with a minimum age of 2695.6 ± 3 Ma (Ayer et al., 2003). Subsequent detrital zircon studies from sandstone samples collected near the Cheminis mine and Martin Bird property yielded Timiskaming ages of 2674 ± 3.7 and

2684.9 ± 1.9 Ma (Ayer et al., 2005) and 2679 ± 3 Ma (Corfu et al., 1991), respectively, suggesting that at least locally the Hearst assemblage is misclassified and instead represents a marine facies of the Timiskaming assemblage as previously suggested by Hyde (1980).

Throughout the Abitibi, numerous intrusions occur in close proximity to the PDF and the CLLF and are constrained in age between 2695-2670 Ma (Ayer et al., 2005). In the Larder Lake area, syntectonic intrusions were originally mapped by Thomson (1941) as "Algoman" intrusives and ranged in composition from syenitic, granitic to dioritic with local lamprophyre dikes. These intrusions are interpreted to be coeval with the Timiskaming assemblage and are the intrusive equivalent of the trachyte volcanic units (Ayer et al., 2005).

### 2.1.3 Structural evolution of Larder Lake area

The southern Abitibi subprovince underwent several deformation events. An early $D_1$ event is represented by regional, east-west striking, isoclinal folds, which either lack (Dimroth et al., 1983) or locally have a weak axial planar $S_1$ cleavage (Hubert et al., 1984). Some authors attribute the formation of these folds to gentle subsidence during early volcanic activity (Dimroth et al., 1983) while others believe that the folds formed during a regional compression event (Desrochers et al., 1993). Whatever their origin, an angular unconformity between the Timiskaming assemblage and the older folded volcanic rocks (Blake River group in the Larder Lake area) indicates that the $D_1$ event predates the deposition of the Timiskaming assemblage (Wilson, 1956; Poulsen, 2017).

The Timiskaming assemblage is spatially associated with major fault zones such as the CLLF (Mueller & Donaldson, 1992; Frieman et al., 2017). The Timiskaming sedimentary rocks are

interpreted to have been deposited either in extensional basins (Dimroth et al., 1982; Corfu et al., 1991; Mueller et al., 1994; Bleeker, 2015), foreland piggy-back basins (Allen and Allen, 2005; Diop, 2011), or strike-slip pull-apart basins (Daigneault et al., 2002; Bedeaux, et al. 2017).

These basins were subsequently deformed during $D_2$ (Cameron, 1993; Bleeker, 2012, 2015), a widespread north-south compressional event, which produced regional isoclinal $F_2$ folds with a moderately to steeply plunging stretching lineation and a pervasive, generally east-west-striking, $S_2$ foliation (Toogood and Hodgson, 1985; Hamilton, 1986; Hodgson & Hamilton, 1989; Robert, 1989; Wilkinson et al., 1999). The strong east-west to northeast trending penetrative foliation and steeply plunging stretching lineation that characterize the CLLF is thought to have formed during this $D_2$ event. The CLLF changes in dip and kinematics from primarily south-dipping and reverse south-side-up in Ontario to north-dipping and reverse north-side-up in Quebec consistent with a major thrusting event (Hodgson and Hamilton, 1989; Wilkinson et al., 1999; Ispolatov et al., 2005; Zhang et al., 2014; Lafrance, 2015). Other studies emphasized transpressional transcurrent movement along the CLLF during the $D_2$ event (Robin and Cruden, 1994; Wilkinson et al., 1999) or postulated that the CLLF formed as early separate segments that later became linked during a $D_3$ event (Bedeaux et al., 2017).

The last regional deformation across the southern Abitibi subprovince resulted in the reactivation of the CLLF during a regional $D_3$ deformation event. Dextral shearing along the CLLF is indicated by dextral asymmetrical shear sense indicators, defined by Z-shaped folds, rotated clasts and a dextral S/C fabric observed in sedimentary units, and the formation of a regional ENE-striking $S_3$ foliation axial planar to Z-shaped $F_3$ folds. (Hodgson and Hamilton, 1989; Robert, 1989;

Wilkinson et al., 1999; Daigneault et al., 2002; Ispolatov et al., 2005; Zhang et al., 2014; Lafrance, 2015).

### 2.1.4 Gold Mineralization

Gold deposits along the CLLF are characterized by intense carbonate, potassic and sodic alteration associated with sulfide minerals (Thomson, 1941, Thomson and Griffis, 1941, Card et al., 1989; Hodgson and Hamilton, 1989; Mueller, 1991; Mueller and Donaldson, 1992; Thurston and Chivers, 1990). Along the Quebec segment of the CLLF, several world-class orogenic gold deposits have collectively produced over 1,700 t (54.6 Moz) of gold (Monecke et al., 2017) and gold-rich volcanogenic massive sulphide (VMS) deposits have produced over 1,100 t of gold (35.4 Moz) (Dubé and Gosselin, 2007; Monecke et al., 2017; Poulsen, 2017). The VMS deposits are interpreted to have formed along ancient syn-volcanic faults, which may be masked by later overprinting ductile deformation whereas the orogenic gold deposits are directly related to brittle-ductile shearing along second-order splays of the CLLF (Robert, 1990, 1995; Neumayr et al., 2000). In contrast, orogenic gold deposits along the Ontario segment of the CLLF are typically in the immediate footwall of the CLLF (Thomson, 1941; Hamilton, 1986; Hodgson and Hamilton, 1989; Smith et al., 1993; Ispolatov et al., 2005, 2008; Lafrance, 2015; Poulsen, 2017)) and gold-rich VMS deposits are absent.

Intrusion-hosted gold deposits, such as Kirkland Lake, and Young Davidson, are associated with intrusions ranging in composition from quartz-monzonite to syenite, which are all located proximal to the CLLF (Robert, 2001, Martin, 2012, Zhang et al., 2014). Intrusion-related gold deposits are characterized by disseminated sulphides within either the intrusion or adjacent wall rocks with

gold-bearing quartz stockwork veins that differ from typical orogenic vein deposits in they are not well defined, “through-going” quartz-carbonate veins (Robert, 2001). The dominant sulfide present in these deposits is pyrite with arsenopyrite present in some deposits such as Beattie. Commonly associated with ore minerals are Cu, Pb, As, Te, Mo and W, where these elements vary in significance between deposit types. Spatially associated with sulfide mineralization and veinlet stockworks are zones of carbonatization, albitization and locally potassic (K-feldspar) and sericitization of the host rocks. However, the predominance of albite and k-feldspar alteration over sericitization distinctly separates these deposit types from orogenic gold deposits. Alteration zonation also does not exhibit a distinct pattern across different deposits (Robert, 2001). Fluid inclusion studies also indicate the ore-bearing fluids were oxidizing, with negative $\delta^{34}S$ values within pyrite.

The Larder Lake area hosts a number of orogenic gold deposits; these include the Omega, Fernland, Cheminis, Bear Lake, Barber Larder, McGarry and the Kerr-Addison / Chesterville deposits (Figure 2), which are roughly spaced 1.0-1.5 km apart and collectively produced a total of 376 tonnes of gold (~12 Moz) (Ispolatov et al., 2008; Monecke et al., 2017). The relative timing of gold mineralization in the Larder Lake area is constrained by mutually overprinting relationships between auriferous pyrite grains and the $S_2$ foliation along the CLLF (Lafrance, 2015). At the Cheminis deposit, the $S_2$ foliation wraps around auriferous pyrite grains but is also truncated against other auriferous pyrite grains, suggesting that pyrite formation and gold mineralization outlasted the development of the $S_2$ foliation (Lafrance, 2015). Similarly, west of Larder Lake, at the Upper Canada deposit, $S_2$ is defined by “bands of deformed hydrothermal mineral aggregates” with auriferous quartz veinlets parallel to the $S_2$ fabric and associated with

strong carbonate alteration (Ispolatov et al., 2005) suggesting that the formation of the gold bearing quartz veins and associated alteration occurred syn-late $D_2$.

Within the study area, the Kerr-Addison mine together with the contiguous Chesterville mine, produced roughly 335 tonnes of gold (~11 Moz; Smith et al., 1993) at an average grade of about 9 g/t making it one of the largest gold deposits in the Abitibi subprovince. The Kerr-Addison deposit, is structurally controlled with gold introduced during post-Timiskaming brittle-ductile deformation associated with the CLLF (Hamilton, 1986; Smith et al., 1993). The deposit is hosted within mafic to ultramafic volcanic units of the Larder Lake group in the immediate structural footwall of the Timiskaming assemblage (Thomson, 1941; Kishida and Kerrich, 1987; Smith et al., 1993). The contact between the Larder Lake group and the Timiskaming assemblage defines the trace of the CLLF in the Larder Lake area (Hamilton, 1986; Smith et al., 1993). The deposit consists of two main styles of mineralization including quartz-carbonate veins in fuchsite-siderite/magnesite-albite-altered ultramafic rocks, the so-called "green carbonate ore", and disseminated pyrite in albite-sericite-carbonate-altered mafic volcanic rocks, the so-called "flow ore" (Smith et al., 1993).

Approximately 6 km to the west of the Kerr-Addison site is the smaller Cheminis deposit which was discovered in 1937 and had minor production between 1937-1940 (Thomson, 1941) and later between 1991-1996 (Lafrance, 2015). Total ounce production is poorly documented but is in the order of approximately 3.7 tonnes of gold (119,200 ounces) averaging 5.35 g/t (0.156 ounce/ton) (Thomson, 1941; Lafrance, 2015). Similar to the Kerr-Addison deposit, ore zones are associated with disseminated pyrite within altered Fe-rich tholeiitic basalts and ultramafic rocks of the Larder

Lake group, with a smaller proportion hosted by the Timiskaming sandstone unit to the south and north of the volcanic panel (Lafrance, 2015).

## 2.2 Rock Descriptions

Three assemblages characterize the study area, from older to younger: the Larder Lake group (2710–2704 Ma), Blake River group (2704–2695 Ma) and Timiskaming assemblage (2677–2670 Ma) (Ayer et al., 2005; Thurston et al., 2008).

### 2.2.1 Larder Lake group

The Larder Lake group, which is time equivalent to the lower Tisdale assemblage 2710–2705 Ma (Ayer et al., 2002), consists of intercalated mafic to ultramafic volcanic rocks and minor sedimentary rocks. Although not observed in the immediate study area, the Larder Lake group locally contains felsic volcanic rocks. Zircons collected from a felsic tuff breccia in Gauthier Township (south of Kirkland Lake) and a felsic fragmental rock in Skead Township (south of Larder Lake) have yielded ages consistent with the Tisdale assemblage (*ca.* 2705 ± 2 Ma, Corfu et al., 1989; 2710 ± 3.9 Ma, Ayer et al., 2002). Along the segment of the CLLF between the Omega mine to the Kerr-Addison mine (Figure 2), the Larder Lake group occurs as a thin but continuous panel of mafic and ultramafic volcanic rocks bounded on both sides by Timiskaming rocks. Individual units within the panel are discontinuous and pinch both laterally and vertically and the panel itself varies in width from 50 m wide at the Cheminis mine site to over 600 m wide at Kerr-Addison (Figure 2; Thomson, 1941; Jensen, 1980; Jensen and Langford, 1985; Hamilton, 1986; Hodgson and Hattori, 1991; Lafrance, 2015).

Ultramafic volcanic units consist of fine- to medium-grained massive flows with little textural variation. Locally, a coarse- to fine-grained spinifex texture is preserved and defines a primary layering that formed during rapid cooling of the ultramafic flows and/or sills (Figure 3a). A notable feature of the ultramafic units at Kerr-Addison is the presence of distinct pseudo-breccias consisting of angular-rounded fragments of wall rock of variable size within a matrix or network of fractures that have been filled with coarse-grained carbonate, quartz and minor albite (Figure 3b). Locally a jigsaw-fit texture is observed. The breccia may result from volume change during the initial carbonate alteration (during the transformation of olivine to serpentine/talc) with the fractures reopening later due to hydraulic fracturing resulting from fluid pressure build up induced by decreasing permeability (Kishida and Kerrich, 1987).

Mafic volcanic units consist of locally variolitic, amygdaloidal, and plagioclase phenocrystic pillowed flows, locally intercalated with massive flows or sills. Pillowed flows are aphanitic to fine-grained and comprise medium to large (20-30 cm wide) ovoid pillows with fine-grained chloritized selvages (0.5-2 cm thick). Spheroidal varioles varying in size from 0.5 – 2 cm in diameter are locally concentrated around pillow selvages and are typically elongate reflecting the local state of strain (Figure 3c). Amygdaloidal variolitic flows are intercalated with plagioclase phenocrystic flows and monomict breccias with shard-like perlitic fractures, interpreted as hyaloclastite (Figure 3d). Auto-brecciation at the top and base of flows is common with angular (2-10 cm long) porphyritic, aphanitic and hyaloclastite clasts with perlitic fractures suspended in graphitic fine-grained matrix and local fine-grained pyrite growth within matrix material.

Two to three meter thick intervals of black graphitic mudstone are intercalated with the mafic volcanic flows and locally occur at their contact with ultramafic rocks indicating eruptions in a submarine environment with deposition of fine sediments during periods of quiescence. These

graphitic mudstones are very fine-grained, finely laminated to thinly bedded, and locally contain coarse-grained concentric to banded pyrite, interpreted as diagenetic pyrite nodules. Graphitic mudstone is locally intermixed with volcanic fragments at contacts with in situ brecciated mafic flows.

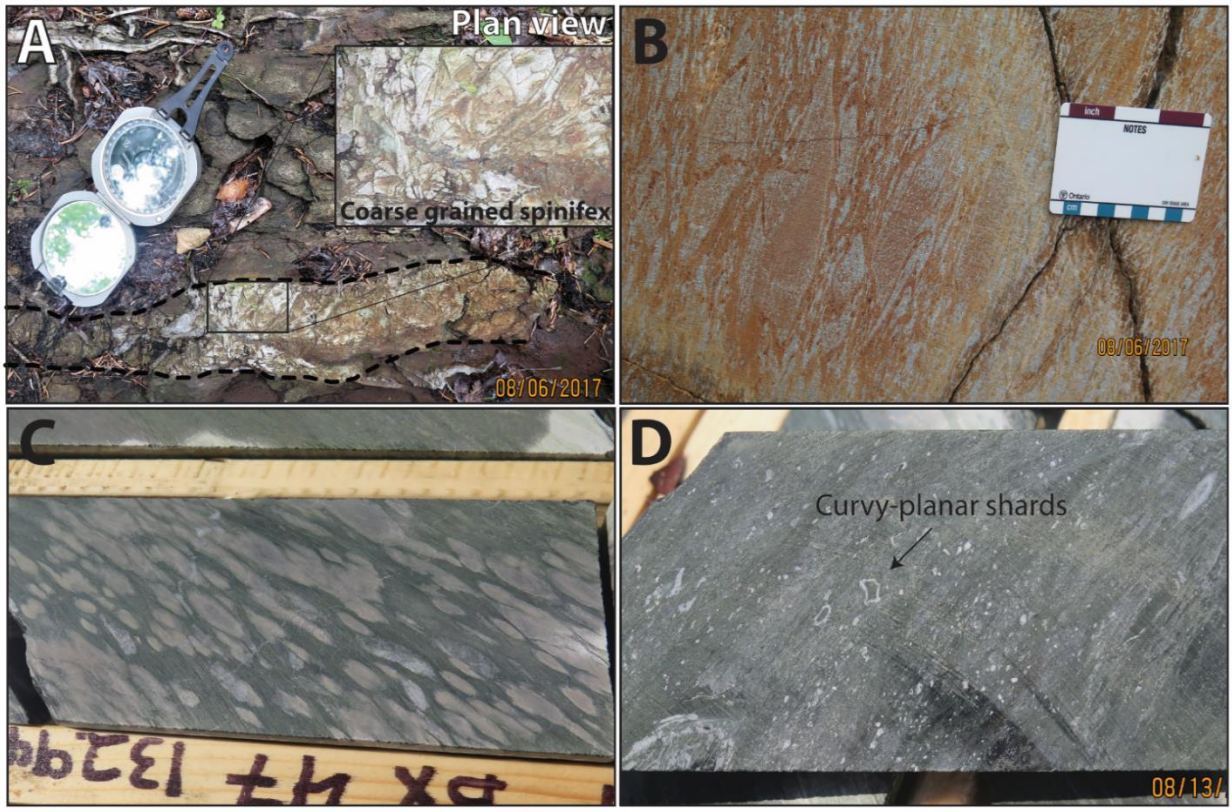


**Figure 3**. Photographs of Larder Lake group lithologies and textures. (**A**) Layers of coarse-grained spinifex within a komatiite flow. Compass indicating north. Co-ordinates: 605367N/5332101E (NAD83, Zone 17N) (**B**) Ultramafic pseudobreccia texture showing fuchsite-quartz-carbonate altered angular clasts within opaque white quartz-carbonate-albite matrix. Outcrop on the Kerr-Addison mine site. (**C**) Variolitic texture within a mafic volcanic flow. Drill hole KAD17-043, hole diameter 63.5 mm. (**D**) Mafic volcanic unit with curvy-planar shards with perlitic fractures interpreted as a hyaloclastite texture. Drill hole KAD17-039, hole diameter 63.5 mm.

## 2.2.2 Blake River group

The Blake River group in the study area consists of the lower units only of the assemblage (2704-2701 Ma; Ayer et al., 2005; referred to as the Garrison subgroup by Goodwin, 1977). It is

correlative with the Hébécourt and Rouyn-Pelletier formations in Quebec. The units have similar lithological and geochemical characteristics (Goodwin, 1977; Goutier and Lacroix, 1992; Péloquin et al., 2008) dominated by Fe-tholeiitic basalts. In the study area, the Blake River group is composed of pillowed to massive mafic volcanic flows.

### 2.2.3 Timiskaming assemblage

The Timiskaming assemblage consists of alluvial-fluvial and marine facies (Hyde, 1980). The marine facies is dominated by grey to green, well-sorted and well-bedded sandstone to mudstone units (Figure 4a) with minor intervals of oxide banded iron formation (Hyde, 1980) and conglomerates. Interbedded sandstone and siltstone exhibit consistently normal graded beds ranging in thickness from less than 1 cm to 50 cm. Sandstone beds are composed dominantly of quartz (5 - 50%), feldspars (20%) with variable amounts of muscovite (10-15%) alongside trace amounts of titanite, rutile and apatite. (Figure 4b).

The alluvial-fluvial facies is dominated by polymictic conglomerates that are grey to beige in color with rounded to angular, cobble- to sand-sized clasts, surrounded by a sandy matrix. Clast composition is highly variable and includes granitic intrusive, mafic to felsic volcanic, mudstone to siltstone and locally quartz vein clasts (Figure 4c). Few fuchsite-altered ultramafic clasts are present (Figure 4d). Intercalated with the conglomerate are massive to cross-bedded sandstones. These sedimentary units are typically poorly sorted, immature and represent a proximal sedimentary facies interpreted as a braided river setting (Hyde, 1980).

### 2.2.4 Dikes

Numerous albitite dikes and mafic dikes cut across and are in sharp contact with the mafic volcanic rocks. Albitite dikes are composed of secondary albite phenocrysts (Figure 4e) surrounded by a groundmass of quartz-albite-carbonate ± pyrite. They are typically present in hydrothermal alteration zones in which they are intensely altered. The mafic dikes are dark green and fine grained with rare, rounded to angular, clasts of granitoid and fine-grained chloritized mafic volcanic rocks surrounded by a groundmass of fine-grained iron- and magnesium-carbonates, chlorite and quartz (Figure 4f).

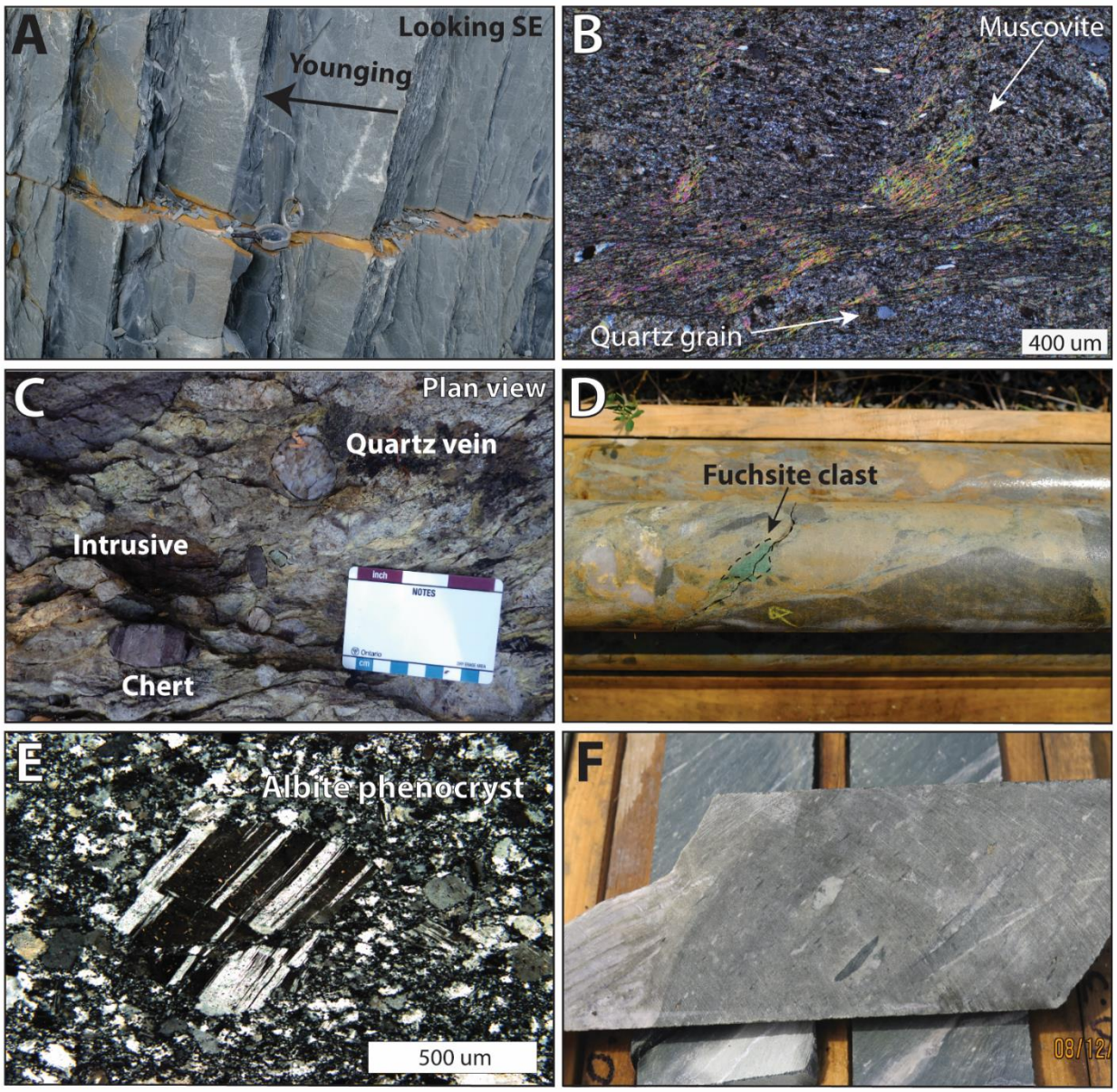


**Figure 4**. Photographs of Timiskaming assemblage lithologies and textures and younger dikes. (**A**) Timiskaming assemblage marine turbidite showing consistently graded sedimentary layers ranging from sandstone to mudstone. Compass for scale. Co-ordinates: 606155N/5333178E (NAD83, Zone 17N) (**B**) Thin section photomicrograph (cross-polarized light) showing composition and texture of typical Timiskaming assemblage marine turbidite. Dominantly composed of large quartz grains within finer grained quartzo-feldspathic matrix with carbonate and muscovite overprinting alteration. (**C**) Timiskaming assemblage alluvial-fluvial facies showing a polymict, unsorted conglomerate. Clasts are typically well-rounded with varying compositions including quartz veins, granitic intrusive, mafic and felsic volcanic, and mudstone to siltstone sedimentary fragments. Co-ordinates: 603581N/5331454E (NAD83, Zone 17N). (**D**) Timiskaming assemblage conglomerate showing a fuchsite altered clast. Drill hole GF-12-125, hole diameter 47.6 mm. (**E**) Thin section photomicrograph of albitite dike showing albite phenocrysts with fractured albite twinning. Groundmass consists of quartz-albite and minor carbonate (XPL). (**F**) Mafic dike with polymict xenoliths of rounded granitic intrusive, fine-grained chloritized volcanic and quartz clasts

within very fine-grained groundmass. Drill hole KAD17-043, hole diameter 63.5 mm.

## 2.2.5 Geochemistry

Samples for whole rock geochemistry were selected from individual rock types with trace to no mineralization or veins. Samples were cut and trimmed to remove surficial alteration and significant zones of hydrothermal alteration.

Analytical Techniques

Forty-two samples of the Larder Lake ultramafic and mafic volcanic rocks, Blake River volcanic rocks, Timiskaming sandstone, and albitite dikes were analyzed for their whole rock major and trace element composition. Sample preparation was completed at the ALS Sudbury branch. Samples were crushed down to < 2 mm sized particles and an aliquot was taken and further pulverized to <75 µm. The aliquot was dissolved at the ALS Vancouver laboratory using a four acid digestion protocol and the solutions were then analyzed by ICP-AES (inductively coupled plasma atomic emission spectroscopy) for major elements, ICP-MS (inductively coupled plasma mass spectroscopy) for trace elements and ICP-AES for base metals. Table 1 in Appendix A lists the data for all samples analyzed, including standards and duplicates.

Quality Assurance / Quality Control

The precision results for major elements (RSD %) vary widely and are less than 10% for $SiO_2$, $TiO_2$, $Al_2O_3$, $Fe_2O_3$, $Cr_2O_3$ and MnO and greater than 15% for MgO, CaO, SrO, $Na_2O$, $K_2O$ and $P_2O_5$. Precision results for trace elements exceeds 10% for As, Bi, Ce, Cr, Cs, Dy, Er, Eu, Gd, Hf, Hg, Ho, In, La, Lu, Nd, Ni, Pr, Rb, Re, Sb, Sm, Sr, Tb, Te, Th, Tm, U, Y, Yb, Zr. The high

variation in precision may be due to heterogeneities of the samples. The accuracy was measured using the international standards IAG OKUM and LK-NP-1 (observed average / certified value x 100) and is within 5% for all major elements (except $K_2O$ and $P_2O_5$) and all trace elements (except Cs, Dy, Ho, La, Nb, Sb, and Yb, which are close to detection limit).

## Results

### *Ultramafic Rocks*

Ultramafic volcanic rocks of the Larder Lake group have been intensely altered in the Kerr-Addison to Cheminis area, to the point where Thomson, (1941) mapped them as exhalative dolomite rocks. These are considered komatiitic flows or sills based on the presence of spinifex textures and local polygonal jointing (Shore and Fowler, 1999), and elevated Cr-Ni values (>1000 ppm Cr and 500-1700 ppm Ni). Immobile elements $Al_2O_3$, $TiO_2$, Zr and Y (incompatible elements within olivine crystal structure; Barnes, 2006) were plotted to compare with other regional ultramafic volcanic rocks. Zr/Y ratios indicate a tholeiitic composition for the ultramafic volcanic rocks (Figure 5a; average ratio of 2.4) and are consistent with the composition of the Larder Lake group from samples collected at the Kerr-Addison mine site (Kerrich and Kishida, 1987), at the Cheminis mine site (Lafrance, 2015) and from the Val d'Or, Rouyn and Halet segments of the CLLF (Bedeaux et al., 2018). Plotted $Al_2O_3/TiO_2$ ratios show a positive linear trend for ultramafic volcanic units of the Larder Lake group (Figure 5b). These ratios are similar to komatiites sampled at Kerr-Addison (Kerrich and Kishida, 1987; Lafrance, 2015), the Piché group from different locations along the CLLF (Bedeaux et al., 2018) as well as other Archean komatiites of the Yilgarn craton (Barnes, 2006). On a binary $TiO_2$ – Zr diagram, they display a linear trend, which may reflect enrichment or dilution during alteration, with a constant $TiO_2$/Zr

ratio of ~0.98 (Figure 5c). Major element composition is plotted on a Jensen ternary diagram, indicating komatiitic to komatiitic basalt composition for the ultramafic volcanic rocks, consistent with regional studies (Figure 5d). However, due to the loss or gain of both Fe and Mg, this plot is indicative only (Jensen, 1976). The effect of alteration is equally observed in the immobile element diagrams exhibiting linear trends (Zr/Y, $Al_2O_3/TiO_2$ and $TiO_2$/Zr), which indicates dilution or concentration of the trace element content.

The igneous mineralogy is not preserved, although igneous textures have been preferentially replaced and preserved by an alteration mineral assemblage of distal to proximal alteration assemblages as shown by the local spinifex textures. Distal alteration is characterized by talc-magnesite-chlorite to chlorite-magnesite. Proximal alteration facies are characterized by a mineral assemblage of magnesite-fuchsite to magnesite-albite (Kishida and Kerrich, 1987). The samples collected by the author were universally altered which is reflected in the trends seen in the immobile elements.

On a rare-earth element (REE) diagram normalized to primitive mantle (Figure 5e), the samples have flat, unfractionated REE patterns with primitive mantle-normalized $La/Yb_{pm}$ ratios of ~0.62, absolute REE abundances that are 7 to 10 times greater than primitive mantle values, and weak positive and negative Eu anomalies. Due to the dilution or concentration of these elements during alteration (mass gain or loss) these patterns will shift vertically depending on the alteration systematics, but the patterns will not change as such are comparable to other studies in the area. (Figure 5e).

*Mafic Volcanic Rocks*

Two samples of Larder Lake mafic volcanic rocks plot in the field of high-Fe to high-Mg tholeiitic basalt (Figure 5a, 5d; Jensen, 1976). They have similar values and $TiO_2$/Zr ratios (~0.82) (Figure 5c) as the ultramafic volcanic rocks yet a higher Y/Zr ratio (Figure 5a) and still within the tholeiitic field. They also have similar flat unfractionated REE patterns (La/Ybpm = ~0.99), and slightly higher absolute REE abundances that are 3 to 7 times greater than primitive mantle values (Figure 5f). Mafic volcanic rocks from the Larder Lake group show a depleted Eu anomaly in comparison with the Blake River group mafic volcanic rocks (Figure 5f). These patterns are similar to trace element signatures observed in the Larder Lake group equivalent, the Piché group, from the Val d'Or, Halet, Rouyn, Bousquet and Beaupré segments of the CLLF (Bedeaux et al., 2018).

Mafic volcanic rocks from the Larder Lake group rocks have been variably altered. The alteration assemblages associated with the mafic volcanic rocks are characterized by a distal chlorite-albite to chlorite-sericite alteration and are overprinted by proximal carbonate-sericite to carbonate-albite, with the dominant composition of the carbonate minerals being $CaCO_3$ (Kerrich and Kishida, 1987).

Two samples of Blake River group mafic volcanic rocks have similar chemistry to the mafic volcanic rocks of the Larder Lake group. They plot within the high-Fe to high-Mg tholeiitic basalts field on a Jensen cation plot and within the transitional field based on their Y/Zr ratio (Figure 5a, 5d; Jensen, 1976), they have similar $TiO_2$/Zr ratio of ~1 (Figure 5c), and similar REE pattern and absolute REE abundance of 8 to 10 ppm (Figure 5f). Previous studies on the

geochemistry of the Blake River group indicate that these are transitional mafic volcanic rocks based on Zr/Y ratios, similar to results from this study (Ross et al., 2011). The mafic volcanic rocks of the Blake River group have been weakly to moderately carbonate altered with proximity to the CLLF.

*Sedimentary rocks*

The analyzed sedimentary rocks are sandstone and mudstone from the Timiskaming turbiditic marine facies and transition zone samples within 2 m of the Larder Lake group-Timiskaming contact. The transition samples contain clasts of ultramafic volcanic rocks, described below. These rocks are characterized by a low $TiO_2$ (<0.75%) and a high Zr content (> 90 ppm) (Figure 5c). The Timiskaming turbidite sedimentary units are enriched in LREE with respect to primitive mantle and show a trace element pattern similar to that of the "transition" zone samples (Figure 5g) indicating a proximal sourcing of continental crust.

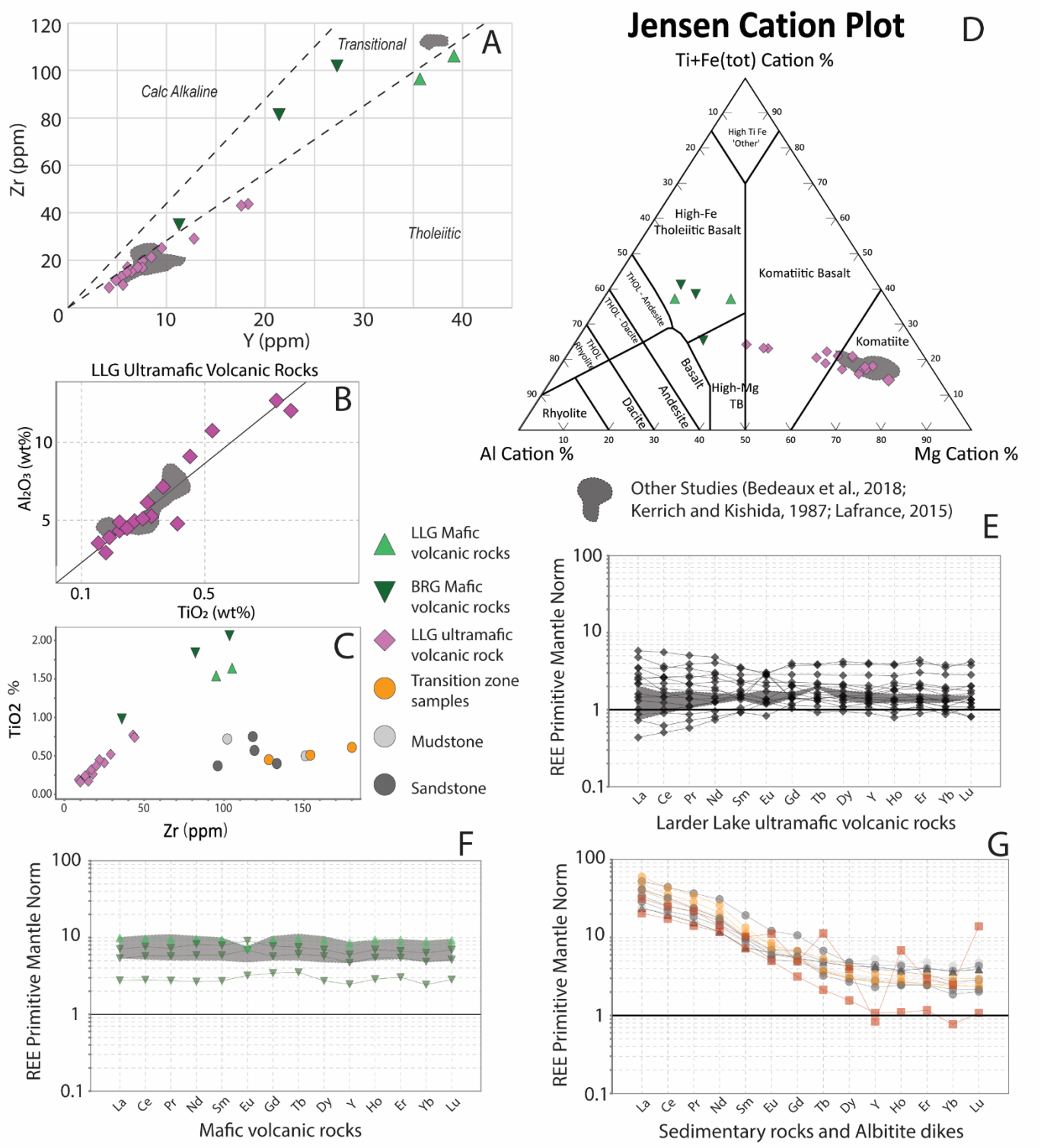


**Figure 5**. Whole rock geochemistry. (**A**). Zr:Y plot of ultramafic and mafic volcanic rocks of the LLG and BRG with regional study data outlined in grey. (**B**) $Al_2O_3/TiO_2$ plot of Larder Lake group ultramafic volcanic rocks from this study and regional study data outlined in grey (**C**). Zr:Ti ratio for 40 samples collected showing a higher Zr content within sedimentary units of the Timiskaming assemblage than the mafic and ultramafic volcanic units, which tend to have lower Zr content and a higher $TiO_2$ percentage. (**D**). Jensen cation plot of

19 whole rock geochemistry samples collected from the Larder Lake area showing the composition of mafic and ultramafic units mapped. Regional study data outlined in grey (**E**). REE normalized to Primitive Mantle values of Sun and McDonough (1989) for 16 samples of ultramafic volcanic units showing a flat REE signature consistent with minimal fractional crystallization. Regional study data outlined in grey. (**F**). REE normalized to Primitive Mantle values of Sun and McDonough (1989) for three samples of Blake River group mafic volcanic units and two samples of Larder Lake group mafic volcanic units showing a slightly higher, yet consistently flat REE pattern. Note the similar trace element signature between the two formations with the exception of an enriched Eu anomaly relative to the Larder Lake group. Regional study data outlined in grey. (**G**). REE normalized to Primitive Mantle values of Sun and McDonough (1989) for 10 samples collected from the Timiskaming sedimentary units and the "transition zone". Results indicate an LREE enrichment relative to Primitive Mantle and show a similar trace element signature as the "transition zone" at the contact with the Larder Lake group.

## 2.3 Structural geology of the Cheminis to Kerr-Addison area

Detailed structural maps of the contact between the Larder Lake group and Timiskaming assemblage, were done at a scale of 1:50 to 1:5,000 at four localities along the CLLF. The structural data and field observations are presented below.

### 2.3.1 Primary features

Younging directions were obtained from normal grading and trough crossbedding in sandstone beds of the Timiskaming assemblage. Normal grading is expressed by sharp lower bed surfaces, scour structures at the base of the beds (Figures 6a, b), and a gradual decrease in grain size from sand- to clay-size from the base to the top of the beds. In pillowed volcanic rocks, the convex rounded top surface of pillows, and apices along their flat lower surface, are the most common younging indicators with less common lenticular drainage cavities. Other primary features include coarse bedding defined by variations in clast size in autobrecciated mafic volcanic (Figure 6c) and nodular diagenetic pyrite in finely bedded mudstone (Figure 6d).

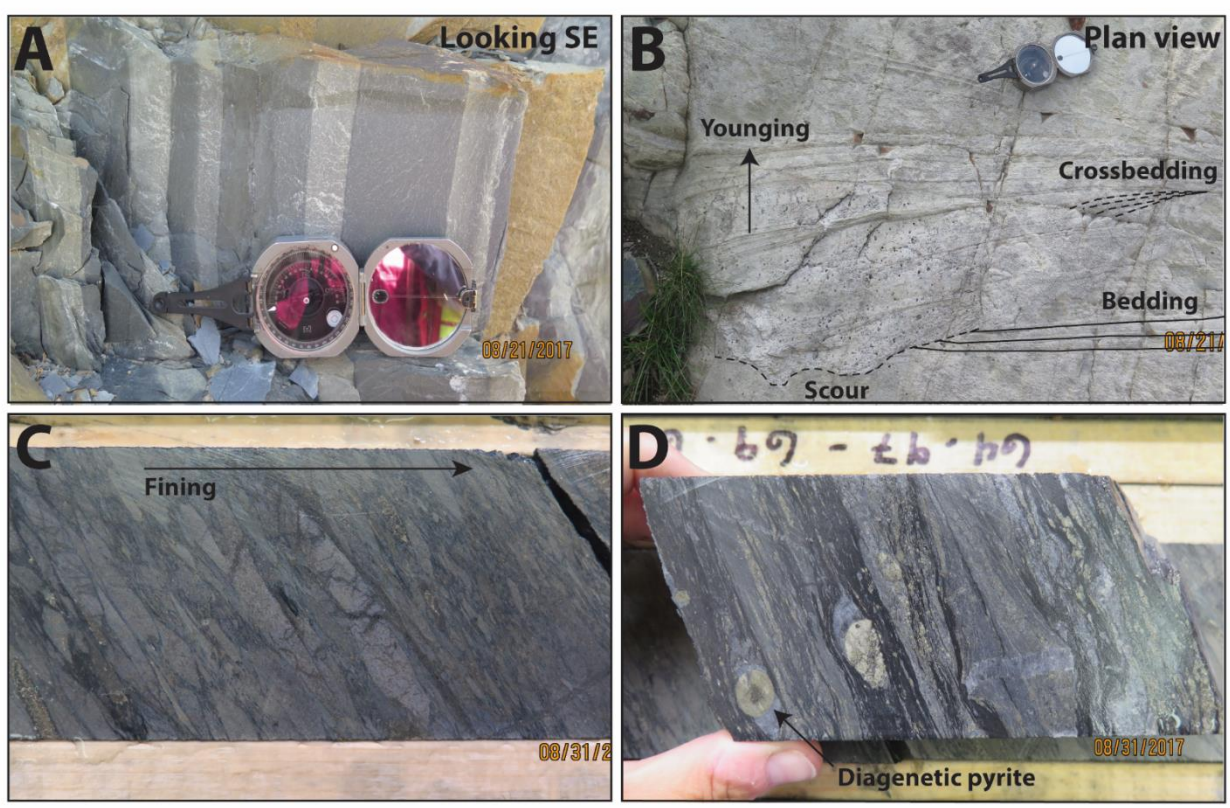


**Figure 6**. Photographs of primary features ($S_0$) (**A**) Timiskaming assemblage marine turbidite showing consistently graded sedimentary units. Compass for scale and indicating north. Co-ordinates: 606177N/5333168E (NAD83, Zone 17N). (**B**) Timiskaming assemblage coarse-grained sandstone unit showing scouring trough and crossbedding. Younging indicated by arrow to the south. Co-ordinates: 605497N/5333194E (NAD83, Zone 17N). (**C**) Larder Lake group mafic volcanic autobreccia with muddy matrix in which fining of clasts from medium to small broadly defines bedding. Drill hole KAD17-009, hole diameter 63.5mm. (**D**) Larder Lake group interflow sedimentary unit. Finely laminated and bedded graphitic mudstone with nodular diagenetic pyrite. Drill hole KAD17-009, hole diameter 63.5mm.

## 2.3.2 Foliations, lineations and folds

Structures associated with an early $D_1$ deformation event are not observed in the study area and this event is inferred from the angular unconformity between the Blake River group and Timiskaming assemblage. This unconformity suggests that the Blake River volcanic rocks were folded and tilted prior to the deposition of the Timiskaming assemblage (Goulet, 1978). The earliest recognized deformation fabrics formed during a $D_2$ deformation event. These include an

$S_2$ foliation and an $L_2$ lineation, which are axial planar and coaxial, respectively, with $F_2$ folds. The $S_2$ foliation is expressed as a penetrative sericitic cleavage in the sedimentary rocks and as a spaced to continuous chloritic / fuchsitic foliation in mafic / ultramafic volcanic rocks. $S_2$ generally strikes east-northeast to northeast and dips steeply northwest or southeast (Figure 7). In thin section, the $S_2$ foliation is defined by the alignment of sericite and elongation of quartz and carbonate grains in sedimentary rocks (Figure 8a), by chlorite, talc, fuchsite in the ultramafic volcanic rocks (Figure 8b), and by chlorite and the elongation of carbonates and albite in mafic volcanic rocks (Figure 8c). $F_2$ folds are defined in outcrop- and map-scale by changes in the younging direction of graded beds and in the relative orientation (anticlockwise or clockwise) of the $S_2$ foliation to bedding. They are open to tight, meter to decimeter in scale folds with east-northeast to northeast striking axial planes and steeply northeast plunging fold axes. An $L_2$ stretching lineation plunges moderately to steeply to the northeast (Figure 7), parallel to $F_2$ fold axes, and is defined by elongate ovoid varioles and pillows in mafic volcanic units and by elongate pseudobreccia clasts in ultramafic rocks (Figure 8d). $F_2$ folds and the $S_2$ foliation are overprinted by a northeast striking, subvertical, spaced $S_3$ foliation (Figure 7) defined by sericite in sedimentary rocks, by chlorite, talc and fuchsite in ultramafic volcanic rocks, and by chlorite in mafic volcanic rocks (Figure 8e). This foliation becomes more intense with proximity to the CLLF where it is the axial planar foliation to $F_3$ folds which crenulate the $S_2$ foliation and is expressed as a spaced differentiated cleavage defined by sericitic foliation planes alternating with more felsic microlithons of quartz and feldspar (Figure 8f, 8g). The $S_3$ cleavage is locally a slip cleavage along which $S_2$ has been dragged in anticlockwise sinistral manner. It is axial planar to meter- to centimeter scale, Z-shaped $F_3$ folds (Figure 8h).

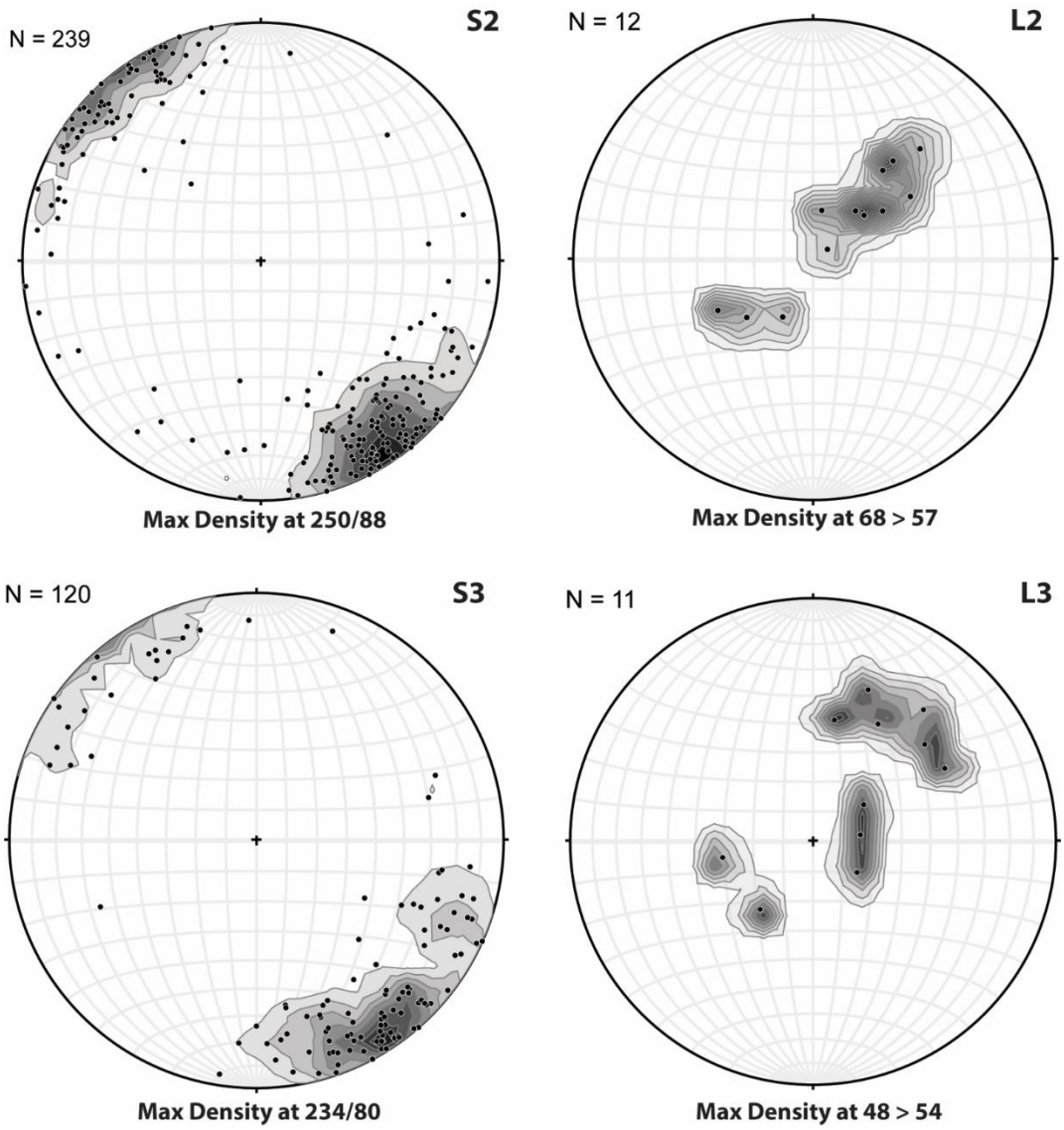


**Figure 7**. Equal-area, lower hemisphere, stereonet diagrams showing the distribution and orientation of the poles to the $S_2$ and $S_3$ foliation, $L_2$ lineations, and $L_3$ lineations. Contours are drawn at intervals of 1% of the total area.

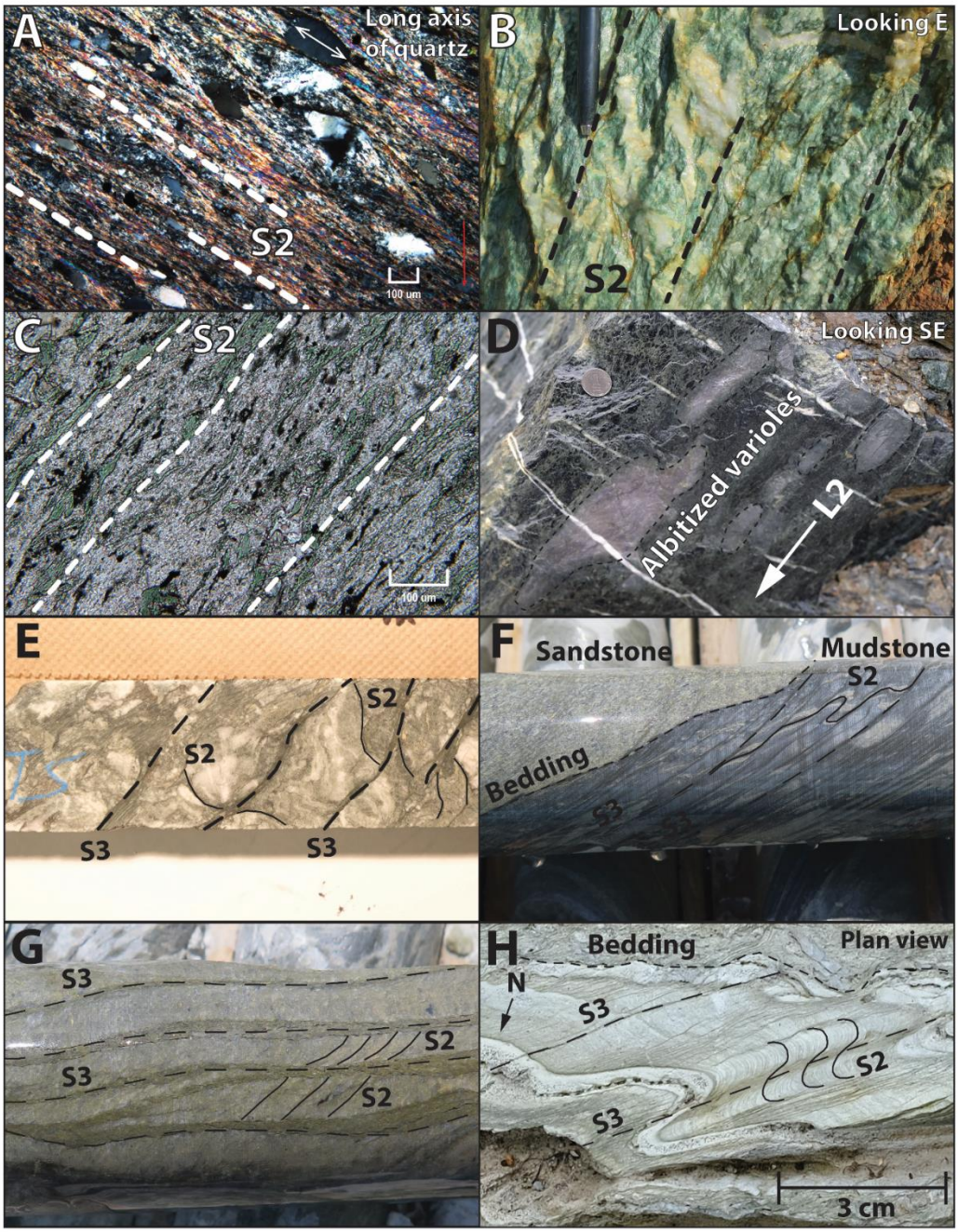


**Figure 8**. Photographs of structural fabrics: (**A**) Thin section photomicrograph (cross-polarized light) of a pervasive $S_2$ foliation defined by sericite and the long axis of quartz grains in Timiskaming turbidites. (**B**) $S_2$ foliation defined by fuchsite and ankerite in Larder Lake ultramafic volcanic rock**.** Pen for scale. Co-ordinates: 605923N/5332881E (NAD83, Zone 17N). (**C**) Thin section photomicrograph (cross-polarized light) of chloritic $S_2$ foliation in Larder Lake group mafic volcanic rock. (**D**) Pink albitized varioles stretched parallel to the moderately northeast-plunging $L_2$ lineation in Larder Lake group mafic volcanic rock. Coin for scale. Co-ordinates: 606362N/5333142E (NAD83, Zone 17N). (**E**) Spaced $S_3$ foliation defined by talc, crosscutting and crenulating the $S_2$ foliation, in altered ultramafic volcanic rock of the Larder Lake group. Drill hole KAD17-041, hole diameter 47.6 mm. (**F**) Spaced sericitic S3 foliation defined by sericite and a

grain preferred orientation of carbonate and quartz in Timiskaming finely laminated mudstone. Drill hole GG-11-04, hole diameter 63.5 mm. (**G**) Spaced sericitic, penetrative, $S_3$ foliation in Timiskaming sandstone proximal to the CLLF and contact with the Larder Lake ultramafic volcanic rocks. Drill hole GG-11-04, hole diameter 63.5 mm. (**H**) Pervasive sericitic $S_2$ foliation in Timiskaming turbidites overprinted by cm-scale Z-shaped $F_3$ fold. $S_2$ and $S_3$ foliations are clockwise and anticlockwise to bedding, respectively, consistent with regional structural observations. Co-ordinates: 599816N/5330490E (NAD83, Zone 17N).

Hydrothermally altered ultramafic rocks are characterized by three distinct alteration facies: talc-chlorite, carbonate-chlorite, to fuchsite-quartz-carbonate-magnesite. These will be further described in the following section. Boundaries between alteration facies are typically gradational. However, locally a series of discrete shear zones mark the boundary between rocks with different alteration facies (Figure 9a). These shear zones generally strike east-northeast to west-southwest with subvertical dips. The shear zones are overprinted by the $S_3$ foliation (Figure 9b) and contain boudinaged, and transposed dark grey quartz veins. Due to the orientation and crosscutting relationship of the $S_3$ foliation, the formation of these shear zones likely formed during $D_2$. Their spatial correlation with alteration facies boundaries could be due to the competency differences. For example, boudin-shaped, inner cores of competent fuchsite-quartz-carbonate-magnesite ultramafic rocks are commonly bordered by discrete, discontinuous, talc-chlorite shear zones (represented as “Barren Talc Rock” in Figure 10).

On the Kerr-Addison mine site, ultramafic volcanic rocks to the northwest are separated from mafic volcanic rocks to the southeast by the NE-trending brittle kerr fault. The kerr fault has been mapped by Thomson (1941) as a steeply north dipping graphitic fault zone and later by Hamilton (1986) as a splay fault off the CLLF as it merges with the CLLF at depth. Later studies reported that the fault was post-mineralization and did not represent the feeder structure to the deposit (Smith et al., 1993; Gold Candle Ltd., internal communications). Brittle-ductile fault zones occur parallel to the kerr fault and appear to be crosscut and offset by it, suggesting that these are an

earlier fault set. These faults are steeply south-dipping to vertical and strike east northeast to northeast. They are characterized by silicified fault breccias with disseminated pyrite and arsenopyrite. The breccias are either within or adjacent to $D_2$ high strain/shear zones. Clasts within the fault breccias are randomly foliated, suggesting that the faults are post-$D_2$ (Figure 9c). The fault breccia matrix is composed of milled wall rock, graphite, albite, quartz, carbonate and is moderately to strongly foliated with the foliation defined by graphite seams and preferred dimensional orientation of quartz and carbonate grains. The sense of movement along these faults is dextral oblique, based on the asymmetry of strain shadows around coarse-grained pyrite and on the rotation of the $S_2$ foliation and bedding in sedimentary units along the margins of the faults. En echelon tensional quartz-carbonate veins are present along some of the fault zones (Figure 9d). The brittle-ductile fault zones typically occur along lithological contacts between ultramafic and mafic volcanic rocks and as they do not have offset markers, the magnitude of the displacements along the faults is not known. At one location, one fault juxtaposes a thin sliver of folded ultramafic rock against a massive mafic volcanic rock, indicating that many of the contacts between the mafic and ultramafic volcanic rocks are not primary. In drill core and cross-section, the faulted contact between the north panel of ultramafic volcanic rocks and the south panel of mafic stratigraphy is marked by a series of these brittle-ductile faults and by the intercalation of both ultramafic and mafic units. This inter-fingering may represent a structurally complex zone in which imbrication of different units has occurred.

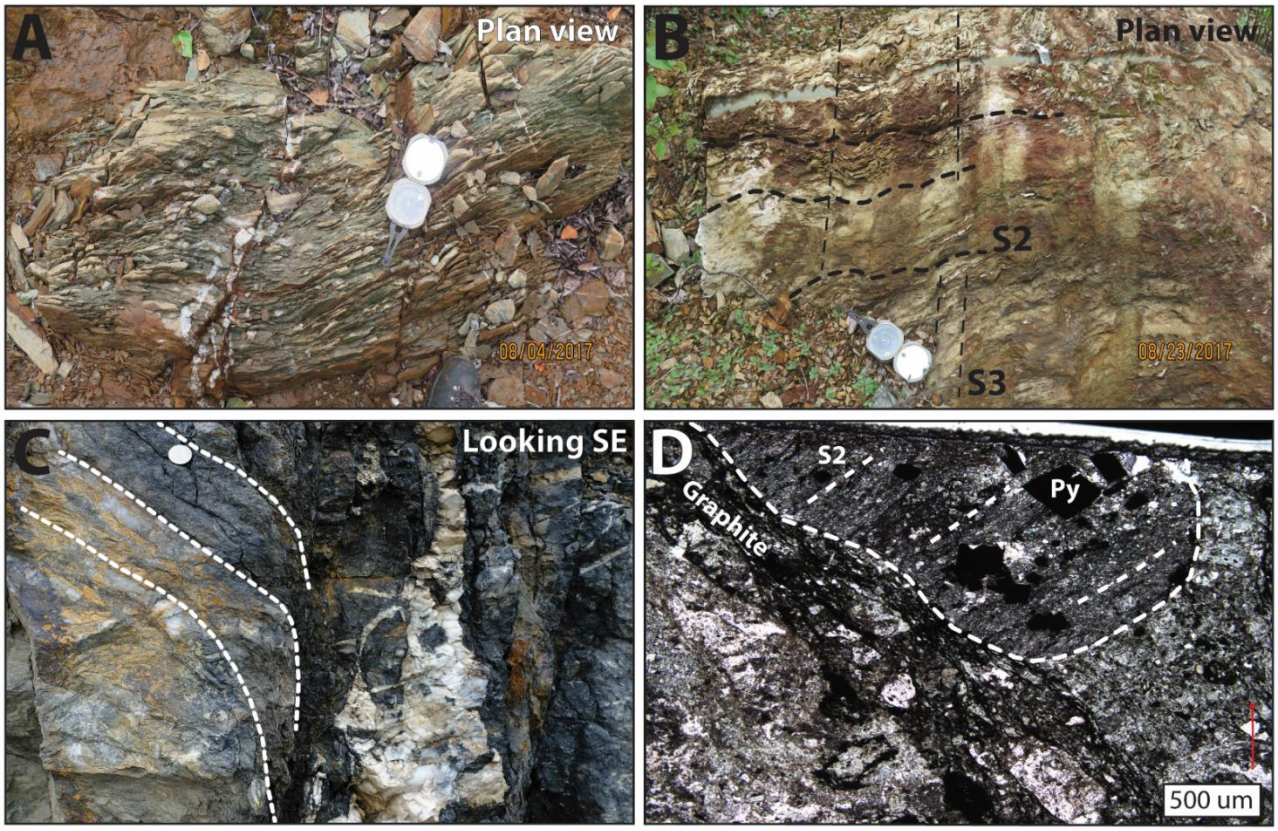


**Figure 9**. Representative photographs of structural features at the Kerr-Addison mine site. (**A**) Discrete, strongly foliated, shear zone separating ankerite-magnesite-fuchsite-quartz-altered ultramafic from ankerite-magnesite-clinochlore-quartz altered ultramafic rocks. Compass for scale and indicating north. Co-ordinates: 605358N/5332461E (NAD83, Zone 17N). (**B**) Fuchsite-altered ultramafic volcanic rock overprinted by a penetrative $S_2$ foliation defined dominantly by fuchsite. The $S_2$ foliation has been crenulated and rotated to a NW-striking orientation, with a moderate dip, by the steeply dipping $S_3$ foliation. The $S_3$ foliation is also defined by fuchsite and is axial planar to the crenulated $S_2$ foliation. Compass for scale and indicating north. Co-ordinates: 605829N/5332817E (NAD83, Zone 17N). (**C**) Brittle-ductile fault separating ultramafic volcanic rocks from mafic volcanic rocks. The fault is characterized by cataclasite filled with graphite, quartz, calcite and pyrite. The rotation of the foliation adjacent to these faults indicates dextral oblique movement. Co-ordinates: 604783N/5331978E (NAD83, Zone 17N). (**D**) Crossed polar thin section photomicrograph of a brittle-ductile fault containing angular clast with a penetrative $S_2$ foliation and euhedral pyrite grains. Pyrite crystals have asymmetrical pressure shadow. The clast is surrounded by a milled fault matrix overprinted by a foliation defined by graphite seams. Sample MEBL17NFS0717.

## 2.3.3 Alteration, veins and gold mineralization

The Kerr-Addison deposit has a wide alteration footprint. The alteration is pervasive and alteration mineral facies vary with rock type and with increasing proximity to the mineralized zones. From

distal to proximal, alteration mineral facies change from talc-chlorite, carbonate-chlorite, to fuchsite-quartz-carbonate-magnesite in ultramafic rocks and from chlorite- albite ± quartz ± ankerite ± sphene to ankerite-sericite-albite ± quartz ± leucoxene in mafic volcanic rocks (Kishida & Kerrich, 1987). A core zone of strong to moderate fuchsite-quartz-ankerite-magnesite alteration, up to 200 m thick, encloses the main ore body and thins out laterally to the northeast and southwest as well as down dip, into wedge-like lenses. At the margins of the inner alteration zone, the fuchsite-quartz-ankerite-magnesite alteration facies interfingers with more distal alteration facies of talc-chlorite and dolomite. The transition between alteration facies is often marked by a discrete zone of high strain or shearing (1-2 m thick) expressed as a fissile to schistose texture defined by micas, which overprints the ultramafic volcanic units. East and west of the Kerr-Addison deposit, along the surface projection of the CLLF, pervasive carbonate alteration is observed in all rock types, including sedimentary rocks of the Timiskaming assemblage, and is most intense within 100 m of the CLLF. The “flow ore” and “green carbonate ore” differ in alteration facies, protolith composition, and the style of mineralization. Within the “flow ore”, gold is typically present as inclusions within disseminated pyrite replacing mafic volcanic rocks, whereas within “green carbonate ore” coarse native gold occurs within quartz-carbonate veins cutting across the ultramafic volcanic rocks. Both styles of mineralization contributed to the mineable ore reserves at Kerr-Addison (Figure 10).

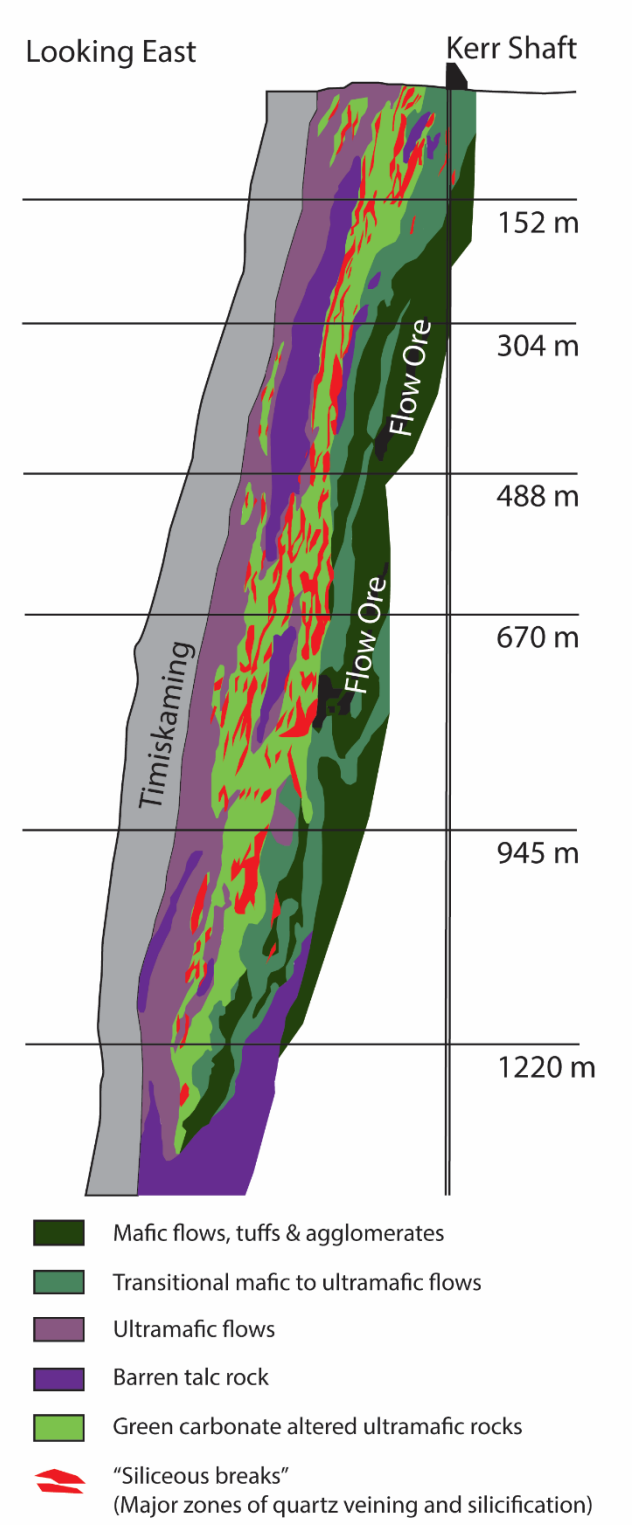


**Figure 10**. Idealized cross-section of the Kerr-Addison deposit compiled from maps of underground workings, showing the distribution of ultramafic rocks altered to talc and fuchsite, other mafic and ultramafic rocks, and major zones of quartz veining and silicification. Modified after Smith et al. 1993.

Three generations of quartz-carbonate veins ($V_1$, $V_2$, and $V_3$) are observed at the Kerr-Addison mine site. $V_1$ veins are present in Timiskaming sandstone only, whereas $V_2$ and $V_3$ veins occur in all rock types and are most abundant in fuchsite-altered ultramafic volcanic rocks, which host the "green carbonate" mineralization as described by Kishida and Kerrich (1987) and Smith et al. (1993). Early $V_1$ veins are typically narrow (<1 cm), white to grey in color, and composed of quartz-carbonate-sericite ± pyrite. They are generally parallel to bedding and locally crenulated parallel to the $S_2$ cleavage (Figure 11a). $V_2$ veins vary in thickness from 1 to 5 cm. They are translucent, dark to light grey, locally laminated and boudinaged, and composed mainly of quartz and carbonate (Figure 11b) with minor albite and trace pyrite, arsenopyrite, tennantite, and gold. $V_2$ veins are commonly found within $D_2$ high strain zones where they are boudinaged and transposed parallel to the $S_2$ foliation (Figure 11c), suggesting that they were emplaced either before or during the $D_2$ event (Figure 11d).

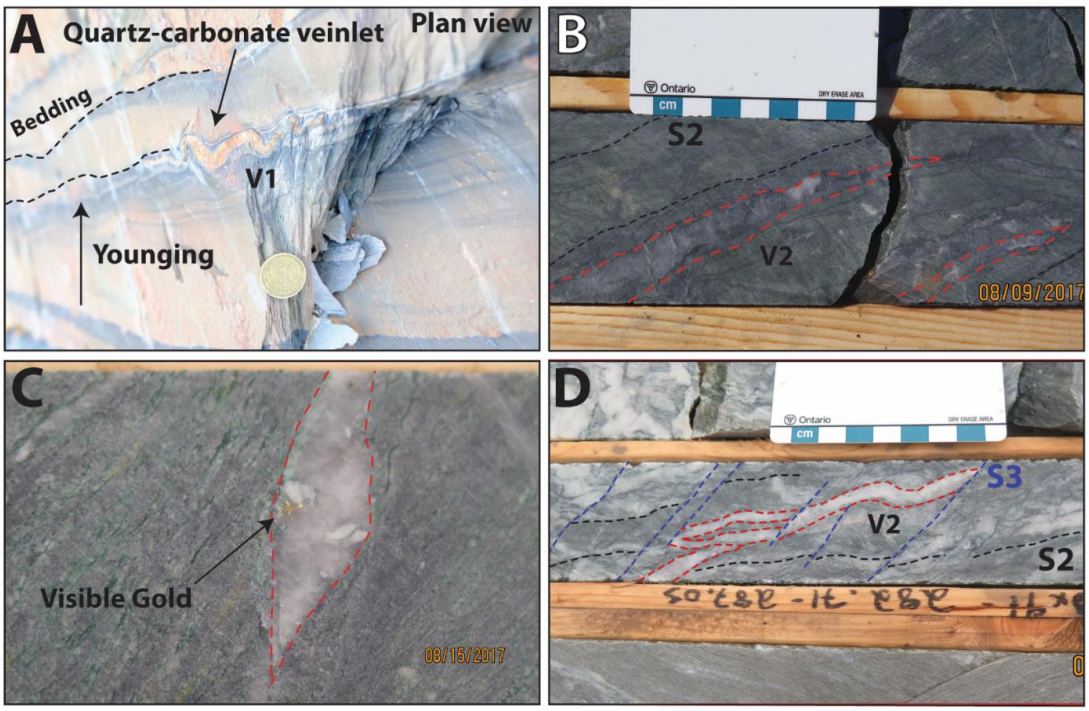


**Figure 11**. Photographs of vein sets (**A**) Bedding parallel quartz-carbonate veinlet ($V_1$). Coin is 20 mm across for scale. Co-ordinates: 606120N/5333218E (NAD83, Zone 17N). (**B**) Dark grey, translucent quartz-

carbonate veins ($V_2$) parallel to the $S_2$ foliation and boudinaged. Drill hole KAD17-039, hole diameter 63.5 mm. (**C**) $V_2$ vein parallel to $S_2$ foliation containing visible gold. Drill hole KAD17-039, hole diameter 47.6 mm. (**D**) Light grey to white quartz-carbonate vein ($V_2$) parallel to the crenulated S2 foliation. $V_2$ veins are locally folded, sheared and transposed. Both $S_2$ and $V_2$ are crenulated and crosscut by the $S_3$ spaced foliation. Drill hole KAD17-039, hole diameter 47.6 mm.

$V_3$ veins are the most common vein set. They vary in thickness from 5 - 50 cm, and are typically over 1 m in length. They are milky white and consist of quartz-carbonate ± chlorite ± albite ± pyrite ± arsenopyrite ± tennantite ± gold. In ultramafic host rocks, the veins locally contain angular clasts of fuchsitic brecciated wall rock (Figures 12a, b). Their walls are lined by euhedral, dog tooth, carbonate crystals and their centres are filled with coarse-grained quartz (Figure 12c). In Timiskaming rocks, the veins occur as en echelon, lensoid arrays which cut across bedding, the $S_2$ cleavage, and $V_2$ veins (Figure 12d). They locally contain angular wallrock fragments (Figure 12e) with 1 - 2 cm thick, chloritic and pyritic alteration halos. In mafic volcanic rocks, the veins are surrounded by 1-5 cm thick, albitic and pyritic, alteration haloes (Figure 12f). Smith et al. (1993) reported that the $V_3$ “milky white quartz veins” host most of the gold in the green carbonate zones as coarse native gold either as inclusions within quartz or carbonate crystals or along their grain boundaries (Figure 12h).

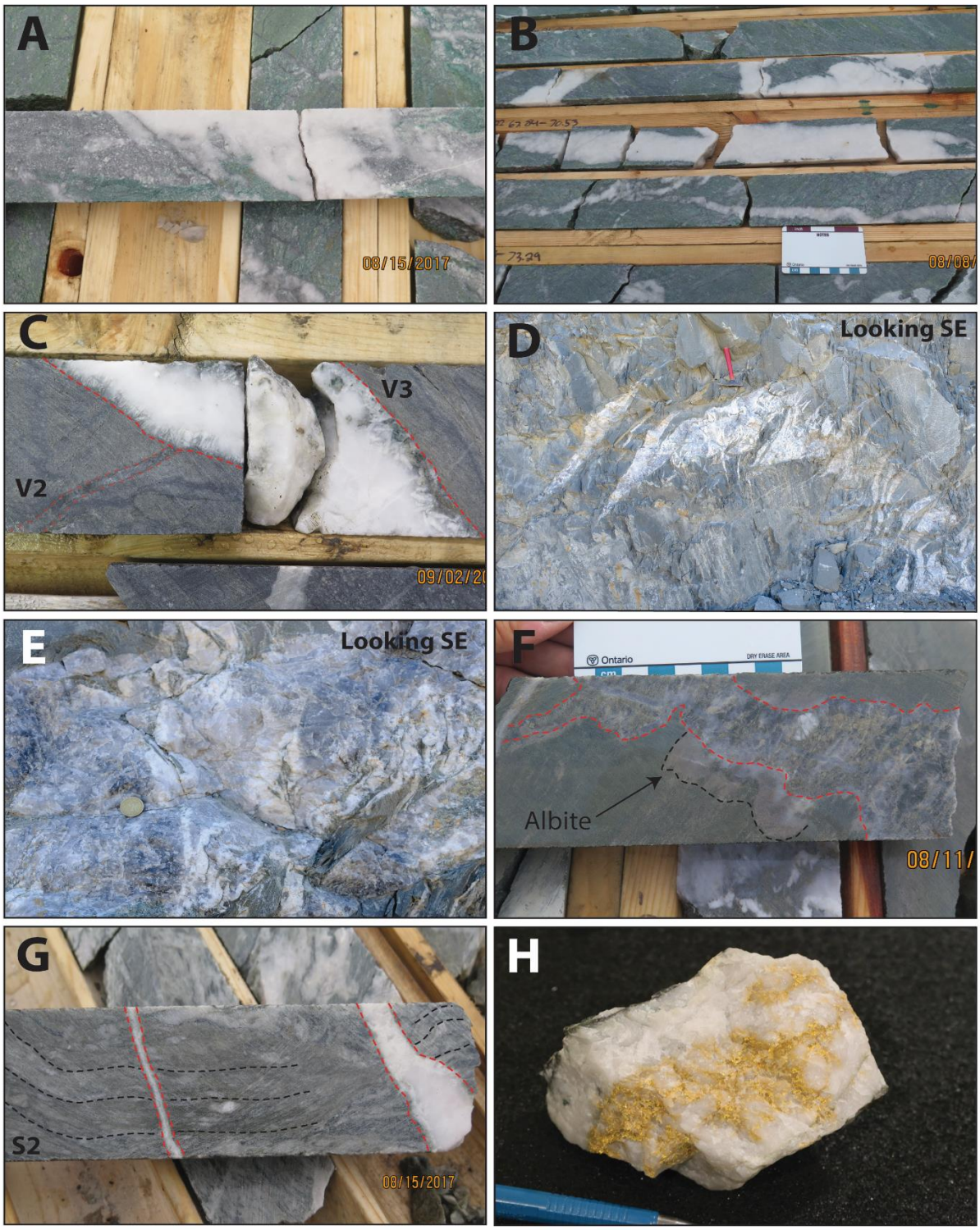


**Figure 12**. Photographs of $V_3$ veins (**A**) Milky white, opaque quartz-carbonate vein ($V_3$) crosscutting fuchsite-altered ultramafic volcanic pseudo-breccia texture. Angular wall rock clasts of previously altered ultramafic units are brecciated during vein emplacement. Drill hole KAD17-043, hole diameter 63.5 mm. (**B**) Milky white, opaque quartz-carbonate veins ($V_3$) crosscutting ultramafic volcanic unit. Drill hole KAD17-037, hole diameter 63.5 mm. (**C**) Milky white, opaque quartz-carbonate vein ($V_3$), with dogtooth

carbonate growth on vein walls, crosscutting dark grey translucent quartz vein ($V_2$). Drill hole KAD17-043, hole diameter 63.5 mm. (**D**) White, opaque quartz-carbonate-chlorite veins ($V_3$) crosscutting the Timiskaming sedimentary rocks. Veins are lensoidal and en echelon. Hammer for scale. Co-ordinates: 606090N/5333208E (NAD83, Zone 17N). (**E**) Close up of 12A showing milky white vein infill surrounding chloritized, angular wall rock clasts. Coin is 20 mm for scale. (**F**) Dark grey, translucent quartz-carbonate-chlorite vein ($V_3$) crosscutting a mafic volcanic unit of the Larder Lake group. A thin alteration selvage of albite surrounds the vein. Drill hole KAD17-041, hole diameter 63.5 mm. (**G**) Milky white, opaque quartz-carbonate veins ($V_3$) crosscutting the crenulated $S_2$ foliation as well as boudinaged $V_2$ veins parallel to the $S_2$ foliation. Drill hole KAD17-043, hole diameter 47.6 mm. (**H**) $V_3$ vein containing visible gold. ROM sample, pen for scale.

$V_3$ veins can be subdivided into three orientation groups: NE-SW striking (210° - 260°) subvertical $V_{3a}$ veins, E-W striking (75° - 110°) subvertical $V_{3b}$ veins, and NW-SE striking (280° - 330°) moderately dipping $V_{3c}$ veins (Figure 13a). $V_{3b}$ and $V_{3c}$ veins are interpreted as conjugate veins. (Figure 13b). The two vein sets are mutually crosscutting and locally form en echelon arrays (Figure 13d). Dextral shearing and rotation of the $S_2$ foliation is observed along the margins of the $V_{3b}$ veins crosscutting the Timiskaming sedimentary units (Figure 13c). The dextral dragging of the $S_2$ foliation along the $V_{3b}$ veins suggests that either the veins were emplaced during the $D_3$ dextral shearing event or, alternatively, they were emplaced late during the $D_2$ deformation event as the vein margins may have acted as weak planar anisotropies that localized later $D_3$ dextral shearing. Most $V_3$ veins also crosscut the $S_2$ foliation (Figure 12g) and are parallel to the $S_3$ foliation and locally, where $V_3$ veins are oriented oblique to the $S_3$ foliation, they are offset or crosscut by $S_3$. This suggest that the $V_3$ veins either pre-date or are syn- $S_3$ foliation.

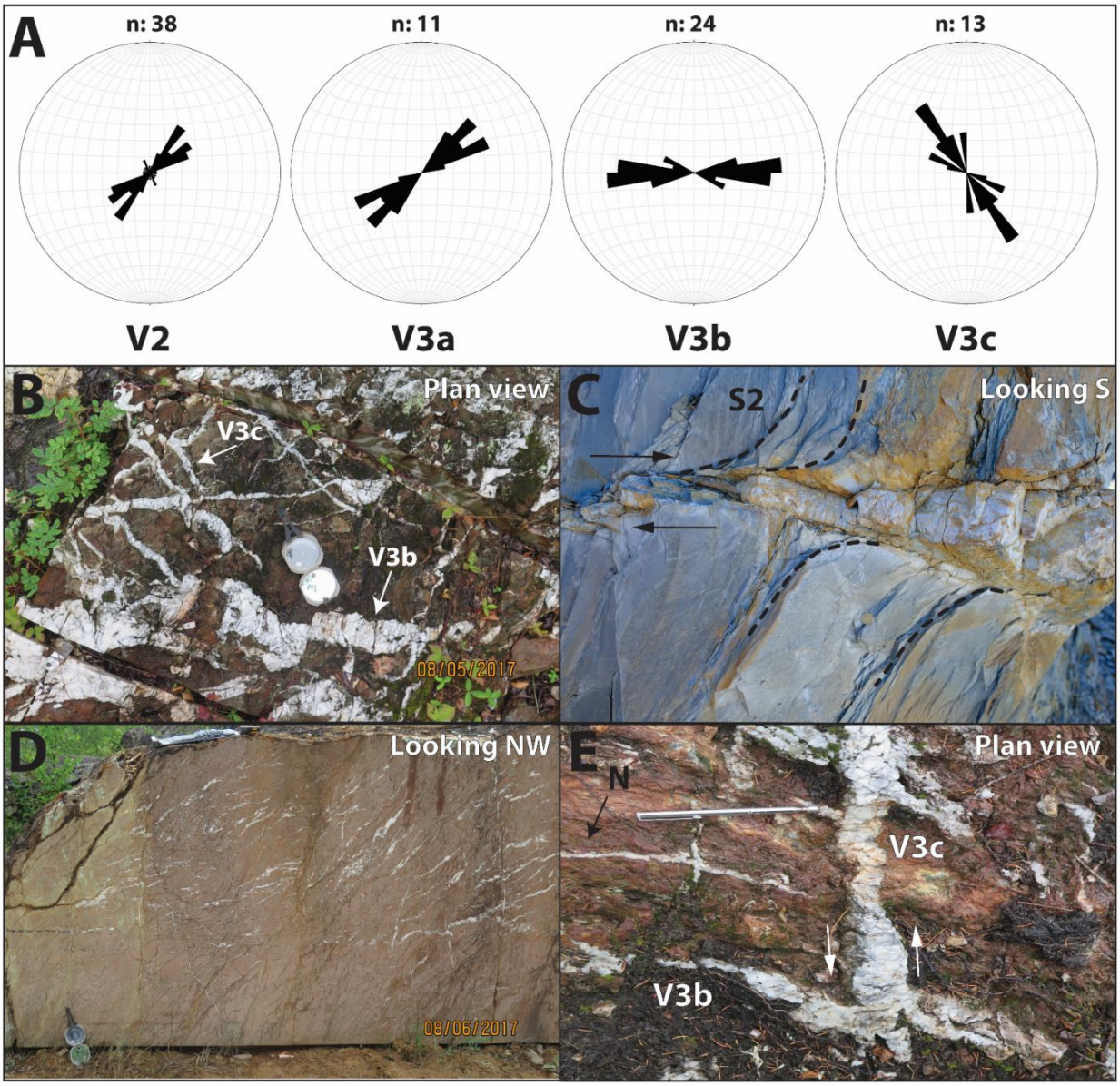


**Figure 13**. Stereonets and representative photos of $V_2$ and $V_3$ vein sets (**A**) Rose diagrams of vein measurements for $V_2$ and $V_3$ vein sets. Measurements were taken from both the Kerr-Addison site and surrounding area. (**B**) Milky white, opaque quartz-carbonate veins crosscutting an ultramafic volcanic unit on the Kerr-Addison site. $V_{3c}$ (NW-striking) and $V_{3b}$ (E-W striking) are conjugate to each other. Compass for scale and indicating north. Co-ordinates: 605370N/5332450E (NAD83, Zone 17N). (**C**) Milky white, opaque $V_{3b}$ quartz-carbonate vein crosscutting $S_2$ and $V_2$ with dextral shearing of $S_2$ along vein margins. $V_{3b}$ veins are lensoidal in outcrop. Coin is 20 mm for scale. Co-ordinates: 605981N/5333234E (NAD83, Zone 17N). (**D**) En echelon, milky white, opaque quartz-carbonate veins ($V_{3a}$) crosscutting a fuchsite-altered ultramafic volcanic unit. Compass for scale. Co-ordinates: 605650N/5332725E (NAD83, Zone 17N). (**E**) Milky white $V_{3b}$ and $V_{3c}$ conjugate vein set showing minor sinistral vein offset of the $V_{3b}$ vein by $V_{3c}$. Magnet for scale. Co-ordinates: 605358N/5332461E (NAD83, Zone 17N).

In summary, gold mineralization at the Kerr-Addison deposit is hosted within both $V_2$ and $V_3$

veins. Gold is also present in association with fuchsite, carbonate, quartz and albite in strongly altered ultramafic rocks (Figure 14a, b, c).

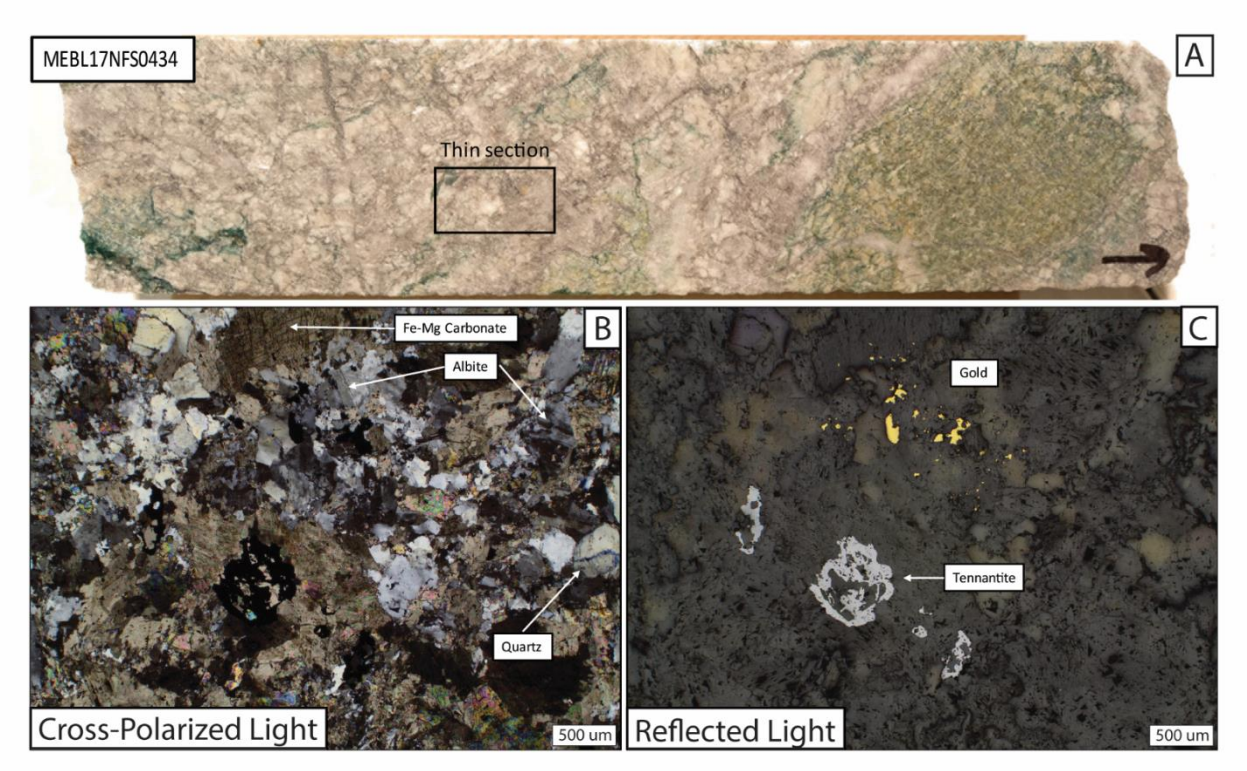


**Figure 14**. Thin section with visible gold in ultramafic breccia matrix. (**A**) Fuchsite altered ultramafic unit showing location of thin section. (**B**) Photomicrograph of ultramafic groundmass composed of medium- to coarse-grained quartz-carbonate-albite. (**C**) Photomicrograph of visible gold and porous tennantite crystal along grain boundaries and as inclusions within quartz, albite and carbonate crystals.

## 2.4 Contact relationships

The CLLF is defined as the contact between the Timiskaming assemblage and the Larder Lake group (Thomson, 1941). This contact was traced and mapped where it crops out at surface to determine structural and stratigraphic relationships between the two rock units. Five excellent exposures of the contact were found and were mapped in detail. Their location is shown and numbered sequentially from east to west in Figure 2.

### 2.4.1 Kearns

The contact is observed north of Highway 66 in the town of Kearns (Location 1 on Figure 2), where fine- to medium-grained sandstone and mudstone of the Timiskaming assemblage are exposed north of ultramafic to mafic volcanic rocks of the Larder Lake group (Figure 15a). The contact is overprinted by a 30-50 cm wide mylonite zone (Figure 15b). The sedimentary rocks are altered to sericite ± carbonate near the contact and the 20 – 40 m thick ultramafic volcanic rocks are pervasively carbonatized and altered to talc and chlorite.

North of the contact, the sedimentary rocks are folded into a large-scale $F_2$ anticline with an axial planar, east-northeast trending $S_2$ cleavage (Figure 15c). The fold becomes tighter to the east and the sedimentary rocks and volcanic rocks adjacent to the contact are repeated either through folding and transposition parallel to the highly strained mylonitic contact, i.e. the CLLF, or by fault imbrication and interleaving. If the former, this suggests that the Timiskaming rocks and Larder Lake volcanic rocks were in contact prior to the $D_2$ deformation event. If the latter, these rocks were either in contact prior to the $D_2$ deformation or were juxtaposed during this event.

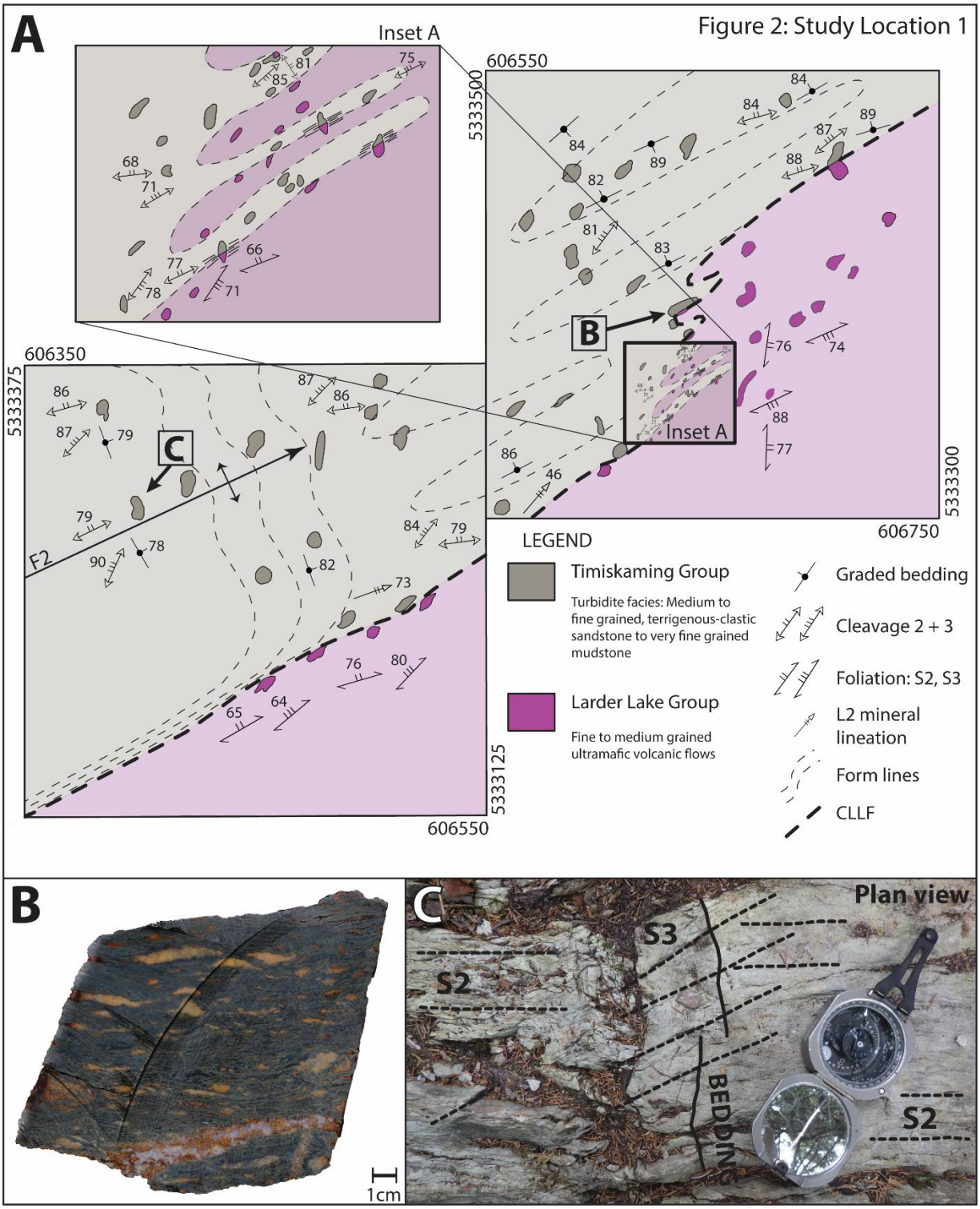


**Figure 15**. Timiskaming-Larder Lake contact in the Kearns area (**A**) Detailed lithologic and structural map of area north of the town of Kearns. The Timiskaming assemblage marine turbidites are open to tightly folded by $F_2$ folds with an axial plane striking east-northeast and axial hinges plunging steeply to the northeast. The CLLF is a high strain zone that is tightly folded by $F_2$ folds as illustrated in Inset A. (**B**) Mylonite located at the contact between the ultramafic volcanic and sedimentary rocks. A strong pervasive

fabric is observed with parallel boudinaged quartz-carbonate veins. (**C**) Timiskaming assemblage sandstone to siltstone showing the relationship between the cleavages and bedding. The $S_2$ cleavage is axial planar or perpendicular to open folded bedding with the $S_3$ foliation crosscutting both.

## 2.4.2 Virginiatown

The contact relationship between Timiskaming sedimentary rocks and ultramafic volcanic rocks of the Larder Lake group is exposed on an outcrop in the yard of an elementary school in Virginiatown, Ontario, approximately 13 km east of Larder Lake on old HWY 66 (Location 2; Figure 2). Rocks of the Timiskaming assemblage consist of matrix-supported pebble conglomerate, sandstone and finely laminated mudstone with local normal graded bedding (Figure 16). The Larder Lake ultramafic rock is altered to an assemblage of iron- and magnesium-carbonate - quartz ± talc ± chlorite and lacks any primary textures. The contact between the two rock types is sharp with mudstone beds that are subparallel and truncated along the contact. Normal graded beds young to the SE, into the ultramafic. The contact has been folded by tight, isoclinal $F_2$ folds with an axial planar, east-northeast striking, $S_2$ foliation. Both units have been overprinted by a pervasive $S_2$ foliation and a weak spaced $S_3$ foliation, expressed as a sericitic foliation or fracture cleavage in the sedimentary rocks and a talc-chlorite foliation in the ultramafic units. The $S_2$ foliation is axial planar to the folds whereas the $S_3$ foliation is consistently oriented anticlockwise with respect to bedding which is consistent with regional mapping relationships. The $F_2$ folds are overprinted by open $F_3$ folds with a northeast striking axial planar $S_3$ fracture cleavage (Figure 16a). Extensional quartz-carbonate veins ($V_2$) crosscut the Timiskaming sedimentary rocks and end abruptly at the contact with the ultramafic rocks (Figure 16b). This abrupt termination of the veins suggest that the contact acted as a rheological boundary that stopped the propagation of the vein-hosting fractures. These veins are interpreted as pre- to syn-

$D_2$ structures because they follow the contour of the $F_2$ folded contact and have locally been dextrally offset along the $S_3$ cleavage.

Similar to the Kearns area, the folded contact and fabric relationships in Virginiatown suggests that the rocks of the Timiskaming assemblage and Larder Lake group were in contact either pre-$D_2$ deformation or were juxtaposed during the $D_2$ deformation.

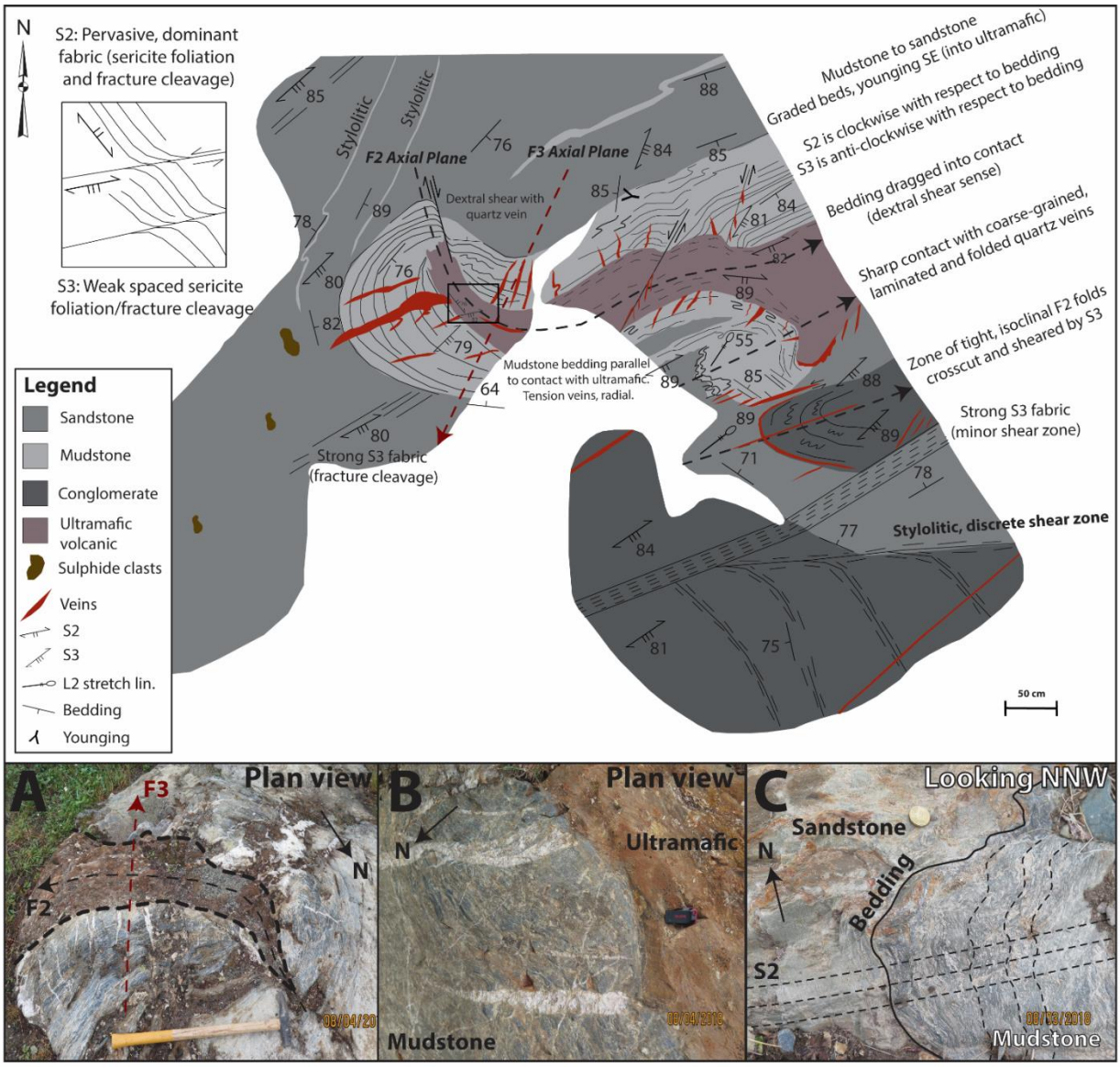


**Figure 16**. Timiskaming-Larder Lake contact in Virginiatown. The map shows an ultramafic volcanic unit in sharp contact with a Timiskaming age sandstone to mudstone. The contact between the two units has been folded by $F_2$ and $F_3$ folds with quartz-carbonate veins perpendicular to the contact. Co-ordinates:

604921N/5332138E (NAD83, zone 17N). (**A**) Photograph of the strongly carbonatized, dark brown ultramafic volcanic unit in contact with a grey mudstone. The two fold axial planes are indicated by dashed lines with arrows showing the plunge direction of the axial hinges. Hammer for scale. (**B**) Close up photograph of the contact between the ultramafic and sedimentary units. The contact is sharp and locally undulating with quartz-carbonate tension veins crosscutting the Timiskaming sedimentary rocks and terminating on the contact. SANDISK USB stick for scale. (**C**) Photograph of the folded sedimentary unit. Bedding has been folded and crenulated by $F_2$ folds with an axial planar $S_2$ fracture cleavage. Coin is 20 mm for scale.

## 2.4.3 Highway 66 Bypass Road Cut

Immediately west of location 2, the contact between the Timiskaming assemblage and the Larder Lake group is exposed along a new road cut. The contact strikes east-northeast, dips steeply to the north, and is represented by a 2 to 4-meter thick transition zone (Figure 17a, 17b). The term transition zone is used to describe an interval of mixed lithology consisting of ultramafic clasts and lenses within a siliciclastic matrix, commonly developed at the contact between the Larder Lake group and the Timiskaming assemblage. The ultramafic lenses or layers are altered to chlorite-fuchsite-carbonate ± talc (Figure 17c, 17d, 17e, 17f) and are oriented parallel to the $S_2$ foliation while the Timiskaming sandstone/siltstone is altered to sericite-carbonate. The $S_2$ foliation is defined by Fe-Mg chlorite in the ultramafic layers and sericite in sandstone. SEM mineral chemical analyses of the carbonate mineral in the ultramafic lenses yielded an average Mg# of 0.76 (0.66 to 0.85 from 6 analyses), which is consistent with alteration of ultramafic rocks. The matrix of the transition zone is interpreted to be sandstone as it consists of large, rounded quartz grains surrounded by sericite ± albite ± carbonate.

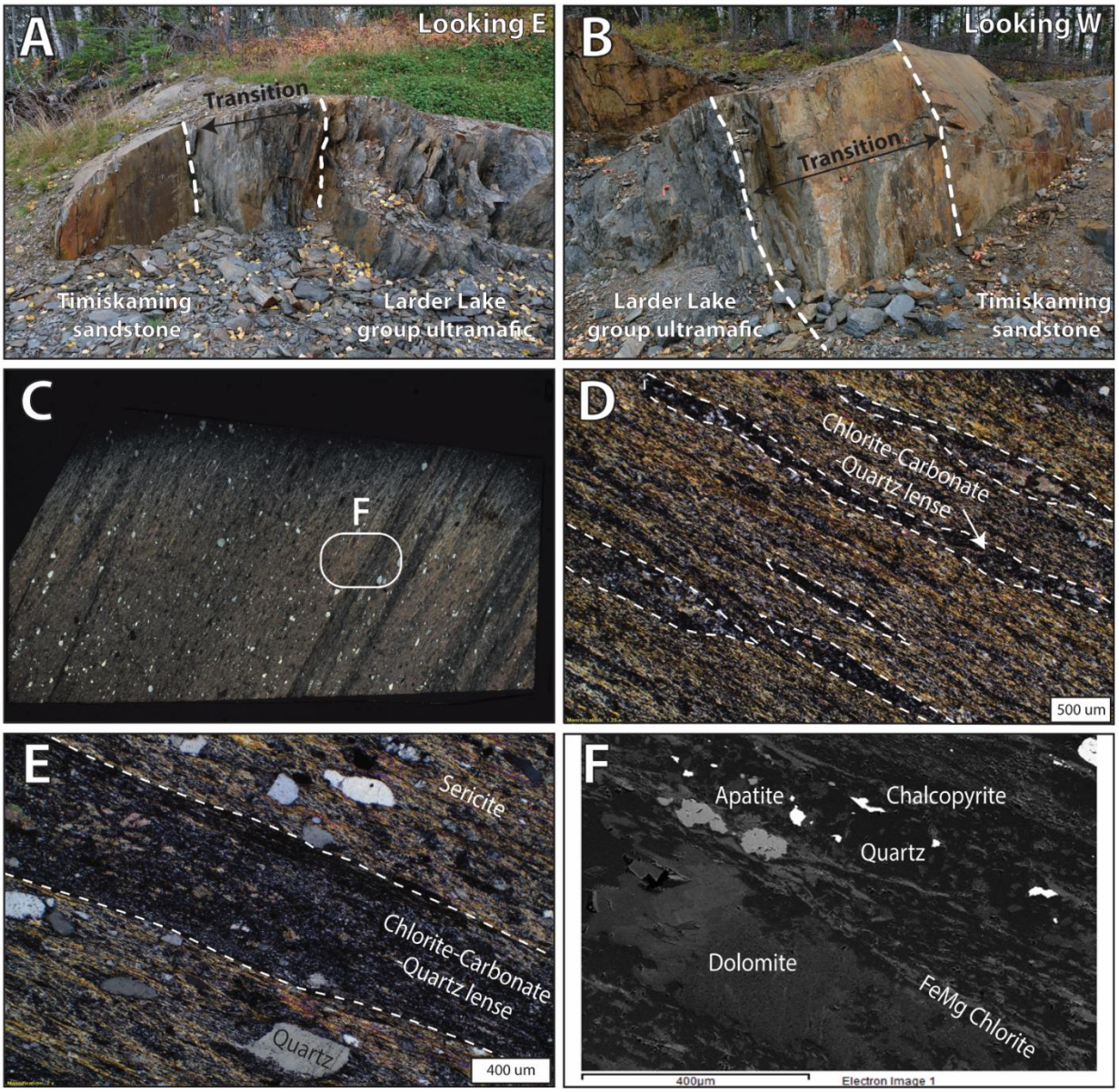


**Figure 17**. Timiskaming-Larder Lake contact north of Hwy #66 and the town of Virginiatown (**A**) East side of the highway bypass outcrop, outside of Virginiatown, of the CLLF defined by a 2 m transition zone between Timiskaming sandstone and Larder Lake ultramafic rocks. Co-ordinates: 604824N/5332038E (NAD83, zone 17N). (**B**) West side of the highway bypass outcrop showing the same transition zone. Co-ordinates: 604791N/5332025E (NAD83, zone 17N). (**C**) Crossed polar thin section scan of sample MEBL17NFS0451 within the transition zone taken from diamond drill hole KAD17-041. Thin section scan shows strongly flattened dark green lenses within siltstone/sandstone. White rectangle indicates location of SEM image illustrated in (**F**). (**D**) Thin section photomicrograph (cross-polarized light) from sample MEBL17NFS0451. Dark grey-green lenses of chlorite-carbonate-quartz material are contained within a very fine-grained sericitic matrix of a Timiskaming siltstone/sandstone. (**E**) Crossed polar thin section photomicrograph from sample MEBL17NFS0451. Close up of a chlorite-carbonate-quartz lens surrounded by a strongly sericitized matrix containing flattened quartz grains. Note the flattening of the lenses is parallel

to the long axis of quartz grains and the dominant $S_2$ fabric. (**F**) Scanning Electron Microprobe image of a chlorite-carbonate-quartz lens.

In both outcrop and drill core, the ultramafic lenses / clasts decrease in abundance away from the contact between the Larder Lake group and Timiskaming rocks, similar to the field observations made at the Cheminis mine site, which will be discussed in more detail below.

### 2.4.4 Kerr-Addison site

Renewed exploration at the Kerr-Addison mine site provided new drill core across the CLLF (Location 3; Figure 2). At Kerr-Addison, the package of Larder Lake volcanic rocks is over 600 m wide, thicker here than elsewhere along the CLLF. It consists of a 100-150 m thick panel of north-dipping massive komatiitic ultramafic rocks with locally preserved spinifex textures in contact with mafic volcanic rocks to the south. This contact is marked by the late, north-dipping, brittle and carbonaceous kerr fault at the western end of the deposit and is relatively undeformed or cut by small-scale fractures at the eastern end of the deposit. South-dipping variolitic, pillowed and autobrecciated mafic volcanic flows with minor intercalated ultramafic volcanic rocks and interflow mafic sedimentary rocks occupy the footwall of the kerr fault (Figure 18). Similar to the contact relationship described at Kearns, Timiskaming sedimentary rocks to the north are in contact with volcanic rocks of the Larder Lake group to the south (Figure 18). This contact is highly strained and the primary relationship between the two rock units is not discernible. Due to the high level of strain observed at the Kerr-Addison site, the transition zone between the two rock units is characterized by a heterogeneous composition, in which primary textures have been completely obscured.

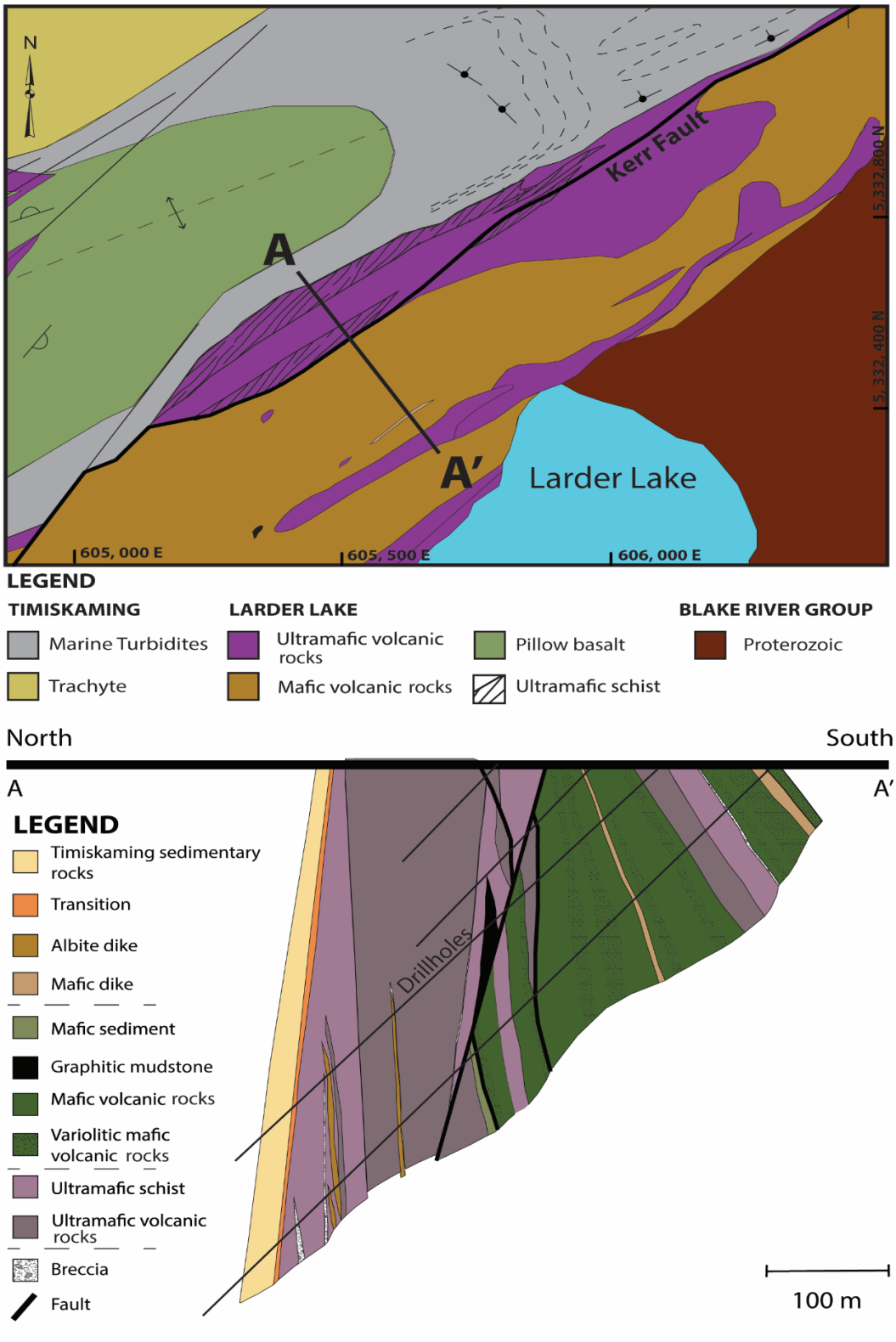


**Figure 18**. Geological map of the Kerr-Addison site, modified after Thomson, 1941. Cross-section A-A' is compiled from diamond drill core logs. The cross-section shows the northern panel of steeply dipping

ultramafic volcanic units in contact with the Timiskaming sedimentary rocks to the north which are separated from the mafic volcanic panel to the south by the steeply north dipping kerr fault and a series of south dipping brittle-ductile faults. Note the thin but consistent transition zone between the Larder Lake group ultramafic units and the Timiskaming sedimentary rocks.

### 2.4.5 Cheminis mine site

At the Cheminis mine site (Location 4; Figure 2), roughly 6 km east of Larder Lake, an interval of Larder Lake group volcanic rocks is bound on the north and south sides by Timiskaming sedimentary rocks. The contacts are well exposed at surface and are intersected by multiple drill holes.

The geology of the Cheminis mine site is similar to that of Kerr-Addison except that the interval of Larder Lake group rocks is only 50 m wide and is surrounded on both sides by Timiskaming sedimentary rocks (Figure 19a, 19b). The Larder Lake group consists of intercalated ultramafic and mafic volcanic rocks (Lafrance, 2015). The Timiskaming rocks to the north are interlayered turbidites and polymictic conglomerates, whereas to the south they are dominated by mudstones and turbidites with minor iron formation (Lafrance, 2015).

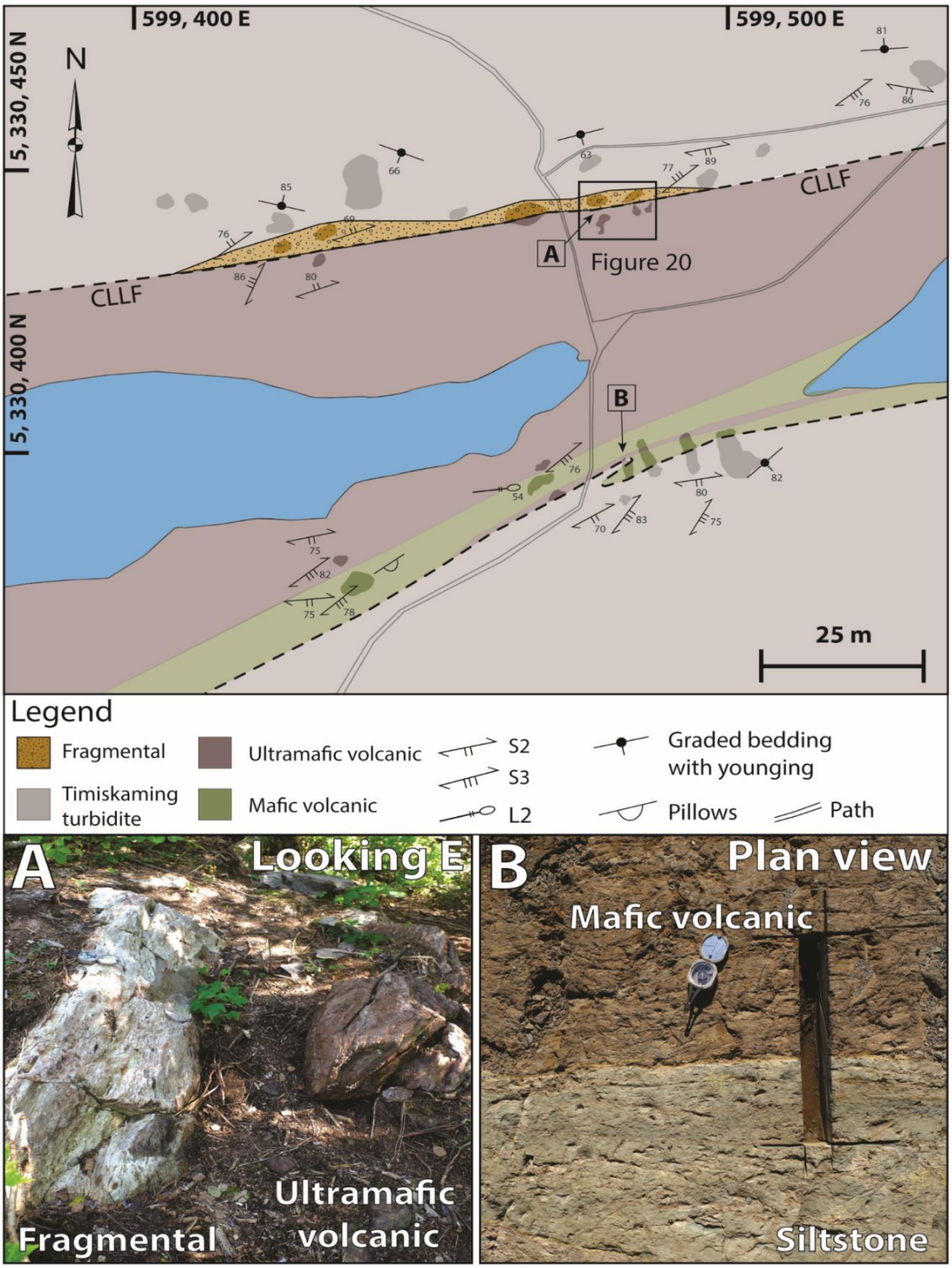


**Figure 19**. Timiskaming-Larder Lake contact at the Cheminis mine site. The site is characterized by a thin segment of Larder Lake group mafic and ultramafic volcanic units bordered to the north and south by Timiskaming assemblage marine turbidites. At the north contact, which defines the CLLF, a fragmental

unit, comprised of a sedimentary matrix and chloritic-carbonatized rounded clasts, separates the Timiskaming sedimentary rocks from the Larder Lake group volcanic rocks, referred to as the Transition Zone. (**A**) Northern contact between the Timiskaming assemblage and Larder Lake group. Co-ordinates: 599554N/5330416E (NAD83, Zone 17N). Compass indicating north. (**B**) Southern contact between the Timiskaming greywacke to siltstone and mafic volcanic rocks of the Larder Lake group. Note the low degree of strain and sharp nature of the contact. Co-ordinates: 599568N/5330332E (NAD83, Zone 17N). Compass indicating north.

The north contact between the Larder Lake volcanic and Timiskaming sedimentary rocks is a 1-2 m thick, transition zone that separates graded and north-younging mudstone and fine-grained sandstone to the north from dark brown, fine-grained and massive, strongly carbonatized, ultramafic rocks to the south (Figure 20a). This transition zone is characterized by rounded to subrounded, carbonatized and chloritic clasts / fragments within a sandy quartzo-feldspathic matrix (Figure 20b). The clasts are similar in appearance to the adjacent ultramafic volcanic rocks (Figure 20c). They are most abundant next to the ultramafic rocks and decrease in abundance across the transition zone forming a gradational contact with the Timiskaming sedimentary rocks. In drill core, normal grading to the north is observed in sandstone beds immediately above the transition zone facing away from the Larder Lake group. There are local reversals in facing direction further away from the transition zone suggesting that these rocks are tightly folded.

In thin section, the ultramafic rocks are composed of chlorite, Fe-Mg-carbonate, quartz with minor albite, talc and up to 5% disseminated pyrite. The clasts in the transition interval are similar in composition and are composed of ankerite, chlorite-quartz, albite, talc and minor pyrite (Figure 20d). The clast composition differs from the sandy matrix, which consists of fine-grained quartz, sericite, albite, ankerite and coarser (50 – 200 μm) rounded detrital quartz grains (Figure 20e). Both $S_2$ and $S_3$ cleavages overprint the volcanic fragments and the sandy matrix of the transitional horizon (Figure 20f, 20g), which is otherwise only weakly deformed as both fragments and detrital

quartz grains in the sandy matrix are equant to weakly elongate.

The north contact was also investigated in drill core. Drill Hole GF-12-125 was drilled from south to north and intersected the northern contact between metavolcanic rocks of the Larder Lake group and metasedimentary rocks of the Timiskaming assemblage to the north. Graded sandstone beds in the Timiskaming assemblage clearly face or young to the north, away from the Larder Lake group (Figure 21).

At surface, 15 m north of the contact, the younging direction in the Timiskaming turbidites is reversed to the south. Two scenarios are possible to explain these relationships: (1) the Timiskaming sedimentary units north of the Larder Lake group are tightly to isoclinally folded and this reversal of younging represents a tight synform, or (2) a fault, parallel to the CLLF, juxtaposed the north-younging Timiskaming turbidites against south-younging Timiskaming turbidites. Both scenarios are possible and explain how north-younging Timiskaming sandstone overlying the metavolcanic Larder Lake group reverse their younging direction 15 m north of the contact. A cross section depicting these structural and stratigraphic relationships is shown in Figure 22. The section was drawn using both surface and drill core orientation data and observations.

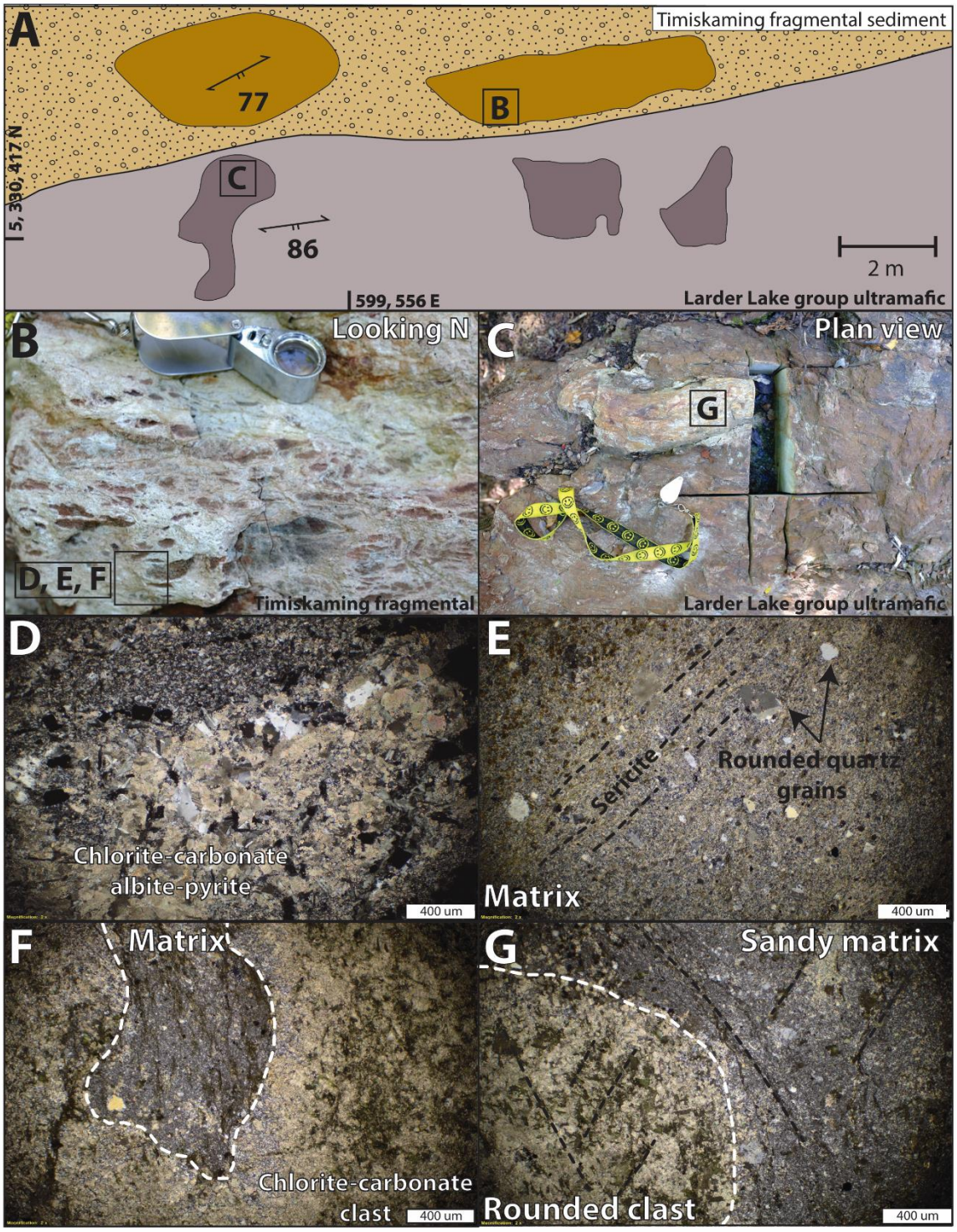


**Figure 20**. (**A**) Geologic map of the northern contact between the Timiskaming assemblage and the Larder Lake group on the Cheminis mine site. (**B**) Photo illustrating the fragmental unit that separates the sedimentary rocks from the volcanic rocks. This unit consists, in outcrop, of a white sandy to silty matrix containing rounded carbonatized clasts. Note the relatively low degree of strain. Hand lens for scale, looking north. (**C**) Strongly carbonatized ultramafic volcanic unit found in contact with the Timiskaming assemblage. Hand lens for scale, plan view. (**D**) Thin section photomicrograph (cross-polarized light) of a

sample taken from the ultramafic volcanic unit. The ultramafic unit is composed of coarse-grained carbonate, euhedral chlorite, minor albite and pyrite. The composition of the adjacent Larder Lake group volcanic rock is identical to the composition of the clasts within the fragmental unit to the north. (**E**) Representative thin section photomicrograph (cross-polarized light) of the matrix material within the fragmental unit. The matrix is composed dominantly of quartz-sericite-carbonate and minor pyrite. (**F**) Thin section photomicrograph (cross-polarized light) of a sample taken from the fragmental unit. Note the distinct difference in composition between the clast and matrix material. (**G**) Thin section photomicrograph (cross-polarized light) of a sample taken from the fragmental unit. The composition of the rounded clasts is dominantly ankerite-chlorite with minor albite and pyrite. The matrix material is composed of quartz grains within a finer sedimentary matrix and abundant sericite.

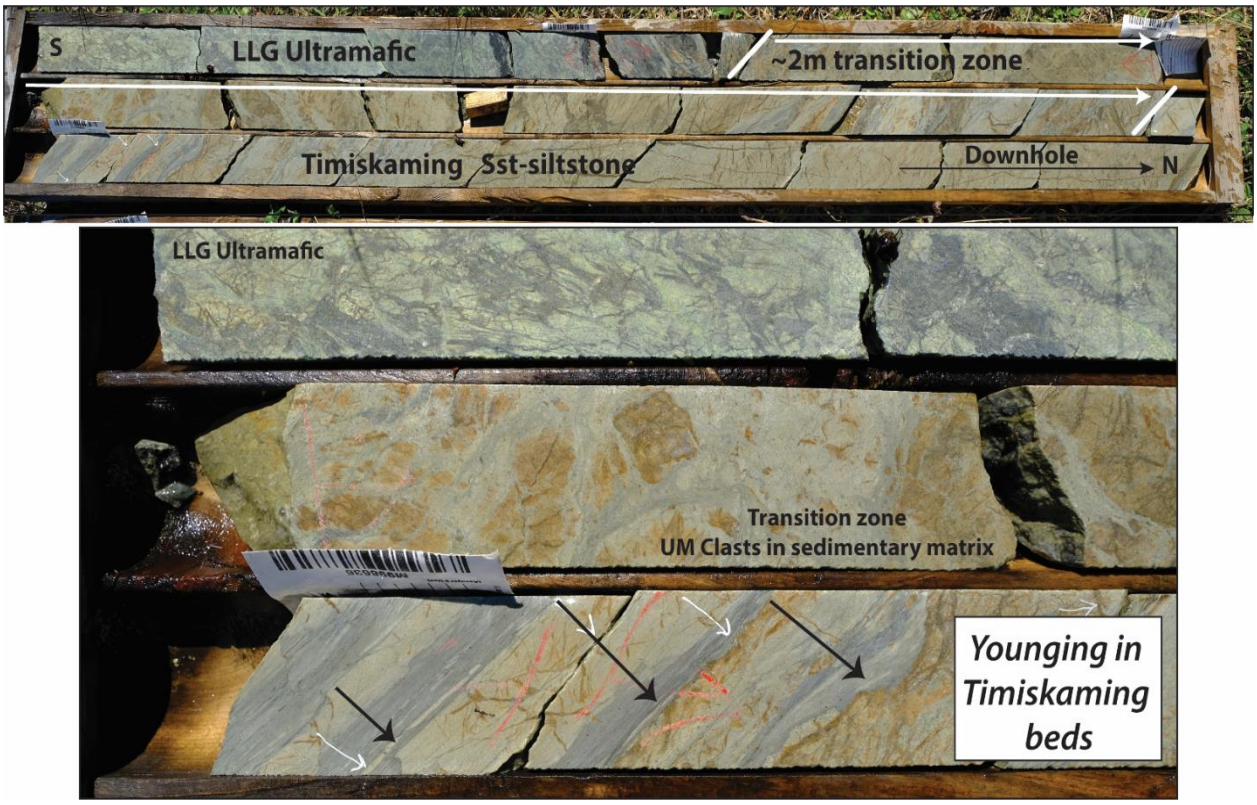


**Figure 21**. Drill hole GF-12-125 from cross section in Figure 21. Fuchsite-altered Larder Lake Group ultramafic flow in contact with a sandstone-siltstone of Timiskaming age. Normal grading in sedimentary beds north of the volcanic rocks indicate younging downhole, towards the north. A 2 m gradational zone marks the contact. It is characterized by carbonatized rounded fragments surrounded by a sedimentary matrix and is similar to the transition zone in the Kerr-Addison area.

At the south contact between the Timiskaming rocks and Larder Lake group (Figure 19b), a very fine-grained greywacke to sandstone is in sharp contact with intercalated mafic to ultramafic volcanic rocks. The greywacke is green to grey with consistent graded beds, younging to the south, away from the Larder Lake group volcanic rocks. The southern contact between the two lithologies

varies from sharp, with no obvious structure or shear sense indicators and equal strain on either side, to moderately strained, with attenuated sedimentary beds proximal to the contact. Unlike the north contact, a transition zone containing ultramafic-mafic volcanic clasts is not present. A pervasive chloritic and sericitic $S_2$ foliation strikes east-northeast and is steeply dipping to the south. The $S_2$ foliation is generally subparallel to lithological contacts and oriented clockwise with respect to bedding. A weak to moderate chloritic and sericitic $S_3$ foliation strikes northeast, and is anticlockwise with respect to bedding. The $S_2$ foliation is sinistrally offset along the $S_3$ foliation. A notable structural feature, consistent with previous mapping at Cheminis (Lafrance, 2015), is the relationship of $S_2$ and $S_3$ foliations with respect to bedding. North of the Larder Lake group volcanic rocks, $S_2$ foliation is oriented clockwise, whereas $S_3$ foliation is anticlockwise, with respect to bedding. South of the Larder Lake group, $S_2$ and $S_3$ foliations are typically oriented anticlockwise to bedding (Lafrance, 2015) where beds young to the south. This relationship is consistent with a large scale anticline with the Larder Lake group lying within the hinge of the fold.

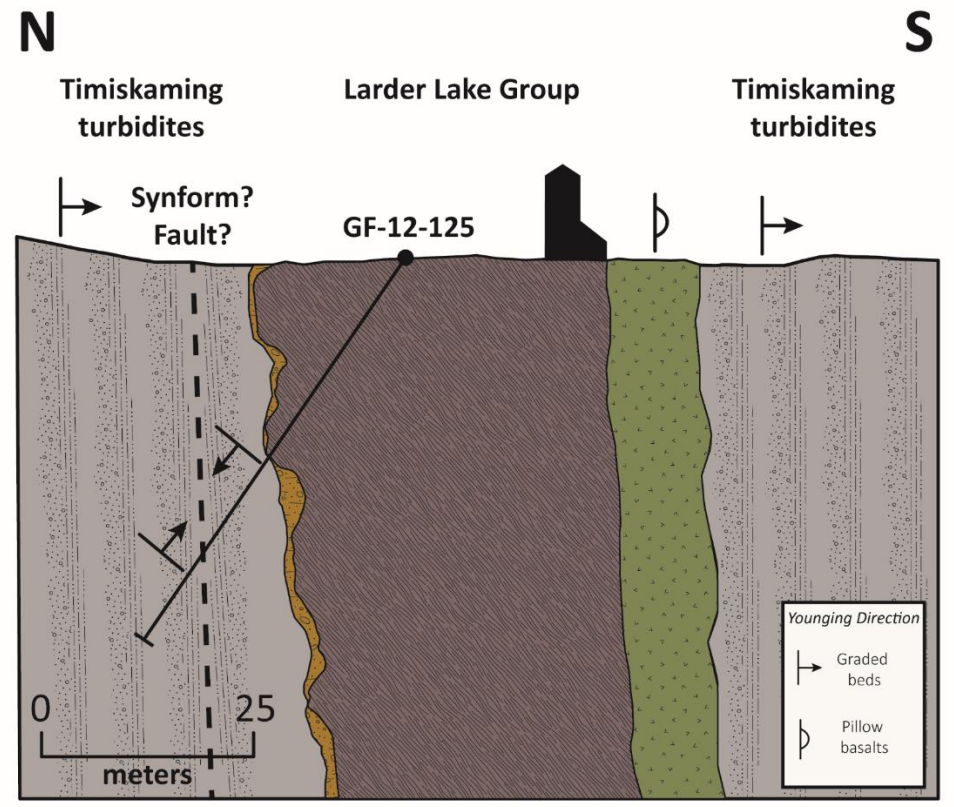


**Figure 22**. Cross-section of the Cheminis mine site showing the relationship between the Timiskaming assemblage and the Larder Lake group. Diamond drill hole GF-12-125 from the Cheminis mine site is collared in the LLG and crosses the contact with the Timiskaming assemblage. At the contact, there is increased shearing, minor graphite and a lower Timiskaming siltstone that contains strongly carbonatized fragments followed by a north-younging sequence of turbidites.

## 2.5 Discussion

### 2.5.1 The nature of the Timiskaming – Larder Lake contact

The contact between the Timiskaming assemblage and Larder Lake group represents an age gap of ca. 27 – 40 Ma and has previously been interpreted to reflect the structural juxtaposition of the two units along the CLLF (Hamilton, 1986; Smith et al., 1993; Jackson and Fyon, 1991). More recent regional scale studies suggest that the CLLF formed prior to the deposition of the Timiskaming assemblage and was later deformed (Bedeaux et al., 2017). Regional compilations

further suggest that although the CLLF is continuous along a 250 km strike length (Poulsen, 2017), there are distinct variations in the orientation of foliations, stretching lineations and their relationship to lithological contacts. Collectively these favor the existence of an ancestral CLLF along which the Timiskaming was deposited within extensional basins above an accreted volcanic substrate (Bedeaux et al., 2017). These interpretations support the results of this study that suggests that although later structurally modified, the contact was originally primary and therefore originated as an unconformity between the metavolcanic rocks of the Larder Lake group and the younger overlying metasedimentary rocks of the Timiskaming assemblage.

Structural modification of this contact was described at the Kearns and Virginiatown locations where the contact underwent shearing, folding and/or imbrication during the $D_2$ deformation event. At the Cheminis mine site, the contact locally escaped this deformation, and the original stratigraphic relationship between the two units is preserved. The transition zone at Cheminis is a clastic sedimentary rock containing clasts of the underlying ultramafic rocks and represents a basal unconformity. Beds young away from the contact along with a decrease in the abundance of ultramafic clasts, and it is overprinted by the regional $S_2$ cleavage, suggesting that the transition zone formed during the erosion of the ultramafic rocks prior to regional deformation.

### 2.5.2 Regional supporting evidence

The presence of an unconformity between the Hearst assemblage and the Larder Lake group has been previously documented (Hewitt, 1951, 1963; St-Jean et al., 2017) in the region. A recently uncovered outcrop in the northeastern part of Skead Township exposes the basal unconformity between the sedimentary rocks of the Hearst assemblage and the underlying Larder Lake group ultramafic volcanic rocks. The underlying komatiite of the Larder Lake group is dark green, fine

grained with polyhedral joints and well developed spinifex textures. The overlying basal conglomerate is matrix supported and contains angular to subangular clasts (up to 90 cm across) composed predominantly of granitoid and coarse-grained spinifex-textured komatiite clasts. The bimodal clast composition, their angularity and their similarity to the underlying komatiite indicates a proximal sourcing of clasts (St-Jean et al., 2017).

Away from the contact, komatiite clasts become increasingly scarce and the conglomerate is polylithic with clasts of gabbro, mudstone, fine-grained mafic volcanic rock, granitoid and minor sulphidized clasts. Younging directions to the NE and ENE suggest that the conglomerate youngs away from the ultramafic rocks and unconformably overlies those rocks (St-Jean et al., 2017).

The Larder Lake group represents the eroded basement on which the Hearst and Timiskaming sediments were deposited. Goulet (1978) described a similar unconformity north of the CLLF between the Timiskaming assemblage and Blake River group. As the latter was also basement to the overlying Timiskaming assemblage, this suggests that the Timiskaming assemblage was deposited on a folded/imbricated basement consisting of at least the Blake River and Larder Lake groups (Wilkinson et al., 1999; Goulet, 1978).

Similarly, in the Malartic area, Gunning and Ambrose (1940) described the contact between mafic volcanic rocks of the Piché Group and younger conglomerate and greywacke of the Cadillac Group as a structurally conformable contact. They suggested that the Cadillac group and overlying Timiskaming group were deposited in a large basin overlying an older basement as proposed here for the Larder Lake area.

### 2.5.3 CLLF evolution

The CLLF has a prolonged deformation history. In the Malartic area, early fault structures, which are located immediately north of the CLLF, are thought to have controlled the emplacement of ca. 2690 Ma intrusions prior to the deposition of Timiskaming assemblage (Bedeaux et al., 2017). The deformation event responsible for the formation of these early structures may also be responsible for the tilting of the volcanic rocks prior to the deposition of the Timiskaming rocks as indicated by the angular unconformable contact relationships between older volcanic rocks and the Timiskaming assemblage in the Rouyn area (Goulet, 1978) and Larder Lake area (this study). This deformation event correlates with the $D_1$ event previously inferred in this study from the angular unconformable relationship between the Blake River group and Timiskaming assemblage. The early $D_1$ structures may have been reactivated as bounding faults of extensional and/or strike-slip basins in which fluvial to shallow marine sedimentary rocks and alkali volcanic rocks of the Timiskaming assemblage were deposited (Bedeaux et al., 2017). Inversion of these basins during the $D_2$ north-south shortening event folded these rocks and tilted the Timiskaming angular unconformity to near-vertical dips (this study) and reactivated these contacts as reverse faults (Lafrance, 2015). The $D_2$ event produced the strong $S_2$ foliation and $L_2$ lineation that characterize the CLLF. Bedeaux et al. (2017) suggested that the Timiskaming rocks were deposited early during the $D_2$ event at ca. 2677 – 2678 Ma (Pilote et al., 2015; De Souza et al., 2015) and were later buried and deformed during the same $D_2$ event at 2672 Ma – 2665 Ma (Wilkinson et al., 1999). However, because the Timiskaming assemblage and ca. 2678 Ma to ca. 2675 Ma intrusions are overprinted by the $D_2$ fabrics in the Malartic area, Samson (2019) suggested that the Timiskaming sedimentary rocks were deposited prior to the $D_2$ event. The Timiskaming basins could therefore have formed either during or before the $D_2$ event. In either

case, overprinting of the $S_2$ cleavage by Z-shaped $F_3$ folds and dextral shear bands suggest that CLLF was subsequently reactivated as a dextral transcurrent fault during the NW-SE-directed $D_3$ deformation event (Hodgson and Hamilton, 1989; Robert, 1989; Wilkinson et al., 1999; Daigneault et al., 2002; Ispolatov et al., 2005; Zhang et al., 2014; Lafrance, 2015).

### 2.5.4 Gold mineralization

Gold mineralization in the southern Abitibi is, in general, spatially associated with the Destor-Porcupine fault zone, to the north, and the Cadillac-Larder Lake fault (CLLF) zone to the south. The gold endowment of the orogenic deposits located along the CLLF totals about 3,471 t (~111.6 Moz; Monecke et al., 2017).

The CLLF is a 250 km long curvilinear structure that has a spatial control on the localization of gold between Matachewan to Val d'Or. This work has focused in the Larder Lake area, however as outlined by Poulsen (2017) the nature of the CLLF, and its relationship to gold mineralization, changes along strike and the relationships discussed here do not necessarily apply to the entire fault system.

In the Larder Lake area, there are a number of gold deposits from west to east, including the Omega, Fernland, Cheminis, Bear Lake, Barber Larder, McGarry and Kerr-Addison Chesterville (Figure 2). Along this trend the northern contact between the Larder Lake group and the Timiskaming assemblage, or the CLLF, is planar and shows little strike variation, although the dip changes from south dipping at Omega to north dipping at Kerr-Addison with the inflection point at the Bear Lake deposit. These deposits are somewhat unique in that they are all located within

the high strain corridor of the CLLF, rather than second or third order faults associated with the main break, which is more typical of orogenic gold deposits (Ispolatov et al., 2008). The geology in all of these deposits is similar, hosted in the Larder Lake group. The Larder Lake group is several hundred meters in thickness and is bound to the north and south by rocks of the Timiskaming assemblage and consists of a continuous panel of mafic and ultramafic rocks with minor sedimentary rocks. Although distinct volcanic facies are recognized along the trend between Omega and Kerr-Addison (~11 km), the panels of stratigraphy are not continuous and are lensoidal in shape, possibly reflecting high degrees of transposition.

All of these deposits show similar characteristics with each having “green carbonate” and “flow ore” style mineralization with gold contained within altered ultramafic and mafic volcanic rocks. Both styles of mineralization are grossly stratabound (Kishida and Kerrich, 1987, Smith et al., 1993). Green carbonate style of mineralization consists of an assemblage of fuchsite-quartz-ankerite-magnesite, which hosts quartz carbonate vein sets. Gold occurs within both quartz carbonate veins and disseminations within the alteration assemblage (Thomson, 1941; Kishida and Kerrich, 1987; Smith et al., 1993).

Flow ore is composed of quartz, chlorite, and carbonate with variable amounts of sericite, albite and arsenopyrite to arsenian pyrite. In this type of ore, most of the gold occurs associated with fine-grained arsenian pyrite (Sandering Taylor, 2017). Relict volcanic textures such as varioles and pillow and flow breccia are recognized (Thomson, 1941; Kishida and Kerrich, 1987; Smith et al., 1993).

Lafrance (2015) suggests that at the Cheminis mine, the styles of gold mineralization varies according to their host rocks, but they have similar alteration mineralogy (sericite or fuchsite, carbonate, chlorite, albite, pyrite, arsenopyrite) and underwent similar elemental mass gains in $CO_2$, S, $K_2O$, As, W ± CaO, $Na_2O$, and Sb, suggesting that they interacted with the same hydrothermal fluids.

The distribution of gold, at these deposits, is almost exclusively within the Larder Lake group and is hosted in both the ultramafic (green carbonate) and mafic (flow ore) volcanic rocks as described above. Gold is located throughout the Larder Lake group and is not dominantly at the contact with the Timiskaming assemblage or the CLLF.

At the Omega deposit, gold occurs throughout the Larder Lake group including both the structural hanging wall and footwall. Whereas immediately to the east, at the Fernland deposit, gold occurs near the southern contact of the Larder Lake group, in the structural hangingwall. At Kerr-Addison, by far the largest deposit along this segment, gold is mainly localized along the northern contact of the Larder Lake group, but also occurs in several poorly defined zones to the south, such as the Town and Mill zones (Smith et al., 1993).

Detailed mapping and core logging at Kerr-Addison has shown a number of roughly east-west trending penetrative shears within the Larder Lake group, in the footwall of the contact with the Timiskaming assemblage. The most significant structure, informally referred to as the kerr fault, juxtaposes “green carbonate” against “flow ore”. Gold in both styles are centered around the late fault, which is superposed on an older structure that played a fundamental control on the

distribution of gold. Poorly defined zones, to the south, at the Town and Mill zone, have similar characteristics with shear zones that juxtapose volcanic units and control the distribution of gold. These faults, as outlined above, developed during $D_2$ with a strong penetrative foliation and steeply east plunging lineations.

Work by Lafrance (2015) on the Cheminis deposit demonstrated that gold was emplaced during $D_2$ south-side-up ductile shear along the CLLF. Wilkinson et al., (1999) suggests that metasomatism, leading to reaction softening, may have localized strain in a linear zone, within the Larder Lake group, during regional $D_2$ deformation (e.g., Kishida and Kerrich 1987). Calcite – Fe carbonate is ubiquitous in rocks located near the CLLF and contributes to the definition of $S_2$ foliation planes, suggesting carbonate metasomatism is synchronous with $D_2$. Similarly Ispolatov et al. (2008) demonstrated that mineralization at Upper Canada deposit, localized along a splay of the CLLF was formed during $D_2$ and demonstrated a similar structural framework for the deposits located in the Larder Lake segment between Omega and Kerr-Addison.

At Kerr-Addison, gold is hosted within the green carbonate alteration assemblages (as inclusions within and along grain boundaries of carbonate, quartz, albite and fuchsite alteration minerals) and within $V_2$ and $V_3$ veins. $V_2$ veins clearly host visible gold and are parallel to the $S_2$ foliation, which was subsequently crenulated during $D_3$ and crosscut by $V_3$ veins. This evidence would suggest that at least one stage of gold introduction preceded the emplacement of the $V_3$ veins, which themselves contain visible gold. Therefore, it is plausible that the $V_3$ veins were associated with a second pulse of gold-bearing hydrothermal fluids. Alternatively, $V_2$ and $V_3$ may have originated from the same protracted event during progressive deformation.

In summary, the distribution of gold is strongly controlled by the location of the CLLF, at Larder Lake and in general the southern Abitibi subprovince. On the Larder Lake segment, gold was introduced during $D_2$ and is associated with veins, or alteration assemblages, that developed during $D_2$. Rocks of the Timiskaming assemblage show similar $D_2$ fabrics as the Larder Lake group, yet are barren of any significant gold mineralization. As suggested by Wilkinson et al. (1999) hydrothermal metasomatic reaction softened the Larder Lake group, partitioning strain into the mafic and ultramafic rocks and localized the distribution gold to penetrative shears that juxtapose the different volcanic rocks in the Larder Lake group.

## Conclusion

Detailed mapping and characterization of the contact between Timiskaming assemblage – Larder Lake group suggests that its nature changes from an unconformity, where it is less deformed, to a shear zone, where it has been structurally modified. At Cheminis, a transition zone between the Timiskaming assemblage – Larder Lake group is characterized by ultramafic-mafic clasts in a sandy matrix. The younging direction in this unit and overlying sedimentary rocks faces away from the Larder Lake group indicating that the sedimentary rocks overlie the volcanic units. Regional studies support that the early metavolcanic stratigraphy was folded and tilted during $D_1$, which likely formed the basement for which the Timiskaming assemblage was unconformably deposited on top of the exposed Larder Lake group. Reactivation of this contact during a $D_2$ deformation event localized the distribution of gold deposits and formed the present day manifestation of the CLLF.

# References


Allen, P. A., & Allen, J. R. (2005). *Basin Analysis: Principles and Applications 2nd ed.*

Ayer, J., Amelin, Y., Corfu, F., Kamo, S., Ketchum, J., Kwok, K., & Trowell, N. (2002). Evolution of the southern Abitibi greenstone belt based on U-Pb geochronology: autochthonous volcanic construction followed by plutonism, regional deformation and sedimentation. *Precambrian Research, 115*, 63–95 pp.

Ayer, J., Barr, E., Bleeker, W., Creaser, R., Hall, G., Ketchum, J., Powers, D. Salier, B., Still, A. & Trowell, N. (2003). Discover Abitibi. New geochronological results from the Timmins area: implications for the timing of late tectonic stratigraphy, magmatism and gold mineralization; Summary of Field Work and Other Activities 2003. *Ontario Geological Survey, OFR 6120,* 33-1 – 33-11 pp.

Ayer, J., Thurston, P. C., Bateman, R., Dubé, B., Gibson, H. L., Hamilton, M. A., Hathway, B., Hocker, S.M., Houlé, M.G., Hudak, G., Ispolatov, V.O., Lafrance, B., Lesher, C.M., Macdonald, P.J., Péloquin, A.S., Piercey, S.J., Reed, L.E., & Thompson, P. H. (2005). *Overview of results from the Greenstone Architecture Project: Discover Abitibi Initiative*. *Ontario Geological Survey, OFR 6154,* 146 pp.

Barnes, S. J. (2006). Komatiites: Petrology, Volcanology, Metamorphism, and Geochemistry. *Special Publication of the Society of Economic Geologists: Nickel Deposits of the Yilgarn Craton: Geology, Geochemistry, and Geophysics Applied to Exploration, 13.* 13-50 p.p.

Bedeaux, P., Pilote, P., Daigneault, R., & Rafini, S., (2017). Synthesis of the structural evolution and associated gold mineralization of the Cadillac Fault, Abitibi, Canada. *Ore Geology Reviews, 82,* 49-69 pp.

Bedeaux, P., Mathieu, L., Pilote, P., Rafini, S., & Daigneault, R. (2018). Origin of the Piché Structural Complex and implications for the early evolution of the Archean crustal-scale Cadillac – Larder Lake Fault Zone, Canada. *Canadian Journal of Earth Sciences, 55* (8), 905–922 pp.

Bleeker, W. (2012). Targeted Geoscience Initiative (TGI-4) Lode Gold Deposits in Ancient Deformed and Metamorphosed Terranes: The role of extension in the formation of Timiskaming basins and large gold deposits, Abitibi greenstone belt – A discussion. *Summary of field work and other activities 2011; Ontario Geological Survey, OFR 6280, 47,* 1-12 pp.

Bleeker, W. (2015). Synorogenic gold mineralization in granite-greenstone terranes: the deep connection between extension, major faults, synorogenic clastic basins, magmatism, thrust inversion, and long-term preservation. *Geological Survey of Canada, OFR 7852,* 25–48 pp.

Burrows, D. R., and Spooner, E.T.C. (1986). The McIntyre Cu-Au deposit, Timmins, Ontario, Canada. *Proceedings of Gold '86, an international symposium on the geology of gold deposits. Edited by A. J. Macdonald, Gold '86,* 23-39 pp.

Cameron, E.M. (1993). Precambrian gold: Perspective from top to bottom of shear zones. *The Canadian Mineralogist, 13,* 917-944 pp.

Camiré, G.E., Laflèche, M.R., Ludden, J.N. (1993). Archean metasedimentary rocks from the northwestern Pontiac Subprovince of the Canadian shield: chemical characterization, weathering and modelling of the source areas. *Precambrian Research, 63 (3),* 285-305 pp.

Card, K. D., Poulsen, K. H., & Robert, F. (1989). The Archean Superior Province of the Canadian Shield and its lode gold deposits. *The Geology of Gold Deposits, The Perspective in 1988*: *Economic Geology Monograph 6,* 19–36 pp.

Cooke, D. L., & Moorhouse, W. W. (1969). Timiskaming volcanism in the Kirkland Lake area, Ontario, Canada. *Canadian Journal of Earth Sciences, 6* (1), 117–132 pp.

Corfu, F., Jackson, S. L., & Sutcliffe, R. H. (1991). U–Pb ages and tectonic significance of late Archean alkalic magmatism and nonmarine sedimentation: Timiskaming Group, southern Abitibi belt, Ontario. *Canadian Journal of Earth Sciences, 28* (4), 489–503 pp.

Corfu, F., Krogh, T. E., Kwok, Y. Y., & Jensen, L. S. (1989). U-Pb zircon geochronology in the

southwestern Abitibi greenstone belt, Superior Province. *Canadian Journal of Earth Sciences*, *26*, 1747–1763 pp.

Corfu, F., & Noble, S. R. (1992). Genesis of the southern Abitibi greenstone belt, Superior Province, Canada: evidence from zircon Hf isotope analyses using a single filament technique. *Geochimica et Cosmochimica Acta*, *56*, 2081–2097 pp.

Daigneault, R., Mueller, W. U., & Chown, E. H. (2002). Oblique Archean subduction: accretion and exhumation of an oceanic arc during dextral transpression, Southern Volcanic Zone, Abitibi Subprovince Canada. *Precambrian Research*, *115* (1–4), 261–290 pp.

Davis, D. W. (2002). U-Pb geochronology of Archean metasedimentary rocks in the Pontiac and Abitibi subprovinces, Québec, constraints on timing, provenance and regional tectonics. *Precambrian Research*, *115*, 97–117 pp.

Desrochers, J.P., Hubert, C., Ludden, J.N., and Pilote, P. (1993). Accretion of Archean oceanic plateau fragments in the Malartic Composite Block, Abitibi Greenstone Belt, Canada. *Geology*, *21*, 451-459 pp.

De Souza, S, Dubé, B., McNicoll, V.J., Mercier-Langevin, P., Creaser, R.A., Kjarsgaard, I.M. (2015). Geology, hydrothermal alteration, and genesis of the world-class Canadian Malartic stockwork-disseminated Archean gold deposit, Abitibi, Quebec. Dubé, B., Mercier-Langevin, P. (Eds,), Targeted Geoscience Initiative 4: Contributions to the Understanding of Precambrian Lode Gold Deposits and Implications for Exploration. *Geological Survey of Canada; OFR 7852*, 113-126 pp.

Dimroth, E., Imreh, L., Rocheleau, M., & Goulet, N. (1982). Evolution of the south-central part of the Archean Abitibi Belt, Quebec. Part I: Stratigraphy and paleogeographic model. *Canadian Journal of Earth Sciences*, *19*, 1729–1758 pp.

Dimroth, E., Imreh, L., Goulet, N, and Rocheleau, M. (1983). Evolution of the south-central segment of the Archean Abitibi Belt, Quebec. Part II: Tectonic evolution and geomechanical model model. *Canadian Journal of Earth Sciences*, *20*, 1355–1373 pp.

Diop, A. (2011). Caractéristiques sédimentologiques, volcanologiques et structurales du bassin de Granada dans la ceinture de roches vertes de l'Abitibi (Québec). *Thèse Du Doctorat, Université Du Québec à Chicoutimi*, 348 pp.

Dubé, B., & Gosselin, P. (2007). Greenstone hosted quartz-carbonate vein deposits, in Goodfellow, W.D., ed., Mineral Deposits of Canada: A synthesis of Major Deposit-Types, District Metallogeny, the Evolution of Geological Provinces, an Exploration Methods. *Geological Association of Canada, Mineral Deposits Division, Special Publication* (5), 49–73 pp.

Frarey, M. J., & Krogh, T. E. (1986). U-Pb zircon ages of late internal plutons of the Abitibi and eastern Wawa Subprovinces, Ontario and Québec. *Geological Survey of Canada, (Part A, Paper 861-A)*, 43–48 pp.

Frieman, B.M., Kuiper, Y.D., Monecke, T., Kelly, N.M., & Kylander-Clark, A. (2017). Constraints on the geodynamic evolution of the southern Superior Province : U-Pb LA-ICP-MS analysis of detrital zircon in successor basins of the Archean Abitibi and Pontiac subprovinces of Ontario and Quebec, Canada. *Precanbrian Research, 292*, 398-416 pp.

Goulet, N. (1978). Stratigraphy and structural relationships across the Cadillac – Larder Lake Fault, Rouyn-Beauchastel area, Quebec. *PhD thesis, Queen's University, Canada*, 141 pp.

Goutier, J., & Lacroix, S., 1992, Géologie du secteur de la faille de Porcupine-Destor dans les cantons de Destor et Duparquet: *Ministère de l'Énergie de des Ressources du Québec Report MB* 92(6), 62 p.

Goodwin, A.M., 1977, Archean volcanism in Superior province, Canadian Shield: *Geological Association of Canada Special Paper 16*, p. 205–241 pp.

Gunning, H.C., Ambrose, J.W. (1940). Malartic Area, Quebec. *Geological Survey of Canada, Memoir 222*, 169 pp.

Hamilton, J. V. (1986). The structural and stratigraphic setting of gold mineralization in the vicinity of Larder Lake, southcentral Abitibi greenstone belt, northeastern Ontario. *M.Sc. Thesis, Queen's University*, 154 pp.

Hewitt, D.F. (1951). Geology of Skead Township, Larder Lake area, Timiskaming District, Ontario.

*Ontario Department of Mines, Annual Report, 1949, 58 (6),* 1-43 pp.
Hewitt, D.F. (1963). The Timiskaming Series of the Kirkland Lake area. *The Canadian Mineralogist, 7 (3),* 497-522 pp.
Hodgson, C. J. A. Y., & Hamilton, J. V. (1989). Gold Mineralization in the Abitibi Greenstone Belt: End-Stage Result of Archean Collisional Tectonics. *The Geology of Gold Deposits: the Perspective in 1988. Economic Geology Monograph 6,* 86–100 pp.
Hodgson, C. J., & Hattori, K. (1991). Gold-related geology in the Kirkland Lake and Timmins camps, Ontario. *Geological Survey of Canada, OFR 2160*, 1–57 pp.
Hubert, C., Trudel, P., & Gelinas, L. (1984). Archean wrench fault tectonics and structural evolution of the Blake River group, Abitibi belt, Quebec. *Canadian Journal of Earth Sciences, 21 (9),* 1024-1032 pp.
Hyde, R. S. (1980). Sedimentary facies in the Archean Timiskaming Group and their tectonic implications, Abitibi greenstone belt, northeastern Ontario, Canada. *Precambrian Research*, *12*, 161–195 pp.
Ispolatov, V., Lafrance, B., Dubé, B., Hamilton, M., & Creaser, R. (2005). Geology, Structure, and Gold Mineralization, Kirkland Lake and Larder Lake Areas (Gauthier and Teck Townships): Discover Abitibi Initiative. *Ontario Geological Survey*, *OFR 6159*, 1–125 pp.
Ispolatov, V., Lafrance, B., Dubé, B., Creaser, R., & Hamilton, M. (2008). Geologic and structural setting of gold mineralization in the Kirkland Lake-Larder Lake gold belt, Ontario. *Economic Geology*, *103* (6), 1309–1340 pp.
Jackson, S. L., & Fyon, J. A. (1991). The Western Abitibi Subprovince in Ontario. *Ontario Geological Survey, Geology of Ontario Special Volume 4 (1),* 405-482 pp.
Jensen, L. S. (1974). Ramore area, Districts of Timiskaming and Cochrane. *Ontario Division of Mines, Miscellaneous Paper*, *59*, 206 pp.
Jensen, L.S. (1976) A New Cation Plot for Classifying Subalkalic Volcanic Rocks; *Ontario Division of Mines*, *Miscellaneous Paper 66*, 22 pp.
Jensen, L. S. (1978a). Archean Komatiitic, Tholeiitic, Calc-alkalic and Alkalic Volcanic Sequences in the Kirkland Lake area. *Geological Association of Canada, (Toronto '78 Field Trip Guidebook),* 237-259 pp.
Jensen, L. S. (1978b). Regional Stratigraphy and Structure of the Timmins-Kirkland Lake area, District of Cochrane and Timiskaming and the Kirkland-Larder Lake area, District of Timiskaming. *Ontario Geological Survey, Miscellaneous Paper, 82,* 235 pp.
Jensen, L. S. (1979). Larder Lake Synoptic Mapping Project, Districts of Cochrane and Timiskaming. *Ontario Geological Survey, Miscellaneous Paper, 90,* 245 pp.
Jensen, L. S. (1980). Kirkland Lake-Larder Lake synoptic mapping project, Districts of Cochrane and Timiskaming. *Ontario Geological Survey, Miscellaneous Paper, 96*, 201 pp.
Jensen, L. S. (1985). Synoptic Mapping of the Kirkland Lake-Larder Lake areas, District of Timiskaming. *Ontario Geological Survey*, *126*, 112–120 pp.
Jensen, L. S., & Langford, F. F. (1985). Geology and Petrogenesis of the Archean Abitibi belt in the Kirkland Lake area, Ontario. *Ontario Geological Survey, Miscellaneous Paper 123,* 130 pp.
Kishida, A., & Kerrich, R. (1987). Hydrothermal alteration zoning and gold concentration at the Kerr-Addison Archean lode gold deposit, Kirkland Lake, Ontario (Canada). *Economic Geology*, *82* (3), 649–690 pp.
Lafrance, B. (2015). Geology of the orogenic Cheminis gold deposit along the Larder Lake – Cadillac deformation zone, Ontario. *Canadian Journal of Earth Sciences*, *52* (12), 1093–1108 pp.
Ludden, J., Hubert, C., & Gariépy, C. (1986). The tectonic evolution of the Abitibi greenstone belt of Canada. *Geological Magazine*, *123*, 153–166 pp.
Martin, R.D. (2012). Syenite-hosted gold mineralization and hydrothermal alteration at the Young-Davidson deposit, Matachewan, Ontario. *MSc thesis, University of Waterloo, Waterloo.* 1-188.
Monecke, T., Mercier-Langevin, P., Dubé, B., & Frieman, B. M. (2017). Geology of the Abitibi Greenstone Belt. *Reviews in Economic Geology*, *19*, 7–49 pp.

Mueller, W. (1991). Volcanism and related slope to shallow marine volcaniclastic sedimentation: an Archean example, Chibougamau, Quebec, Canada. *Precambrian Research, 49*, 1–22 pp.

Mueller, W., & Donaldson, J. A. (1992). Development of Sedimentary Basins in the Archean Abitibi Belt, Canada - an Overview. *Canadian Journal of Earth Sciences, 29* (10), 2249–2265 pp.

Mueller, W., Donaldson, J. A., & Doucet, P. (1994). Volcanic and tectono-plutonic influences on sedimentation in the Archean Kirkland Basin Abitibi greenstone belt, Canada. *Precambrian Research, 68*, 201–230 pp.

Neumayr, P., Hagemann, S. G., & Couture, J.-F. (2000). Structural setting, textures, and timing of hydrothermal vein systems in the Val d'Or camp, Abitibi, Canada: implications for the evolution of transcrustal, second- and third-order fault zones and gold mineralization. *Canadian Journal of Earth Sciences, 37 (1),* 95–114 pp.

Péloquin, A.S., Piercey, S.J., Hamilton, M.A. (2008). The Ben Nevis Volcanic Complex, Ontario, Canada: Part of the Late Volcanic Phase of the Blake River Group, Abitibi Subprovince. *Economic Geology; 103 (6),* 1219-1241 pp.

Perrouty, S., Gaillard, N., Piette-Lauziere, N., Mir, R., Bardoux, M. Olivo, G.R., Linnen, R.L., Bérubé, C.L., Lypaczewski, P., Guilmette, C. Feltrin, L., Morris, W.A. (2017). Structural setting for Canadian Malartic style of gold mineralization in the Pontiac Subprovince, south of the Cadillac Larder Lake Deformation Zone, Québec, Canada. *Ore Geology Reviews 84,* 185-201 pp.

Pilote, P., Scott, C.R., Mueller, W., Lavoie, S. & Riopel, P. (1999). Géologie des formations de Val-d'Or, Héva et Jacola: Nouvelle interprétation du groupe de Malartic; in Explorer au Québec : le défi de la connaissance. Séminaire d'information sur la recherche géologique ; *Ministère de l'Énergie et des Ressources du Québec, programme et résumés, DV 99 (3),* 52 pp.

Pilote, P., Daigneault, R., David, J., McNicoll, V. (2015). Architecture of the Malartic, Piché and Cadillac groups and the Cadillac Fault : Geological revisions, new dates and interpretations. *Ministère de l'Énergie et des Ressources Naturelles. DV 2015-04*, 37 pp.

Poulsen, K. H. (2017). The Larder Lake-Cadillac Break and Its Gold Districts. *Reviews in Economic Geology, 19*, 133–167 pp.

Poulsen, K. H., Robert, F., & Dubé, B. (2000). Geological Classification of Canadian Gold Deposits. *Geological Survey of Canada, Bulletin 540,* 106 pp.

Robert, F. (1989). Internal structure of the Cadillac tectonic zone southeast of Val d'Or, Abitibi greenstone belt, Quebec. *Canadian Journal of Earth Sciences, 26*(12), 2661–2675 pp.

Robert, F. (1990). Structural setting and control of gold-quartz veins of the Val d'Or area, southeastern Abitibi subprovince. *Geology Department (Key Centre) and University Extension, University of Western Australia Short Course Notes, 24*, 167–210 pp.

Robert, F. (1995). Quartz-carbonate vein gold. *Geological Survey of Canada*, (Geology of Canadian Mineral Deposits, No. 8), 350–366 pp.

Robert, F. (2001). Syenite-associated disseminated gold deposits in the Abitibi greenstone belt, Canada. *Mineralium Deposita, 36* (6), 503–516 pp.

Robin, P.-Y., and Cruden, A.R. (1994). Strain and vorticity in ideally ductile transpression zones. *Journal of Structural Geology, 16*, 447-466 pp.

Ross, P.-S., McNicoll, V., Goutier, J., Mercier-Langevin, P., Dubé, B. (2011). Basaltic t andesitic volcaniclastic rocks in the Blake River Group, Abitibi Greenstone Belt: 2. Origin, geochemistry, and geochronology. *Canadian Journal of Earth Sciences, 48 (4),* 757-777 pp.

Samson, B. (2019). Deformation history and gold mineralization of the Cadillac Group north of the Larder Lake-Cadillac deformation zone, southern Abitibi greenstone belt, Quebec. *M.Sc. Thesis, Laurentian University.* 136 pp.

Sandering Taylor, M. (2017). Deportment of Gold Within Green Carbonate Ore and Flow Ore in the Kerr-Addison Mine, Virginiatown, Ontario, HBSc thesis Department of Earth Science, Western University, London, Ontario, 104 pp.

Shore, M., and Fowler, A.D. (1999). The origin of spinifex texture in komatiites. *Nature, 397*, 691-694 p.p.

Sibson, R. H., Robert, F., & Poulsen, K. H. (1988). High-angle reverse faults, fluid-pressure cycling, and mesothermal gold-quartz deposits. *Geology*, *16*, 551–555 pp.

Smith, J. P., Spooner, E. T. C., Broughton, D. W., & Ploeger, F. R. (1993). Archean Au-Ag-(W) Quartz Vein/Disseminated Mineralisation within the Larder Lake - Cadillac Break, Kerr Addison - Chesterville System, North East Ontario, Canada. *Ontario Geological Survey*, *OFR 5831*, 310 pp.

St-Jean, N., Hunt, L., & Sherlock, R. L. (2017). Preliminary Results from Mapping a New Exposure of the Basal Unconformity Between the Hearst and Larder Lake Assemblages, Skead Township, Northeastern Ontario. *Ontario Geological Survey*, *OFR 6333*, 37-1-37–7 pp.

Sun, S., & McDonough, W.F. (1989). Chemical and isotopic systematics of oceanic basalts: implications for mantle composition and processes. *Geological Society of London, Special Publications, 42,* 313-345 pp.

Thomson, J. E. (1941). Geology of McGarry and McVittie Townships, Larder Lake area: *Ontario Department of Mines Annual Report, Part VII* (50), 93 pp.

Thomson, J. E., & Griffis, A. T. (1941). Geology of Gauthier Township, East Kirkland Lake area. *Ontario Department of Mines Annual Report, 50* (8), 68-94 pp.

Thurston, P. C., Ayer, J. A., Goutier, J., & Hamilton, M. A. (2008). Depositional Gaps in Abitibi Greenstone Belt Stratigraphy: A Key to Exploration for Syngenetic Mineralization. *Economic Geology, 103,* 1097–1134 pp.

Thurston, P. C., & Chivers, K. M. (1990). Secular variation in Greenstone sequence development emphasizing Superior Province, Canada. *Precambrian Research*, *46*, 21–58 pp.

Tihor, L. A., & Crocket, J. H. (1977). Gold Distribution in the Kirkland Lake-Larder Lake area, with emphasis on the Kerr Addison-type ore deposits - a progress report. *In: Report of Activities, Part A, Geological Survey of Canada, 77–1A*, 363–370 pp.

Toogood, D. J., & Hodgson, C. J. (1985). A structural investigation between Kirkland Lake and Larder Lake gold camps. *Ontario Geological Survey, Miscellaneous Paper*, *127*, 200–205 pp.

Wilkinson, L., Cruden, A. R., & Krogh, T. E. (1999). Timing and kinematics of post-Timiskaming deformation within the Larder Lake - Cadillac deformation zone, southwest Abitibi greenstone belt, Ontario, Canada. *Canadian Journal of Earth Sciences, 36*(4), 627–647 pp.

Wilson, M. E. (1912). Geology and economic resources of the Larder Lake District, Ontario and adjoining portions of Pontiac County, Quebec; *Geological Survey of Canada Memoir 17-E,*1-70 pp.

Wilson, M.E. (1956). Early Precambrian rocks of the Timiskaming region, Quebec and Ontario. *Geological Society of America, Bulletin 67,* 1397-1430 pp.

Winchester, J.A. and Floyd, P.A. (1977). Geochemical discrimination of different magma series and their differentiation products using immobile elements. *Chemical Geology, 20,* 325-343 pp.

Zhang, J., Lin, S., Linnen, R., & Martin, R. (2014). Structural setting of the Young-Davidson syenite-hosted gold deposit in the Western Cadillac-Larder Lake Deformation Zone, Abitibi Greenstone Belt, Superior Province, Ontario. *Precambrian Research*, *248*, 39–59 pp.

# Appendix A: Geochemical Results

**Table 1.** Analytical results for major and trace elements for all collected samples:

| Analyte | Assemblage | Unit | Easting | Northing | SiO2 |
|---|---|---|---|---|---|
| **Unit** | | | | | wt. % |
| **L.O.D.*** | | | | | 0.01 |
| **MEBL17NFS0778** | LL | Komatiite | 604786 | 5331998 | 39.7 |
| **MEBL17NFS0768** | LL | Komatiite | 604823 | 5332030 | 33.1 |
| **MEBL17NFS0772** | LL | Komatiite | 604789 | 5332017 | 59.1 |
| **MEBL17NFS0789** | LL | Mudstone | 604778 | 5331949 | 66.6 |
| **MEBL17NFS0777** | LL | Mudstone | 604790 | 5332035 | 59.1 |
| **MEBL17NFS0788B** | LL | Basalt | 604780 | 5331958 | 63.4 |
| **MEBL17NFS0831** | LL | Komatiite | 606352 | 5333163 | 14.05 |
| **MEBL17NFS0834** | Tm | Sandstone | 606360 | 5333167 | 37.2 |
| **MEBL17NFS0775** | LL | Komatiite | 604789 | 5332004 | 34.8 |
| **MEBL17NFS0760** | LL | Komatiite | 604840 | 5332070 | 44.1 |
| **MEBL17NFS0769** | LL | Komatiite | 604823 | 5332025 | 38.2 |
| **MEBL17NFS0765** | LL | Komatiite | 604825 | 5332038 | 59.8 |
| **MEBL17NFS0767** | LL | Komatiite | 604824 | 5332031 | 28.7 |
| **MEBL17NFS0766** | LL | Komatiite | 604824 | 5332035 | 34.1 |
| **MEBL17NFS0770** | LL | Komatiite | 604823 | 5332025 | 37.8 |
| **MEBL17NFS0786B** | LL | Komatiite | 604782 | 5331962 | 36.6 |
| **MEBL17NFS0786** | LL | Komatiite | 604782 | 5331962 | 37.2 |
| **MEBL17NFS0689** | LL | Komatiite | 604787 | 5332026 | 41.5 |
| **MEBL17NFS0798** | LL | Mudstone | 604779 | 5331956 | 59.4 |
| **MEBL17NFS0771** | LL | Mudstone | 604789 | 5332017 | 55.5 |
| **IAG OKUM- X258634** | - | Standard | - | - | 44.5 |
| **MEBL18NFS1148AG01** | Tm | Sandstone | 599816 | 5330491 | 40.5 |
| **MEBL18NFS1103AG01** | LL | Basalt | 599568 | 5330333 | 39.9 |
| **MEBL18NFS1103BG01** | LL | Sandstone | 599568 | 5330333 | 53.4 |
| **MEBL18NFS1011AG01** | LL | Komatiite | 599554 | 5330416 | 36.4 |
| **LK-NP-1** | - | Standard | - | - | 48.3 |
| **IAG OKUM - X259169** | - | Standard | - | - | 43.6 |
| **MEBL18NFS1107AG01** | LL | Komatiite | 599559 | 5330417 | 32.5 |
| **MEBL18NFS1006AG01** | LL | Transition | 599539 | 5330415 | 63.1 |
| **MEBL18NFS1105AG01** | LL | Transition | 599544 | 5330419 | 60.5 |
| **MEBL18NFS1010AG01** | LL | Transition | 599560 | 5330417 | 62.6 |
| **MEBL18NFS1106AG01** | LL | Komatiite | 599555 | 5330418 | 45.9 |
| **MEBL18NFS1033AG01** | LL | Komatiite | 604791.1 | 5332013 | 28.8 |
| **MEBL18NFS1034AG01** | BR | Basalt | 604819.2 | 5332201 | 41.7 |
| **MEBL18NFS0959AG01** | LL | Basalt | 604785.5 | 5331973 | 49.4 |
| **MEBL18NFS0984AG01** | BR | Basalt | 605485.4 | 5333083 | 39.6 |
| **MEBL18NFS1032AG01** | LL | Basalt | 604789.1 | 5332016 | 46.7 |
| **MEBL18NFS0961BG01** | LL | Lamprophyre | 604788.3 | 5331986 | 35.1 |
| **MEBL18NFS0965BG01** | LL | Komatiite | 604791.4 | 5332022 | 32.2 |
| **MEBL18NFS0964AG01** | LL | Komatiite | 604788.4 | 5332000 | 35.6 |
| **MEBL18NFS0967AG01** | Tm | Sandstone | 604792.6 | 5332028 | 69.9 |
| **MEBL18NFS1031AG01** | LL | Albite dike | 604790 | 5332017 | 62.3 |
| **MEBL18NFS0961AG01** | LL | Komatiite | 604788.3 | 5331986 | 40.3 |
| **MEBL18NFS1036AG01** | LL | Albite dike | 604840.1 | 5332071 | 70 |
| **MEBL18NFS1034AG02** | Br | Basalt | 604819.2 | 5332201 | 42.2 |

** L.O.D.: Limit of Detection*

*Br: Blake River group; LL: Larder Lake group; Tm: Timiskaming assemblage*

**Table 1. (Continued)**

| Analyte | TiO2 | Al2O3 | Fe2O3 | Cr2O3 | MnO | MgO | CaO |
|---|---|---|---|---|---|---|---|
| **Unit** | wt. % | wt. % | wt. % | wt. % | wt. % | wt. % | wt. % |
| **L.O.D.** | 0.01 | 0.01 | 0.01 | 0.002 | 0.01 | 0.01 | 0.01 |
| **MEBL17NFS0778** | 0.41 | 4.76 | 6 | 0.17 | 0.32 | 8.68 | 14.45 |
| **MEBL17NFS0768** | 0.32 | 5.36 | 8.68 | 0.3 | 0.31 | 11.55 | 15.5 |
| **MEBL17NFS0772** | 0.46 | 13.6 | 5.88 | <0.01 | 0.05 | 7.84 | 2.54 |
| **MEBL17NFS0789** | 0.43 | 13.75 | 2.06 | 0.01 | 0.01 | 0.72 | 0.28 |
| **MEBL17NFS0777** | 0.49 | 13.45 | 6.77 | 0.09 | 0.1 | 4.14 | 1.67 |
| **MEBL17NFS0788B** | 0.58 | 12.65 | 9.41 | 0.01 | 0.12 | 2.41 | 1.62 |
| **MEBL17NFS0831** | 0.46 | 7.25 | 11.8 | 0.5 | 0.34 | 11.05 | 20 |
| **MEBL17NFS0834** | 0.57 | 9.51 | 7.19 | 0.09 | 0.13 | 10.1 | 11.2 |
| **MEBL17NFS0775** | 0.24 | 4.99 | 8.84 | 0.23 | 0.14 | 17.95 | 7.29 |
| **MEBL17NFS0760** | 0.77 | 12.1 | 12.45 | 0.13 | 0.11 | 12.45 | 5.68 |
| **MEBL17NFS0769** | 0.23 | 4.54 | 8.81 | 0.29 | 0.11 | 23.7 | 6.78 |
| **MEBL17NFS0765** | 0.51 | 14.3 | 3.95 | 0.04 | 0.07 | 3.62 | 3.67 |
| **MEBL17NFS0767** | 0.22 | 4.22 | 8.31 | 0.24 | 0.34 | 13.2 | 17.65 |
| **MEBL17NFS0766** | 0.19 | 3.72 | 8.12 | 0.21 | 0.2 | 15.85 | 12.1 |
| **MEBL17NFS0770** | 0.23 | 4.46 | 8.23 | 0.26 | 0.12 | 18.5 | 10.35 |
| **MEBL17NFS0786B** | 0.17 | 2.91 | 5.91 | 0.13 | 0.49 | 9.17 | 17.9 |
| **MEBL17NFS0786** | 0.16 | 3.32 | 5.62 | 0.17 | 0.41 | 8.26 | 17.15 |
| **MEBL17NFS0689** | 0.52 | 10.7 | 10.35 | 0.03 | 0.15 | 8.58 | 6.99 |
| **MEBL17NFS0798** | 0.5 | 13.65 | 6.56 | 0.09 | 0.1 | 4.17 | 1.83 |
| **MEBL17NFS0771** | 0.72 | 12.25 | 7.25 | 0.03 | 0.13 | 5.64 | 3.88 |
| **IAG OKUM** | 0.38 | 8.14 | 12.05 | 0.36 | 0.18 | 21.7 | 7.97 |
| **MEBL18NFS1148AG01** | 0.37 | 10.3 | 5.72 | 0.021 | 0.16 | 6.92 | 15.3 |
| **MEBL18NFS1103AG01** | 0.66 | 9.93 | 8.5 | 0.083 | 0.15 | 9.71 | 10.2 |
| **MEBL18NFS1103BG01** | 0.75 | 15.3 | 14.85 | 0.031 | 0.08 | 4.94 | 1.57 |
| **MEBL18NFS1011AG01** | 0.29 | 5.09 | 7.97 | 0.275 | 0.16 | 16.65 | 9.59 |
| **LK-NP-1** | 1.12 | 15.2 | 13.35 | 0.021 | 0.18 | 7.21 | 10.2 |
| **IAG OKUM** | 0.36 | 7.76 | 11.7 | 0.341 | 0.17 | 21.4 | 7.67 |
| **MEBL18NFS1107AG01** | 0.27 | 4.87 | 8.65 | 0.266 | 0.17 | 17.75 | 9.37 |
| **MEBL18NFS1006AG01** | 0.61 | 17.2 | 4.21 | 0.031 | 0.05 | 1.72 | 2.2 |
| **MEBL18NFS1105AG01** | 0.45 | 13.3 | 5.11 | 0.025 | 0.08 | 2.96 | 4.04 |
| **MEBL18NFS1010AG01** | 0.51 | 15.8 | 5.14 | 0.027 | 0.05 | 2.85 | 2.04 |
| **MEBL18NFS1106AG01** | 0.74 | 12.6 | 12.7 | 0.01 | 0.05 | 12.3 | 2.71 |
| **MEBL18NFS1033AG01** | 0.45 | 9.12 | 11.5 | 0.407 | 0.16 | 18.4 | 9.77 |
| **MEBL18NFS1034AG01** | 1.84 | 12 | 16 | 0.008 | 0.22 | 3.3 | 10.65 |
| **MEBL18NFS0959AG01** | 1.64 | 12.2 | 13.6 | 0.002 | 0.3 | 3.25 | 7.44 |
| **MEBL18NFS0984AG01** | 0.98 | 13.4 | 10.55 | 0.03 | 0.12 | 6.37 | 9.42 |
| **MEBL18NFS1032AG01** | 1.54 | 11.65 | 18.2 | 0.002 | 0.18 | 7.51 | 2.51 |
| **MEBL18NFS0961BG01** | 0.74 | 7.83 | 10.1 | 0.118 | 0.19 | 18.5 | 8.51 |
| **MEBL18NFS0965BG01** | 0.24 | 4.61 | 8.7 | 0.251 | 0.19 | 16.8 | 9.72 |
| **MEBL18NFS0964AG01** | 0.32 | 6 | 8.57 | 0.281 | 0.15 | 18.75 | 9.79 |
| **MEBL18NFS0967AG01** | 0.4 | 13.55 | 4.33 | 0.035 | 0.05 | 1.93 | 0.76 |
| **MEBL18NFS1031AG01** | 0.51 | 15.9 | 3.38 | 0.002 | 0.03 | 2.73 | 2.12 |
| **MEBL18NFS0961AG01** | 0.37 | 7.02 | 9.17 | 0.283 | 0.17 | 17.4 | 7.89 |
| **MEBL18NFS1036AG01** | 0.24 | 13.25 | 1.78 | 0.008 | 0.04 | 2.01 | 2.8 |
| **MEBL18NFS1034AG02** | 2.11 | 12.95 | 16.75 | 0.007 | 0.26 | 4.86 | 8.21 |

**Table 1. (Continued)**

| Analyte | SrO | BaO | Na2O | K2O | P2O5 | LOI | Total |
|---|---|---|---|---|---|---|---|
| **Unit** | wt. % | wt. % | wt. % | wt. % | wt. % | wt. % | wt. % |
| **L.O.D.** | 0.01 | 0.01 | 0.01 | 0.01 | 0.01 | 0.01 | 0.01 |
| **MEBL17NFS0778** | 0.02 | 0.04 | 0.14 | 1.07 | 0.04 | 22.5 | 98.3 |
| **MEBL17NFS0768** | 0.03 | <0.01 | 1.3 | 0.01 | <0.01 | 24 | 100.46 |
| **MEBL17NFS0772** | 0.02 | 0.01 | 3.96 | 0.27 | 0.2 | 6.46 | 100.39 |
| **MEBL17NFS0789** | <0.01 | 0.06 | 4.68 | 2.15 | 0.09 | 7.54 | 98.38 |
| **MEBL17NFS0777** | 0.04 | 0.08 | 0.44 | 3.32 | 0.16 | 9.74 | 99.59 |
| **MEBL17NFS0788B** | <0.01 | 0.05 | 2.85 | 1.49 | 0.13 | 4.76 | 99.48 |
| **MEBL17NFS0831** | 0.08 | 0.1 | 0.07 | 2.22 | <0.01 | 30.1 | 98.02 |
| **MEBL17NFS0834** | 0.03 | 0.04 | 2.35 | 0.64 | 0.36 | 18.6 | 98.01 |
| **MEBL17NFS0775** | 0.02 | <0.01 | 0.02 | 0.05 | 0.01 | 20.6 | 95.18 |
| **MEBL17NFS0760** | 0.03 | <0.01 | 0.03 | 0.24 | 0.04 | 13.2 | 101.33 |
| **MEBL17NFS0769** | <0.01 | <0.01 | 0.01 | <0.01 | 0.02 | 15.4 | 98.09 |
| **MEBL17NFS0765** | 0.04 | 0.03 | 6.01 | 0.6 | 0.16 | 6.63 | 99.43 |
| **MEBL17NFS0767** | 0.02 | <0.01 | 0.61 | <0.01 | 0.01 | 27.3 | 100.82 |
| **MEBL17NFS0766** | 0.02 | <0.01 | 0.02 | <0.01 | 0.02 | 25.5 | 100.05 |
| **MEBL17NFS0770** | 0.02 | <0.01 | 0.02 | <0.01 | 0.01 | 19 | 99 |
| **MEBL17NFS0786B** | 0.01 | 0.02 | 0.05 | 0.72 | 0.02 | 25.7 | 99.8 |
| **MEBL17NFS0786** | 0.01 | 0.02 | 0.05 | 0.87 | 0.02 | 24.8 | 98.06 |
| **MEBL17NFS0689** | 0.03 | 0.06 | 0.47 | 1.98 | 0.04 | 17.1 | 98.5 |
| **MEBL17NFS0798** | 0.04 | 0.08 | 0.45 | 3.34 | 0.16 | 9.76 | 100.13 |
| **MEBL17NFS0771** | 0.01 | <0.01 | 4.58 | 0.1 | 0.15 | 7.38 | 97.62 |
| **IAG OKUM** | <0.01 | <0.01 | 1.19 | 0.04 | 0.02 | 4.75 | 101.28 |
| **MEBL18NFS1148AG01** | 0.04 | 0.02 | 2.43 | 0.74 | 0.13 | 16.45 | 99.1 |
| **MEBL18NFS1103AG01** | 0.06 | 0.03 | 2.08 | 0.67 | 0.3 | 16.9 | 99.17 |
| **MEBL18NFS1103BG01** | 0.01 | 0.01 | 4.02 | 0.13 | 0.24 | 5 | 100.33 |
| **MEBL18NFS1011AG01** | 0.08 | <0.01 | 0.02 | <0.01 | 0.01 | 22.4 | 98.94 |
| **LK-NP-1** | 0.02 | 0.02 | 2.41 | 0.45 | 0.11 | 0.32 | 98.91 |
| **IAG OKUM** | <0.01 | <0.01 | 1.14 | 0.04 | 0.01 | 4.72 | 98.91 |
| **MEBL18NFS1107AG01** | 0.07 | <0.01 | 0.01 | 0.01 | 0.03 | 24.1 | 98.07 |
| **MEBL18NFS1006AG01** | 0.03 | 0.12 | 2.26 | 3.8 | 0.2 | 4.39 | 99.92 |
| **MEBL18NFS1105AG01** | 0.04 | 0.09 | 2.14 | 2.88 | 0.16 | 7.12 | 98.9 |
| **MEBL18NFS1010AG01** | 0.03 | 0.08 | 3.09 | 2.69 | 0.2 | 4.63 | 99.74 |
| **MEBL18NFS1106AG01** | 0.03 | <0.01 | 2.47 | 0.03 | 0.06 | 8.47 | 98.07 |
| **MEBL18NFS1033AG01** | 0.02 | <0.01 | 0.02 | <0.01 | 0.01 | 20.3 | 98.96 |
| **MEBL18NFS1034AG01** | 0.01 | <0.01 | 3.11 | 0.02 | 0.23 | 9.66 | 98.75 |
| **MEBL18NFS0959AG01** | 0.01 | 0.01 | 2.76 | 0.25 | 0.13 | 8.32 | 99.31 |
| **MEBL18NFS0984AG01** | 0.02 | <0.01 | 1.58 | 0.35 | 0.07 | 16.95 | 99.44 |
| **MEBL18NFS1032AG01** | <0.01 | 0.02 | 0.29 | 0.55 | 0.1 | 9.25 | 98.5 |
| **MEBL18NFS0961BG01** | 0.02 | <0.01 | 0.01 | <0.01 | 0.56 | 17.1 | 98.78 |
| **MEBL18NFS0965BG01** | 0.04 | <0.01 | 0.02 | <0.01 | 0.01 | 25.3 | 98.08 |
| **MEBL18NFS0964AG01** | 0.01 | <0.01 | 0.01 | <0.01 | 0.01 | 20.1 | 99.59 |
| **MEBL18NFS0967AG01** | 0.02 | 0.1 | 0.93 | 3.41 | 0.14 | 5.52 | 101.08 |
| **MEBL18NFS1031AG01** | 0.02 | 0.04 | 6.27 | 1.27 | 0.23 | 4.12 | 98.92 |
| **MEBL18NFS0961AG01** | 0.02 | <0.01 | 0.02 | 0.01 | 0.02 | 16.45 | 99.12 |
| **MEBL18NFS1036AG01** | 0.02 | 0.04 | 1.54 | 3.22 | 0.09 | 5.59 | 100.63 |
| **MEBL18NFS1034AG02** | 0.02 | <0.01 | 1.93 | 0.07 | 0.29 | 6.39 | 96.05 |

**Table 1. (Continued)**

| Analyte | C | S | H2O+** | Cl | F | S.G.* | Ag |
|---|---|---|---|---|---|---|---|
| **Unit** | % | % | % | ppm | ppm | | ppm |
| **L.O.D.** | 0.01 | 0.01 | 0.01 | 50 | 20 | 0.01 | 0.5 |
| **MEBL17NFS0778** | 6.1 | 0.1 | 0.88 | <50 | 270 | 2.82 | <0.5 |
| **MEBL17NFS0768** | 6.37 | 0.09 | 1.74 | 50 | 280 | 2.83 | <0.5 |
| **MEBL17NFS0772** | 0.99 | 0.2 | 3.19 | <50 | 500 | 2.83 | <0.5 |
| **MEBL17NFS0789** | 5.69 | 0.9 | 1.1 | <50 | 440 | 2.6 | <0.5 |
| **MEBL17NFS0777** | 2.58 | 0.2 | 1.78 | <50 | 590 | 2.87 | <0.5 |
| **MEBL17NFS0788B** | 1.48 | 1.42 | 2.65 | <50 | 410 | 2.81 | <0.5 |
| **MEBL17NFS0831** | 8.62 | 1.73 | 1.17 | <50 | 440 | 2.96 | <0.5 |
| **MEBL17NFS0834** | 4.69 | 0.34 | 2.37 | <50 | 540 | 2.8 | <0.5 |
| **MEBL17NFS0775** | 4.82 | 0.02 | 3.78 | <50 | 240 | 2.87 | <0.5 |
| **MEBL17NFS0760** | 2.49 | 0.07 | 5.84 | <50 | 470 | 2.83 | <0.5 |
| **MEBL17NFS0769** | 3.06 | 0.01 | 5.44 | <50 | 290 | 2.82 | <0.5 |
| **MEBL17NFS0765** | 1.65 | 0.27 | 0.86 | <50 | 370 | 2.71 | <0.5 |
| **MEBL17NFS0767** | 7.3 | 0.07 | 1.79 | <50 | 250 | 2.86 | <0.5 |
| **MEBL17NFS0766** | 6.68 | 0.03 | 2.1 | <50 | 260 | 2.88 | <0.5 |
| **MEBL17NFS0770** | 4.41 | 0.24 | 3.77 | <50 | 240 | 2.81 | <0.5 |
| **MEBL17NFS0786B** | 7.15 | 0.03 | 0.51 | <50 | 240 | 2.85 | <0.5 |
| **MEBL17NFS0786** | 6.92 | 0.04 | 0.63 | <50 | 250 | 2.87 | <0.5 |
| **MEBL17NFS0689** | 4.33 | 0.11 | 2.96 | <50 | 350 | 2.9 | <0.5 |
| **MEBL17NFS0798** | 2.6 | 0.19 | 1.64 | <50 | 590 | 2.86 | <0.5 |
| **MEBL17NFS0771** | 1.93 | 0.83 | 2.81 | <50 | 380 | 2.79 | <0.5 |
| **IAG OKUM** | 0.02 | 0.02 | 5.7 | 50 | 190 | 2.95 | <0.5 |
| **MEBL18NFS1148AG01** | 4 | 0.08 | N/A | N/A | N/A | N/A | <0.5 |
| **MEBL18NFS1103AG01** | 4.21 | 0.08 | N/A | N/A | N/A | N/A | <0.5 |
| **MEBL18NFS1103BG01** | 0.54 | 0.44 | N/A | N/A | N/A | N/A | <0.5 |
| **MEBL18NFS1011AG01** | 5.63 | 0.16 | N/A | N/A | N/A | N/A | <0.5 |
| **LK-NP-1** | 0.02 | 0.03 | N/A | N/A | N/A | N/A | <0.5 |
| **IAG OKUM** | 0.05 | 0.02 | 6.11 | 110 | 120 | 2.91 | <0.5 |
| **MEBL18NFS1107AG01** | 6.19 | 0.08 | N/A | N/A | N/A | N/A | <0.5 |
| **MEBL18NFS1006AG01** | 0.71 | 0.12 | N/A | N/A | N/A | N/A | <0.5 |
| **MEBL18NFS1105AG01** | 2.07 | 0.16 | N/A | N/A | N/A | N/A | <0.5 |
| **MEBL18NFS1010AG01** | 0.77 | 0.16 | N/A | N/A | N/A | N/A | <0.5 |
| **MEBL18NFS1106AG01** | 1.17 | 3.23 | N/A | N/A | N/A | N/A | 1.8 |
| **MEBL18NFS1033AG01** | 4.23 | 0.01 | 8.4 | <50 | 240 | 2.78 | <0.5 |
| **MEBL18NFS1034AG01** | 2.03 | 0.15 | 4.14 | <50 | 270 | 2.82 | <0.5 |
| **MEBL18NFS0959AG01** | 1.65 | 0.2 | 4.41 | 70 | 280 | 2.78 | <0.5 |
| **MEBL18NFS0984AG01** | 4.11 | 0.07 | 3.38 | <50 | 240 | 2.88 | <0.5 |
| **MEBL18NFS1032AG01** | 1.54 | 0.1 | 6.31 | <50 | 250 | 2.83 | <0.5 |
| **MEBL18NFS0961BG01** | 3.4 | 0.01 | 7.19 | <50 | 1020 | 2.78 | <0.5 |
| **MEBL18NFS0965BG01** | 6.55 | 0.01 | 2.76 | <50 | 210 | 2.8 | <0.5 |
| **MEBL18NFS0964AG01** | 4.5 | 0.04 | 5 | 70 | 190 | 2.75 | <0.5 |
| **MEBL18NFS0967AG01** | 1.11 | 0.25 | 1.27 | <50 | 440 | 2.73 | <0.5 |
| **MEBL18NFS1031AG01** | 0.75 | 0.85 | 1.19 | <50 | 320 | 2.67 | <0.5 |
| **MEBL18NFS0961AG01** | 3.35 | 0.07 | 6.25 | <50 | 640 | 2.86 | <0.5 |
| **MEBL18NFS1036AG01** | 1.12 | 0.58 | 1.01 | <50 | 260 | 2.69 | <0.5 |
| **MEBL18NFS1034AG02** | 0.85 | 0.21 | 5.16 | <50 | 320 | 2.93 | <0.5 |

**S.G.: Specific Gravity*
***H2O+: Water of Crystallization – Combustion furnace and infrared absorption*

**Table 1. (Continued)**

| Analyte | Co | Cu | Mo | Ni | Cr | W | Ga |
|---|---|---|---|---|---|---|---|
| **Unit** | ppm | ppm | ppm | ppm | ppm | ppm | ppm |
| **L.O.D.** | 1 | 1 | 1 | 01 | 10 | 1 | 0.1 |
| **MEBL17NFS0778** | 55 | 41 | 1 | 571 | 1280 | 2 | 6 |
| **MEBL17NFS0768** | 90 | 62 | <1 | 1250 | 2210 | 3 | 7.5 |
| **MEBL17NFS0772** | 15 | 48 | <1 | 100 | 30 | 21 | 14.1 |
| **MEBL17NFS0789** | 11 | 245 | 4 | 55 | 50 | 2 | 15.5 |
| **MEBL17NFS0777** | 37 | 53 | 2 | 235 | 720 | 3 | 16.9 |
| **MEBL17NFS0788B** | 25 | 284 | 2 | 93 | 80 | 4 | 16.9 |
| **MEBL17NFS0831** | 137 | 385 | 8 | 1550 | 3810 | 21 | 21.4 |
| **MEBL17NFS0834** | 39 | 69 | 2 | 147 | 700 | 10 | 12.8 |
| **MEBL17NFS0775** | 67 | 39 | <1 | 1025 | 1850 | 6 | 5.9 |
| **MEBL17NFS0760** | 60 | 133 | <1 | 424 | 930 | 5 | 14.9 |
| **MEBL17NFS0769** | 93 | 27 | <1 | 1680 | 2160 | 4 | 5.4 |
| **MEBL17NFS0765** | 23 | 65 | 3 | 115 | 310 | 6 | 15.6 |
| **MEBL17NFS0767** | 71 | 15 | <1 | 1060 | 1750 | 2 | 6.1 |
| **MEBL17NFS0766** | 69 | 27 | <1 | 1035 | 1550 | 4 | 4.7 |
| **MEBL17NFS0770** | 88 | 47 | <1 | 1385 | 1970 | 5 | 5.6 |
| **MEBL17NFS0786B** | 43 | 15 | <1 | 685 | 1000 | 1 | 4.4 |
| **MEBL17NFS0786** | 55 | 22 | <1 | 855 | 1250 | 8 | 4.5 |
| **MEBL17NFS0689** | 49 | 72 | <1 | 181 | 190 | 4 | 10.8 |
| **MEBL17NFS0798** | 39 | 46 | 1 | 259 | 660 | 3 | 16.6 |
| **MEBL17NFS0771** | 25 | 36 | 1 | 150 | 210 | 5 | 15.3 |
| **IAG OKUM** | 15 | 104 | 1 | 58 | 160 | 1 | 11.1 |
| **MEBL18NFS1148AG01** | 37 | 63 | <1 | 192 | 610 | 15 | 14.1 |
| **MEBL18NFS1103AG01** | 30 | 76 | 1 | 152 | 230 | 21 | 19.2 |
| **MEBL18NFS1103BG01** | 77 | 98 | <1 | 1105 | 2000 | 3 | 6.5 |
| **MEBL18NFS1011AG01** | 57 | 174 | 1 | 156 | 170 | <1 | 18.6 |
| **LK-NP-1** | 71 | 39 | <1 | 1080 | 2050 | 1 | 6.8 |
| **IAG OKUM** | 20 | 45 | 1 | 77 | 240 | 3 | 21.4 |
| **MEBL18NFS1107AG01** | 18 | 37 | 1 | 64 | 190 | 2 | 15.9 |
| **MEBL18NFS1006AG01** | 18 | 51 | 1 | 72 | 210 | 2 | 19.2 |
| **MEBL18NFS1105AG01** | 39 | 121 | 1 | 107 | 80 | 6 | 10.6 |
| **MEBL18NFS1010AG01** | 84 | 108 | <1 | 917 | 3000 | 5 | 11.8 |
| **MEBL18NFS1106AG01** | 57 | 99 | 1 | 88 | 60 | <1 | 19 |
| **MEBL18NFS1033AG01** | 49 | 86 | 1 | 133 | 20 | 2 | 21.9 |
| **MEBL18NFS1034AG01** | 53 | 110 | 1 | 134 | 220 | 5 | 17.2 |
| **MEBL18NFS0959AG01** | 41 | 89 | 1 | 38 | 10 | 6 | 23 |
| **MEBL18NFS0984AG01** | 52 | 106 | <1 | 258 | 860 | 4 | 12.6 |
| **MEBL18NFS1032AG01** | 77 | 31 | <1 | 1175 | 1840 | 3 | 8 |
| **MEBL18NFS0961BG01** | 80 | 41 | 1 | 955 | 2080 | 7 | 8.7 |
| **MEBL18NFS0965BG01** | 17 | 38 | 2 | 97 | 250 | 3 | 18.6 |
| **MEBL18NFS0964AG01** | 10 | 27 | <1 | 26 | 20 | 6 | 20.1 |
| **MEBL18NFS0967AG01** | 82 | 70 | <1 | 1075 | 2020 | 1 | 10.4 |
| **MEBL18NFS1031AG01** | 6 | 6 | 1 | 21 | 100 | 9 | 25.8 |
| **MEBL18NFS0961AG01** | 54 | 110 | <1 | 58 | 50 | <1 | 22 |
| **MEBL18NFS1036AG01** | 90 | 46 | <1 | 955 | 2480 | <1 | 11.7 |
| **MEBL18NFS1034AG02** | 55 | 41 | 1 | 571 | 1280 | 2 | 6 |

**Table 1. (Continued)**

| Analyte | Ga | In | Tl | Cd | Li | Rb | Pb |
|---|---|---|---|---|---|---|---|
| **Unit** | ppm | ppm | ppm | ppm | ppm | ppm | ppm |
| **L.O.D.** | 0.1 | 0.05 | 0.02 | 0.5 | 10 | 0.2 | 2 |
| **MEBL17NFS0778** | <5 | 0.021 | 0.08 | <0.5 | 20 | 31.2 | 5 |
| **MEBL17NFS0768** | <5 | 0.031 | <0.02 | 0.5 | 30 | 0.5 | 12 |
| **MEBL17NFS0772** | <5 | 0.016 | <0.02 | <0.5 | 70 | 6.7 | <2 |
| **MEBL17NFS0789** | <5 | 2.28 | 0.07 | 8 | 10 | 64.3 | 14 |
| **MEBL17NFS0777** | <5 | 0.024 | 0.06 | <0.5 | 10 | 111.5 | 9 |
| **MEBL17NFS0788B** | <5 | 0.938 | 0.05 | 5 | 40 | 40.8 | 5 |
| **MEBL17NFS0831** | <5 | 0.103 | 0.03 | 0.9 | 20 | 48.5 | 5 |
| **MEBL17NFS0834** | <5 | 0.031 | <0.02 | <0.5 | 50 | 15.5 | 3 |
| **MEBL17NFS0775** | <5 | 0.024 | <0.02 | <0.5 | 10 | 0.3 | <2 |
| **MEBL17NFS0760** | <5 | 0.028 | <0.02 | <0.5 | 150 | 7.3 | <2 |
| **MEBL17NFS0769** | <5 | 0.015 | <0.02 | 0.6 | 10 | 0.2 | <2 |
| **MEBL17NFS0765** | <5 | 0.027 | 0.03 | <0.5 | 30 | 18.6 | 9 |
| **MEBL17NFS0767** | <5 | 0.012 | <0.02 | <0.5 | 30 | 0.3 | 4 |
| **MEBL17NFS0766** | <5 | 0.02 | <0.02 | 0.5 | 30 | 0.2 | 3 |
| **MEBL17NFS0770** | <5 | 0.019 | <0.02 | <0.5 | 10 | 0.2 | <2 |
| **MEBL17NFS0786B** | <5 | 0.016 | 0.03 | <0.5 | 10 | 21 | 3 |
| **MEBL17NFS0786** | <5 | 0.015 | 0.04 | <0.5 | 10 | 26.2 | 3 |
| **MEBL17NFS0689** | <5 | 0.03 | 0.03 | 0.6 | 60 | 55.9 | <2 |
| **MEBL17NFS0798** | <5 | 0.027 | 0.07 | <0.5 | 10 | 106 | 12 |
| **MEBL17NFS0771** | <5 | 0.024 | 0.02 | <0.5 | 60 | 1 | 10 |
| **IAG OKUM** | <5 | 0.037 | 0.03 | <0.5 | 30 | 16.9 | 2 |
| **MEBL18NFS1148AG01** | <5 | 0.039 | 0.02 | 0.7 | 40 | 15.8 | 6 |
| **MEBL18NFS1103AG01** | <5 | 0.054 | <0.02 | <0.5 | 60 | 2.8 | 7 |
| **MEBL18NFS1103BG01** | <5 | 0.025 | <0.02 | <0.5 | 60 | 0.2 | 6 |
| **MEBL18NFS1011AG01** | <5 | 0.018 | 0.08 | 0.6 | 10 | 12.4 | 4 |
| **LK-NP-1** | <5 | 0.024 | <0.02 | 0.6 | 60 | 0.4 | 3 |
| **IAG OKUM** | <5 | 0.017 | 0.07 | <0.5 | 10 | 123.5 | 2 |
| **MEBL18NFS1107AG01** | <5 | 0.02 | 0.06 | <0.5 | 10 | 95.2 | 2 |
| **MEBL18NFS1006AG01** | <5 | 0.019 | 0.06 | <0.5 | 20 | 86.7 | 5 |
| **MEBL18NFS1105AG01** | <5 | 0.015 | <0.02 | <0.5 | 50 | 0.8 | 8 |
| **MEBL18NFS1010AG01** | <5 | 0.027 | <0.02 | <0.5 | 30 | 0.2 | <2 |
| **MEBL18NFS1106AG01** | <5 | 0.06 | <0.02 | <0.5 | 30 | 0.2 | <2 |
| **MEBL18NFS1033AG01** | <5 | 0.082 | 0.02 | <0.5 | 50 | 6.3 | <2 |
| **MEBL18NFS1034AG01** | <5 | 0.038 | <0.02 | 0.5 | 80 | 12.8 | <2 |
| **MEBL18NFS0959AG01** | <5 | 0.069 | <0.02 | <0.5 | 110 | 13.3 | <2 |
| **MEBL18NFS0984AG01** | <5 | 0.047 | <0.02 | <0.5 | 20 | 0.3 | 3 |
| **MEBL18NFS1032AG01** | <5 | 0.022 | <0.02 | <0.5 | 80 | 0.2 | <2 |
| **MEBL18NFS0961BG01** | <5 | 0.023 | <0.02 | <0.5 | 10 | 0.2 | <2 |
| **MEBL18NFS0965BG01** | <5 | 0.02 | 0.04 | <0.5 | <10 | 100.5 | 11 |
| **MEBL18NFS0964AG01** | <5 | 0.01 | 0.02 | <0.5 | 20 | 32.6 | <2 |
| **MEBL18NFS0967AG01** | <5 | 0.027 | <0.02 | <0.5 | 20 | 0.3 | <2 |
| **MEBL18NFS1031AG01** | <5 | 0.012 | 0.04 | <0.5 | <10 | 99.3 | 11 |
| **MEBL18NFS0961AG01** | <5 | 0.027 | <0.02 | <0.5 | 30 | 0.7 | <2 |
| **MEBL18NFS1036AG01** | <5 | 0.009 | <0.02 | <0.5 | 10 | 0.9 | <2 |
| **MEBL18NFS1034AG02** | <5 | 0.021 | 0.08 | <0.5 | 20 | 31.2 | 5 |

**Table 1. (Continued)**

| Analyte | Zn | Bi | Hg | Sb | Sn | As | Te |
|---|---|---|---|---|---|---|---|
| **Unit** | ppm | ppm | ppm | ppm | ppm | ppm | ppm |
| **L.O.D.** | 2 | 0.01 | 0.005 | 0.05 | 1 | 0.1 | 0.01 |
| **MEBL17NFS0778** | 30 | 0.01 | 0.189 | 16.55 | <1 | 88.3 | 0.02 |
| **MEBL17NFS0768** | 60 | <0.01 | 0.01 | 0.13 | <1 | 13.3 | <0.01 |
| **MEBL17NFS0772** | 73 | 0.02 | 0.017 | 1.05 | 1 | 3 | 0.11 |
| **MEBL17NFS0789** | 3780 | 0.24 | 1.185 | 2.92 | 6 | 68.7 | 0.05 |
| **MEBL17NFS0777** | 41 | 0.22 | 0.098 | 11.5 | 1 | 236 | 0.17 |
| **MEBL17NFS0788B** | 1930 | 0.16 | 0.537 | 0.66 | 5 | 16.6 | 0.41 |
| **MEBL17NFS0831** | 56 | 0.29 | 0.032 | 12.05 | 3 | >250 | 0.06 |
| **MEBL17NFS0834** | 23 | 0.15 | 0.005 | 0.55 | 2 | >250 | 0.01 |
| **MEBL17NFS0775** | 46 | <0.01 | 0.04 | 1.79 | <1 | 71.7 | 0.01 |
| **MEBL17NFS0760** | 170 | 0.02 | 0.011 | 0.35 | <1 | 38.8 | 0.02 |
| **MEBL17NFS0769** | 54 | <0.01 | 0.006 | 0.15 | <1 | 39.7 | 0.06 |
| **MEBL17NFS0765** | 39 | 0.25 | 0.014 | 1.44 | 1 | 30.2 | 0.01 |
| **MEBL17NFS0767** | 53 | <0.01 | 0.01 | 0.79 | <1 | 38 | 0.01 |
| **MEBL17NFS0766** | 44 | <0.01 | 0.006 | 40 | <1 | >250 | 0.03 |
| **MEBL17NFS0770** | 42 | 0.01 | 0.014 | 0.53 | <1 | 49.7 | 0.03 |
| **MEBL17NFS0786B** | 30 | 0.02 | 0.384 | >250 | 1 | >250 | 0.05 |
| **MEBL17NFS0786** | 30 | 0.03 | 0.685 | >250 | <1 | >250 | <0.01 |
| **MEBL17NFS0689** | 72 | 0.02 | 0.017 | 1.29 | <1 | 34.2 | 0.04 |
| **MEBL17NFS0798** | 42 | 0.2 | 0.141 | 14 | 1 | >250 | 0.08 |
| **MEBL17NFS0771** | 112 | 0.12 | 0.018 | 0.67 | 1 | 22.9 | 0.03 |
| **IAG OKUM** | 38 | 0.24 | 0.005 | 0.5 | 1 | 4.9 | 0.01 |
| **MEBL18NFS1148AG01** | 125 | 0.21 | 0.01 | 0.58 | 1 | 46.9 | 0.03 |
| **MEBL18NFS1103AG01** | 128 | 0.19 | 0.006 | 1.01 | 1 | 49.1 | 0.02 |
| **MEBL18NFS1103BG01** | 60 | 0.02 | 0.006 | 21.9 | <1 | >250 | <0.01 |
| **MEBL18NFS1011AG01** | 103 | 0.02 | 0.017 | 0.05 | 1 | 1.4 | 0.03 |
| **LK-NP-1** | 61 | 0.02 | <0.005 | 26.9 | <1 | >250 | 0.06 |
| **IAG OKUM** | 52 | 0.35 | <0.005 | 3.95 | 1 | 141.5 | 0.03 |
| **MEBL18NFS1107AG01** | 24 | 0.13 | 0.027 | 2.63 | 1 | 107 | 0.05 |
| **MEBL18NFS1006AG01** | 46 | 0.36 | 0.019 | 2.7 | 1 | 77.6 | 0.06 |
| **MEBL18NFS1105AG01** | 105 | 0.05 | 0.017 | 40.5 | <1 | 245 | 0.03 |
| **MEBL18NFS1010AG01** | 94 | 0.03 | 0.018 | 0.33 | <1 | 50.7 | 0.06 |
| **MEBL18NFS1106AG01** | 113 | 0.07 | 0.092 | 0.29 | <1 | 45 | 0.02 |
| **MEBL18NFS1033AG01** | 103 | 0.04 | 0.01 | 0.15 | 1 | 15.5 | 0.03 |
| **MEBL18NFS1034AG01** | 90 | 0.01 | 0.031 | 26.4 | <1 | 20.8 | 0.01 |
| **MEBL18NFS0959AG01** | 147 | 0.02 | 0.007 | 0.46 | 1 | 43.1 | 0.01 |
| **MEBL18NFS0984AG01** | 71 | 0.03 | 0.19 | 0.11 | 1 | 15 | 0.02 |
| **MEBL18NFS1032AG01** | 58 | 0.02 | 0.009 | 32 | <1 | 149.5 | 0.01 |
| **MEBL18NFS0961BG01** | 52 | <0.01 | 0.012 | 1.04 | <1 | 67.9 | 0.04 |
| **MEBL18NFS0965BG01** | 87 | 0.24 | 0.164 | 4.28 | 1 | 65 | 0.02 |
| **MEBL18NFS0964AG01** | 26 | 0.05 | 0.019 | 0.61 | 1 | 2.6 | 0.01 |
| **MEBL18NFS0967AG01** | 63 | 0.05 | 0.09 | 1.79 | <1 | 65.6 | 0.1 |
| **MEBL18NFS1031AG01** | 6 | 0.19 | 0.019 | 0.52 | 1 | 2.5 | 0.02 |
| **MEBL18NFS0961AG01** | 129 | 0.01 | 0.023 | 0.58 | 1 | 69.7 | 0.02 |
| **MEBL18NFS1036AG01** | 66 | <0.01 | 0.07 | 0.05 | <1 | 0.3 | 0.01 |
| **MEBL18NFS1034AG02** | 30 | 0.01 | 0.052 | 16.55 | <1 | 88.3 | 0.02 |

**Table 1. (Continued)**

| Analyte | Se | Sc | Ba | Cs | Y | Sr | Hf |
|---|---|---|---|---|---|---|---|
| **Unit** | ppm | ppm | ppm | ppm | ppm | ppm | ppm |
| **L.O.D.** | 0.2 | 1 | 0.5 | 0.01 | 0.1 | 0.1 | 0.2 |
| **MEBL17NFS0778** | 0.3 | 18 | 366 | 0.58 | 9.4 | 199 | 0.7 |
| **MEBL17NFS0768** | 0.3 | 20 | 9.7 | 0.14 | 6.3 | 344 | 0.5 |
| **MEBL17NFS0772** | <0.2 | 6 | 82.9 | 0.19 | 5.6 | 181.5 | 2.5 |
| **MEBL17NFS0789** | 1.4 | 8 | 528 | 0.64 | 19.2 | 25.6 | 4 |
| **MEBL17NFS0777** | 0.2 | 16 | 756 | 2.47 | 14 | 355 | 4.2 |
| **MEBL17NFS0788B** | 1.9 | 12 | 463 | 0.38 | 16.4 | 21.7 | 3.2 |
| **MEBL17NFS0831** | 1 | 29 | 919 | 1.23 | 11.3 | 763 | 0.8 |
| **MEBL17NFS0834** | <0.2 | 22 | 366 | 0.48 | 18 | 313 | 3.2 |
| **MEBL17NFS0775** | 0.2 | 17 | 7 | 0.01 | 6 | 160 | 0.4 |
| **MEBL17NFS0760** | 0.4 | 35 | 32.8 | 0.16 | 17.7 | 306 | 1.3 |
| **MEBL17NFS0769** | 0.2 | 16 | 3.6 | 0.07 | 6.6 | 83.4 | 0.5 |
| **MEBL17NFS0765** | <0.2 | 14 | 275 | 0.38 | 13.6 | 334 | 3.6 |
| **MEBL17NFS0767** | 0.4 | 15 | 8.4 | 0.14 | 4.9 | 217 | 0.4 |
| **MEBL17NFS0766** | 0.2 | 14 | 4 | <0.01 | 4.1 | 263 | 0.3 |
| **MEBL17NFS0770** | 0.6 | 15 | 4.9 | 0.05 | 2.5 | 239 | 0.4 |
| **MEBL17NFS0786B** | 0.8 | 11 | 147 | 0.38 | 5.9 | 152.5 | 0.5 |
| **MEBL17NFS0786** | 0.8 | 11 | 172.5 | 0.42 | 5.5 | 134 | 0.3 |
| **MEBL17NFS0689** | 0.2 | 33 | 516 | 1.12 | 12.8 | 286 | 0.8 |
| **MEBL17NFS0798** | <0.2 | 16 | 729 | 2.39 | 13.3 | 327 | 4.2 |
| **MEBL17NFS0771** | 0.9 | 19 | 32.9 | 0.05 | 24.1 | 89.3 | 2.9 |
| **IAG OKUM** | <0.2 | 8 | 147.5 | 0.67 | 12.6 | 297 | 2.4 |
| **MEBL18NFS1148AG01** | <0.2 | 29 | 235 | 0.36 | 16 | 466 | 2.8 |
| **MEBL18NFS1103AG01** | 0.3 | 23 | 46.9 | 0.15 | 20.3 | 68.8 | 3.1 |
| **MEBL18NFS1103BG01** | <0.2 | 18 | 5.9 | 0.02 | 6.2 | 672 | 0.4 |
| **MEBL18NFS1011AG01** | 0.2 | 31 | 140.5 | 0.57 | 21.6 | 169.5 | 2.4 |
| **LK-NP-1** | 0.2 | 17 | 13.4 | 0.05 | 6.9 | 620 | 0.6 |
| **IAG OKUM** | <0.2 | 14 | 1135 | 2.72 | 15.5 | 226 | 4.9 |
| **MEBL18NFS1107AG01** | <0.2 | 11 | 831 | 2.19 | 12 | 378 | 3.5 |
| **MEBL18NFS1006AG01** | 0.2 | 11 | 713 | 2 | 13 | 202 | 4 |
| **MEBL18NFS1105AG01** | 0.6 | 38 | 14.3 | 0.09 | 18.3 | 226 | 1.3 |
| **MEBL18NFS1010AG01** | <0.2 | 30 | 3.5 | 0.14 | 8.5 | 174 | 0.6 |
| **MEBL18NFS1106AG01** | 0.3 | 42 | 9.2 | 0.09 | 21.4 | 82.1 | 2.1 |
| **MEBL18NFS1033AG01** | 0.4 | 43 | 103 | 0.13 | 39.1 | 67.6 | 3 |
| **MEBL18NFS1034AG01** | 0.3 | 37 | 36.6 | 1.46 | 11.2 | 202 | 1 |
| **MEBL18NFS0959AG01** | 0.3 | 41 | 138.5 | 0.41 | 35.6 | 52.5 | 2.6 |
| **MEBL18NFS0984AG01** | <0.2 | 32 | 5.8 | 0.17 | 17.8 | 219 | 3.8 |
| **MEBL18NFS1032AG01** | 0.2 | 18 | 4 | 0.06 | 5.4 | 349 | 0.4 |
| **MEBL18NFS0961BG01** | <0.2 | 22 | 6.5 | 0.09 | 7.3 | 140.5 | 0.5 |
| **MEBL18NFS0965BG01** | 0.2 | 9 | 899 | 1.99 | 10.5 | 189 | 3.3 |
| **MEBL18NFS0964AG01** | 0.2 | 7 | 392 | 0.77 | 4.9 | 170.5 | 2.4 |
| **MEBL18NFS0967AG01** | 0.2 | 21 | 4.8 | 0.11 | 7.6 | 178 | 0.6 |
| **MEBL18NFS1031AG01** | 0.2 | 2 | 421 | 2.05 | 3.8 | 136.5 | 3.9 |
| **MEBL18NFS0961AG01** | 0.3 | 47 | 9.3 | 0.12 | 27.3 | 154 | 2.7 |
| **MEBL18NFS1036AG01** | <0.2 | 27 | 7.6 | 0.2 | 8.6 | 15.9 | 0.5 |
| **MEBL18NFS1034AG02** | 0.3 | 18 | 366 | 0.58 | 9.4 | 199 | 0.7 |

**Table 1. (Continued)**

| Analyte | Ta | Nb | Zr | V | Re | La | Ce |
|---|---|---|---|---|---|---|---|
| **Unit** | ppm | ppm | ppm | ppm | ppm | ppm | ppm |
| **L.O.D.** | 0.1 | 0.2 | 2 | 5 | 0.001 | 0.1 | 0.1 |
| **MEBL17NFS0778** | <0.1 | 0.8 | 25 | 123 | 0.001 | 1.5 | 3.9 |
| **MEBL17NFS0768** | <0.1 | 0.5 | 16 | 137 | 0.001 | 0.7 | 1.8 |
| **MEBL17NFS0772** | 0.1 | 2.3 | 85 | 64 | 0.001 | 13.5 | 29.5 |
| **MEBL17NFS0789** | 0.4 | 5.6 | 144 | 54 | 0.005 | 16.4 | 34.8 |
| **MEBL17NFS0777** | 0.3 | 5 | 155 | 111 | 0.003 | 27.9 | 57.3 |
| **MEBL17NFS0788B** | 0.2 | 4.3 | 119 | 105 | 0.004 | 14.4 | 32.6 |
| **MEBL17NFS0831** | <0.1 | 1 | 25 | 249 | 0.002 | 2.2 | 5.2 |
| **MEBL17NFS0834** | 0.2 | 4.4 | 119 | 165 | <0.001 | 36.2 | 78.6 |
| **MEBL17NFS0775** | <0.1 | 0.4 | 16 | 115 | <0.001 | 1.1 | 2.8 |
| **MEBL17NFS0760** | <0.1 | 1.5 | 43 | 263 | 0.001 | 4 | 9.9 |
| **MEBL17NFS0769** | <0.1 | 0.3 | 15 | 107 | <0.001 | 0.3 | 0.9 |
| **MEBL17NFS0765** | 0.3 | 5.2 | 132 | 115 | 0.002 | 31 | 63.9 |
| **MEBL17NFS0767** | <0.1 | 0.4 | 11 | 102 | <0.001 | 0.6 | 1.6 |
| **MEBL17NFS0766** | <0.1 | 0.2 | 9 | 89 | <0.001 | 0.5 | 1.1 |
| **MEBL17NFS0770** | <0.1 | 0.3 | 12 | 104 | 0.001 | 0.2 | 0.7 |
| **MEBL17NFS0786B** | <0.1 | 0.4 | 15 | 55 | <0.001 | 1.5 | 3.3 |
| **MEBL17NFS0786** | <0.1 | 0.3 | 10 | 59 | <0.001 | 2.4 | 4.6 |
| **MEBL17NFS0689** | <0.1 | 1 | 29 | 194 | <0.001 | 1.7 | 4.7 |
| **MEBL17NFS0798** | 0.3 | 4.8 | 151 | 116 | 0.001 | 26.4 | 54.1 |
| **MEBL17NFS0771** | 0.2 | 3.3 | 102 | 158 | 0.001 | 16.5 | 35.8 |
| **IAG OKUM** | 0.4 | 3.5 | 96 | 69 | <0.001 | 19.8 | 38.8 |
| **MEBL18NFS1148AG01** | 0.3 | 2.6 | 103 | 188 | <0.001 | 58.4 | 108.5 |
| **MEBL18NFS1103AG01** | 0.4 | 4.8 | 118 | 181 | <0.001 | 23.4 | 45 |
| **MEBL18NFS1103BG01** | 0.1 | 0.5 | 16 | 135 | <0.001 | 1 | 2.6 |
| **MEBL18NFS1011AG01** | 0.3 | 4.4 | 85 | 305 | 0.001 | 8.7 | 18.3 |
| **LK-NP-1** | 0.2 | 0.7 | 17 | 119 | <0.001 | 3.3 | 6.5 |
| **IAG OKUM** | 0.6 | 6.8 | 180 | 126 | <0.001 | 41.3 | 77 |
| **MEBL18NFS1107AG01** | 0.5 | 4.7 | 128 | 102 | 0.001 | 27.9 | 52.8 |
| **MEBL18NFS1006AG01** | 0.5 | 5.6 | 154 | 99 | <0.001 | 33.3 | 63.4 |
| **MEBL18NFS1105AG01** | 0.2 | 1.5 | 44 | 273 | 0.001 | 2.4 | 6.1 |
| **MEBL18NFS1010AG01** | <0.1 | 0.8 | 22 | 188 | <0.001 | 0.9 | 2.2 |
| **MEBL18NFS1106AG01** | 0.2 | 3.9 | 82 | 422 | 0.002 | 3.7 | 10.2 |
| **MEBL18NFS1033AG01** | 0.2 | 4.4 | 105 | 436 | 0.002 | 6.9 | 17.6 |
| **MEBL18NFS1034AG01** | 0.1 | 2.4 | 36 | 291 | 0.001 | 1.9 | 5 |
| **MEBL18NFS0959AG01** | 0.2 | 4.2 | 95 | 436 | 0.002 | 6.7 | 16.6 |
| **MEBL18NFS0984AG01** | 0.2 | 5.4 | 143 | 172 | <0.001 | 87.4 | 203 |
| **MEBL18NFS1032AG01** | <0.1 | 0.4 | 13 | 102 | <0.001 | 1.1 | 2.6 |
| **MEBL18NFS0961BG01** | <0.1 | 0.6 | 17 | 130 | 0.001 | 2 | 3 |
| **MEBL18NFS0965BG01** | 0.3 | 4.7 | 133 | 57 | <0.001 | 28.4 | 57.2 |
| **MEBL18NFS0964AG01** | 0.1 | 2.7 | 95 | 69 | <0.001 | 14 | 30.9 |
| **MEBL18NFS0967AG01** | <0.1 | 0.8 | 20 | 142 | <0.001 | 1.8 | 4.7 |
| **MEBL18NFS1031AG01** | 0.4 | 3 | 118 | 20 | <0.001 | 21.6 | 44.3 |
| **MEBL18NFS0961AG01** | 0.2 | 4.5 | 103 | 466 | 0.003 | 4.9 | 13.5 |
| **MEBL18NFS1036AG01** | <0.1 | 0.3 | 18 | 168 | <0.001 | 0.5 | 1.3 |
| **MEBL18NFS1034AG02** | <0.1 | 0.8 | 25 | 123 | 0.001 | 1.5 | 3.9 |

**Table 1. (Continued)**

| Analyte | Pr | Nd | Sm | Eu | Gd | Tb | Dy |
|---|---|---|---|---|---|---|---|
| **Unit** | ppm | ppm | ppm | ppm | ppm | ppm | ppm |
| **L.O.D.** | 0.03 | 0.1 | 0.03 | 0.03 | 0.05 | 0.01 | 0.05 |
| **MEBL17NFS0778** | 0.6 | 3.1 | 1.06 | 0.38 | 1.36 | 0.24 | 1.54 |
| **MEBL17NFS0768** | 0.3 | 1.7 | 0.69 | 0.23 | 0.83 | 0.15 | 1.09 |
| **MEBL17NFS0772** | 3.7 | 15.4 | 2.88 | 0.8 | 1.79 | 0.21 | 1.1 |
| **MEBL17NFS0789** | 4.32 | 16 | 3.32 | 1.06 | 3.23 | 0.52 | 3.16 |
| **MEBL17NFS0777** | 6.74 | 25.1 | 4.55 | 1.12 | 3.32 | 0.45 | 2.49 |
| **MEBL17NFS0788B** | 4.12 | 16.6 | 3.33 | 0.86 | 2.93 | 0.45 | 2.66 |
| **MEBL17NFS0831** | 0.81 | 3.7 | 1.32 | 0.71 | 1.86 | 0.32 | 1.92 |
| **MEBL17NFS0834** | 10.15 | 41.8 | 8.54 | 2.04 | 6.35 | 0.73 | 3.52 |
| **MEBL17NFS0775** | 0.43 | 2.1 | 0.77 | 0.18 | 0.86 | 0.15 | 0.97 |
| **MEBL17NFS0760** | 1.4 | 6.5 | 1.52 | 0.51 | 2.22 | 0.41 | 2.86 |
| **MEBL17NFS0769** | 0.16 | 1 | 0.41 | 0.14 | 0.71 | 0.16 | 1.01 |
| **MEBL17NFS0765** | 7.6 | 28.5 | 4.99 | 1.18 | 3.52 | 0.46 | 2.44 |
| **MEBL17NFS0767** | 0.24 | 1.3 | 0.47 | 0.23 | 0.68 | 0.12 | 0.8 |
| **MEBL17NFS0766** | 0.2 | 1.1 | 0.41 | 0.21 | 0.62 | 0.1 | 0.7 |
| **MEBL17NFS0770** | 0.11 | 0.6 | 0.33 | 0.16 | 0.41 | 0.07 | 0.43 |
| **MEBL17NFS0786B** | 0.49 | 2.4 | 0.7 | 0.48 | 0.84 | 0.15 | 0.91 |
| **MEBL17NFS0786** | 0.59 | 2.6 | 0.6 | 0.51 | 0.83 | 0.14 | 0.81 |
| **MEBL17NFS0689** | 0.72 | 3.9 | 1.26 | 0.48 | 1.7 | 0.31 | 2.05 |
| **MEBL17NFS0798** | 6.32 | 24.2 | 4.44 | 1.03 | 3.08 | 0.42 | 2.39 |
| **MEBL17NFS0771** | 4.52 | 18.5 | 3.68 | 1.19 | 3.42 | 0.57 | 3.56 |
| **IAG OKUM** | 5.09 | 19.1 | 3.96 | 0.87 | 2.95 | 0.4 | 2.19 |
| **MEBL18NFS1148AG01** | 14.3 | 53.2 | 9.14 | 2.25 | 5.61 | 0.67 | 3.37 |
| **MEBL18NFS1103AG01** | 5.88 | 22.2 | 4.55 | 1.17 | 3.97 | 0.53 | 3.5 |
| **MEBL18NFS1103BG01** | 0.45 | 2 | 0.8 | 0.29 | 0.99 | 0.15 | 1.13 |
| **MEBL18NFS1011AG01** | 2.49 | 11.2 | 3.13 | 1.01 | 3.64 | 0.59 | 3.98 |
| **LK-NP-1** | 0.94 | 4.1 | 1.03 | 0.34 | 1.21 | 0.17 | 1.12 |
| **IAG OKUM** | 9.56 | 35.2 | 5.95 | 1.31 | 4.04 | 0.58 | 3.04 |
| **MEBL18NFS1107AG01** | 6.49 | 24.1 | 4.68 | 1.45 | 3.12 | 0.38 | 2.24 |
| **MEBL18NFS1006AG01** | 7.86 | 28.4 | 4.97 | 1.12 | 3.31 | 0.41 | 2.28 |
| **MEBL18NFS1105AG01** | 1.08 | 5.5 | 1.58 | 0.48 | 2.38 | 0.42 | 3.1 |
| **MEBL18NFS1010AG01** | 0.31 | 1.7 | 0.76 | 0.23 | 1.2 | 0.23 | 1.58 |
| **MEBL18NFS1106AG01** | 1.58 | 8 | 2.62 | 1.15 | 3.4 | 0.66 | 4.21 |
| **MEBL18NFS1033AG01** | 2.67 | 13.2 | 4.11 | 1.28 | 5.56 | 1.07 | 7.01 |
| **MEBL18NFS1034AG01** | 0.76 | 3.6 | 1.21 | 0.54 | 2.05 | 0.38 | 2.01 |
| **MEBL18NFS0959AG01** | 2.55 | 12.9 | 4.21 | 1.2 | 5.64 | 0.96 | 6.28 |
| **MEBL18NFS0984AG01** | 26.5 | 106 | 17.25 | 3.06 | 9.67 | 0.85 | 4.58 |
| **MEBL18NFS1032AG01** | 0.39 | 1.7 | 0.64 | 0.21 | 0.87 | 0.14 | 0.97 |
| **MEBL18NFS0961BG01** | 0.38 | 1.9 | 0.64 | 0.2 | 0.93 | 0.18 | 1.29 |
| **MEBL18NFS0965BG01** | 6.56 | 23.6 | 4.29 | 1 | 3.4 | 0.35 | 1.99 |
| **MEBL18NFS0964AG01** | 3.91 | 16 | 3.2 | 0.84 | 1.88 | 0.23 | 1.15 |
| **MEBL18NFS0967AG01** | 0.76 | 3.5 | 0.95 | 0.46 | 1.24 | 0.21 | 1.46 |
| **MEBL18NFS1031AG01** | 6.03 | 19.5 | 4.53 | 1.88 | 2.92 | 1.22 | 2.9 |
| **MEBL18NFS0961AG01** | 2.01 | 11.1 | 3.51 | 1.52 | 4.6 | 0.81 | 5.12 |
| **MEBL18NFS1036AG01** | 0.22 | 1.2 | 0.78 | 0.3 | 1.14 | 0.22 | 1.54 |
| **MEBL18NFS1034AG02** | 0.6 | 3.1 | 1.06 | 0.38 | 1.36 | 0.24 | 1.54 |

**Table 1. (Continued)**

| Analyte | Ho | Er | Tm | Yb | Lu | U | Th |
|---|---|---|---|---|---|---|---|
| **Unit** | ppm | ppm | ppm | ppm | ppm | ppm | ppm |
| **L.O.D.** | 0.01 | 0.03 | 0.01 | 0.03 | 0.01 | 0.05 | 0.05 |
| **MEBL17NFS0778** | 0.3 | 1.05 | 0.15 | 0.97 | 0.15 | 0.06 | 0.05 |
| **MEBL17NFS0768** | 0.21 | 0.67 | 0.09 | 0.65 | 0.1 | <0.05 | 1.66 |
| **MEBL17NFS0772** | 0.18 | 0.45 | 0.07 | 0.44 | 0.06 | 0.58 | 2.92 |
| **MEBL17NFS0789** | 0.62 | 1.93 | 0.3 | 1.81 | 0.29 | 0.95 | 5.91 |
| **MEBL17NFS0777** | 0.46 | 1.43 | 0.21 | 1.26 | 0.2 | 1.79 | 2.69 |
| **MEBL17NFS0788B** | 0.56 | 1.68 | 0.26 | 1.51 | 0.24 | 0.61 | 0.16 |
| **MEBL17NFS0831** | 0.37 | 1.14 | 0.16 | 0.93 | 0.15 | 0.2 | 6.51 |
| **MEBL17NFS0834** | 0.6 | 1.59 | 0.21 | 1.34 | 0.21 | 2.28 | 0.11 |
| **MEBL17NFS0775** | 0.2 | 0.55 | 0.09 | 0.64 | 0.09 | 0.21 | 0.2 |
| **MEBL17NFS0760** | 0.62 | 1.91 | 0.29 | 1.88 | 0.28 | 0.13 | <0.05 |
| **MEBL17NFS0769** | 0.23 | 0.72 | 0.1 | 0.64 | 0.1 | <0.05 | 6.24 |
| **MEBL17NFS0765** | 0.44 | 1.37 | 0.19 | 1.33 | 0.2 | 2.43 | 0.05 |
| **MEBL17NFS0767** | 0.15 | 0.55 | 0.08 | 0.47 | 0.06 | <0.05 | <0.05 |
| **MEBL17NFS0766** | 0.13 | 0.43 | 0.06 | 0.5 | 0.06 | <0.05 | <0.05 |
| **MEBL17NFS0770** | 0.09 | 0.31 | 0.04 | 0.28 | 0.05 | <0.05 | 0.23 |
| **MEBL17NFS0786B** | 0.19 | 0.6 | 0.08 | 0.54 | 0.08 | 0.09 | 0.11 |
| **MEBL17NFS0786** | 0.17 | 0.51 | 0.08 | 0.43 | 0.08 | 0.06 | 0.11 |
| **MEBL17NFS0689** | 0.45 | 1.46 | 0.2 | 1.41 | 0.21 | <0.05 | 5.65 |
| **MEBL17NFS0798** | 0.42 | 1.34 | 0.2 | 1.24 | 0.22 | 1.7 | 2.06 |
| **MEBL17NFS0771** | 0.75 | 2.3 | 0.36 | 2.13 | 0.35 | 0.62 | 4.53 |
| **IAG OKUM** | 0.41 | 1.17 | 0.14 | 0.92 | 0.15 | 1.16 | 9.66 |
| **MEBL18NFS1148AG01** | 0.65 | 1.58 | 0.2 | 1.31 | 0.19 | 1.79 | 4.33 |
| **MEBL18NFS1103AG01** | 0.71 | 1.92 | 0.32 | 1.84 | 0.32 | 1.35 | 0.12 |
| **MEBL18NFS1103BG01** | 0.22 | 0.65 | 0.1 | 0.69 | 0.09 | <0.05 | 1.66 |
| **MEBL18NFS1011AG01** | 0.76 | 2.4 | 0.29 | 2.12 | 0.33 | 0.41 | 0.85 |
| **LK-NP-1** | 0.29 | 0.66 | 0.11 | 0.63 | 0.09 | 0.06 | 9.47 |
| **IAG OKUM** | 0.52 | 1.56 | 0.19 | 1.48 | 0.22 | 2.63 | 6.26 |
| **MEBL18NFS1107AG01** | 0.44 | 1.21 | 0.17 | 1.22 | 0.17 | 1.87 | 8.12 |
| **MEBL18NFS1006AG01** | 0.45 | 1.21 | 0.17 | 1.18 | 0.18 | 2.28 | 0.22 |
| **MEBL18NFS1105AG01** | 0.64 | 2.12 | 0.38 | 1.74 | 0.31 | 0.07 | 0.2 |
| **MEBL18NFS1010AG01** | 0.37 | 1 | 0.16 | 0.93 | 0.13 | <0.05 | 0.25 |
| **MEBL18NFS1106AG01** | 0.9 | 2.62 | 0.35 | 2.39 | 0.38 | 0.06 | 0.45 |
| **MEBL18NFS1033AG01** | 1.56 | 4.55 | 0.68 | 4.49 | 0.69 | 0.14 | 0.17 |
| **MEBL18NFS1034AG01** | 0.47 | 1.46 | 0.21 | 1.2 | 0.21 | 0.05 | 0.48 |
| **MEBL18NFS0959AG01** | 1.45 | 3.9 | 0.61 | 3.87 | 0.63 | 0.1 | 10.4 |
| **MEBL18NFS0984AG01** | 0.75 | 1.75 | 0.21 | 1.21 | 0.19 | 2.46 | 0.11 |
| **MEBL18NFS1032AG01** | 0.22 | 0.61 | 0.1 | 0.54 | 0.1 | <0.05 | 0.05 |
| **MEBL18NFS0961BG01** | 0.3 | 0.91 | 0.13 | 0.76 | 0.12 | <0.05 | 6.68 |
| **MEBL18NFS0965BG01** | 0.4 | 1.19 | 0.18 | 1.06 | 0.16 | 1.45 | 1.87 |
| **MEBL18NFS0964AG01** | 0.18 | 0.56 | 0.08 | 0.38 | 0.08 | 0.61 | 0.1 |
| **MEBL18NFS0967AG01** | 0.34 | 0.92 | 0.11 | 0.86 | 0.15 | 0.05 | 3.96 |
| **MEBL18NFS1031AG01** | 1.12 | 1.4 | 1.06 | 1.22 | 1.03 | 2.16 | 0.35 |
| **MEBL18NFS0961AG01** | 1.14 | 3.19 | 0.48 | 3.11 | 0.51 | 0.1 | <0.05 |
| **MEBL18NFS1036AG01** | 0.37 | 0.97 | 0.16 | 1.04 | 0.15 | <0.05 | 0.11 |
| **MEBL18NFS1034AG02** | 0.3 | 1.05 | 0.15 | 0.97 | 0.15 | 0.06 | 0.05 |

**Table 2. Precision and Accuracy of standard material and duplicate results**

| | SiO2 | TiO2 | Al2O3 | Fe2O3 | Cr2O3 | MnO | MgO | CaO | SrO | BaO | Na2O | K2O | P2O5 | LOI |
|---|---|---|---|---|---|---|---|---|---|---|---|---|---|---|
| **MEBL18NFS1034AG01** | 41.7 | 1.84 | 12 | - | 16 | 0.008 | 0.22 | 3.3 | 10.65 | 0.01 | <0.01 | 3.11 | 0.02 | 0.23 |
| **MEBL18NFS1034AG02 Duplicate** | 42.2 | 2.11 | 12.95 | - | 16.75 | 0.007 | 0.26 | 4.86 | 8.21 | 0.02 | <0.01 | 1.93 | 0.07 | 0.29 |
| **STD** | 0.35 | 0.19 | 0.67 | - | 0.53 | 0.00 | 0.03 | 1.10 | 1.73 | 0.01 | - | 0.83 | 0.04 | 0.04 |
| **Mean** | 41.95 | 1.975 | 12.47 | - | 16.37 | 0.007 | 0.24 | 4.08 | 9.43 | 0.015 | - | 2.52 | 0.045 | 0.26 |
| **RSD (%) - Precision** | 0.84 | 9.67 | 5.38 | - | 3.24 | 9.43 | 11.79 | 27.04 | 18.30 | 47.14 | - | 33.11 | 78.57 | 16.32 |

| | **Total** | **C** | **S** | **H2O+**** | **Cl** | **F** | **S.G.*** | **Ag** | **As** | **Ba** | **Bi** | **Cd** | **Ce** | **Co** |
|---|---|---|---|---|---|---|---|---|---|---|---|---|---|---|
| **MEBL18NFS1034AG01** | 98.75 | 2.03 | 0.15 | 4.14 | <50 | 270 | 2.82 | <0.5 | 45 | 9.2 | 0.07 | <0.5 | 10.2 | 57 |
| **MEBL18NFS1034AG02 Duplicate** | 96.05 | 0.85 | 0.21 | 5.16 | <50 | 320 | 2.93 | <0.5 | 69.7 | 9.3 | 0.01 | <0.5 | 13.5 | 54 |
| **STD** | 1.91 | 0.83 | 0.04 | 0.72 | - | 35.36 | - | - | 17.47 | 0.07 | 0.04 | - | 2.33 | 2.12 |
| **Mean** | 97.4 | 1.44 | 0.18 | 4.65 | - | 295 | - | - | 57.35 | 9.25 | 0.04 | - | 11.85 | 55.5 |
| **RSD (%) - Precision** | 1.96 | 57.94 | 23.57 | 15.51 | - | 11.98 | - | - | 30.45 | 0.76 | 106 | - | 19.69 | 3.82 |

**S.G.: Specific Gravity*
***H2O+: Water of Crystallization – Combustion furnace and infrared absorption*

| | **Cr** | **Cs** | **Cu** | **Dy** | **Er** | **Eu** | **Ga** | **Gd** | **Ge** | **Hf** | **Hg** | **Ho** | **In** | **La** |
|---|---|---|---|---|---|---|---|---|---|---|---|---|---|---|
| **MEBL18NFS1034AG01** | 60 | 0.09 | 99 | 4.21 | 2.62 | 1.15 | 19 | 3.4 | <5 | 2.1 | 0.031 | 0.9 | 0.06 | 3.7 |
| **MEBL18NFS1034AG02 Duplicate** | 50 | 0.12 | 110 | 5.12 | 3.19 | 1.52 | 22 | 4.6 | <5 | 2.7 | 0.052 | 1.14 | 0.027 | 4.9 |
| **STD** | 7.07 | 0.02 | 7.78 | 0.64 | 0.40 | 0.26 | 2.12 | 0.85 | - | 0.42 | 0.01 | 0.17 | 0.02 | 0.85 |
| **Mean** | 55 | 0.105 | 104.5 | 4.665 | 2.905 | 1.335 | 20.5 | 4 | - | 2.4 | 0.041 | 1.02 | 0.043 | 4.3 |

| | | | | | | | | | | | | | | |
|---|---|---|---|---|---|---|---|---|---|---|---|---|---|---|
| **RSD (%) - Precision** | 12.86 | 20.20 | 7.44 | 13.79 | 13.87 | 19.60 | 10.35 | 21.21 | - | 17.68 | 35.78 | 16.64 | 53.64 | 19.73 |

| | **Li** | **Lu** | **Mo** | **Nb** | **Nd** | **Ni** | **Pb** | **Pr** | **Rb** | **Re** | **Sb** | **Sc** | **Se** | **Sm** |
|---|---|---|---|---|---|---|---|---|---|---|---|---|---|---|
| **MEBL18NFS1034AG01** | 30 | 0.38 | 1 | 3.9 | 8 | 88 | <2 | 1.58 | 0.2 | 0.002 | 0.29 | 42 | 0.3 | 2.62 |
| **MEBL18NFS1034AG02 Duplicate** | 30 | 0.51 | <1 | 4.5 | 11.1 | 58 | <2 | 2.01 | 0.7 | 0.003 | 0.58 | 47 | 0.3 | 3.51 |
| **STD** | 0.00 | 0.09 | - | 0.42 | 2.19 | 21.21 | - | 0.30 | 0.35 | 0.00 | 0.21 | 3.54 | 0.00 | 0.63 |
| **Mean** | 30 | 0.445 | - | 4.2 | 9.55 | 73 | - | 1.795 | 0.45 | 0.0025 | 0.435 | 44.5 | 0.3 | 3.065 |
| **RSD (%) - Precision** | 0.00 | 20.66 | - | 10.10 | 22.95 | 29.06 | - | 16.94 | 78.57 | 28.28 | 47.14 | 7.95 | 0.00 | 20.53 |

| | **Sn** | **Sr** | **Ta** | **Tb** | **Te** | **Th** | **Tl** | **Tm** | **U** | **V** | **W** | **Y** | **Yb** | **Zn** |
|---|---|---|---|---|---|---|---|---|---|---|---|---|---|---|
| **MEBL18NFS1034AG01** | - | 82.1 | 0.2 | 0.66 | 0.06 | 0.25 | <0.02 | 0.35 | 0.06 | 422 | <1 | 21.4 | 2.39 | 113 |
| **MEBL18NFS1034AG02 Duplicate** | - | 154 | 0.2 | 0.81 | 0.02 | 0.35 | <0.02 | 0.48 | 0.1 | 466 | <1 | 27.3 | 3.11 | 129 |
| **STD** | - | 50.84 | 0.00 | 0.11 | 0.03 | 0.07 | - | 0.09 | 0.03 | 31.11 | - | 4.17 | 0.51 | 11.31 |
| **Mean** | - | 118.05 | 0.2 | 0.735 | 0.04 | 0.3 | - | 0.415 | 0.08 | 444 | - | 24.35 | 2.75 | 121 |
| **RSD (%) - Precision** | - | 43.07 | 0.00 | 14.43 | 70.71 | 23.57 | - | 22.15 | 35.36 | 7.01 | - | 17.13 | 18.51 | 9.35 |

| | **SiO2** | **TiO2** | **Al2O3** | **Fe2O3** | **Cr2O3** | **MnO** | **MgO** | **CaO** | **SrO** | **BaO** | **Na2O** | **K2O** |
|---|---|---|---|---|---|---|---|---|---|---|---|---|
| **Certified Value** | 44.14 | 0.38 | 7.97 | 11.81 | - | 0.1813 | 21.29 | 7.85 | - | - | 1.136 | 0.044 |
| **X258634** | 44.5 | 0.38 | 8.14 | 12.05 | 0.36 | 0.18 | 21.7 | 7.97 | <0.01 | <0.01 | 1.19 | 0.04 |
| **X259169** | 43.6 | 0.36 | 7.76 | 11.7 | 0.341 | 0.17 | 21.4 | 7.67 | <0.01 | <0.01 | 1.14 | 0.04 |
| **Mean1** | 44.32 | 0.38 | 8.06 | 11.93 | 0.36 | 0.18 | 21.5 | 7.91 | - | - | 1.16 | 0.042 |

| | | | | | | | | | | | | |
|---|---|---|---|---|---|---|---|---|---|---|---|---|
| **Mean2** | 43.87 | 0.37 | 7.87 | 11.76 | 0.34 | 0.18 | 21.3 | 7.76 | - | - | 1.14 | 0.042 |
| **Accuracy1** | 99.59 | 100 | 99 | 99 | - | 100 | 99 | 99 | - | - | 98 | 105 |
| **Accuracy2** | 99.39 | 97.37 | 98.68 | 99.53 | - | 96.88 | 100.26 | 98.85 | - | - | 100.18 | 95.45 |

| | **Total** | **C** | **S** | **H2O+** | **Cl** | **F** | **S.G.** | **Ag** | **As** | **Ba** | **Bi** | **Cd** |
|---|---|---|---|---|---|---|---|---|---|---|---|---|
| **Certified Value** | | - | - | - | - | - | - | - | - | 6.2 | - | - |
| **X258634** | 101.28 | 0.02 | 0.02 | 5.7 | 50 | 190 | 2.95 | <0.5 | 0.4 | 6.6 | <0.01 | <0.5 |
| **X259169** | 98.91 | 0.05 | 0.02 | 6.11 | 110 | 120 | 2.91 | <0.5 | 0.3 | 7.6 | <0.01 | <0.5 |
| **Mean1** | 101.28 | 0.02 | 0.02 | 5.7 | 50 | 190 | 2.95 | - | 0.4 | 6.4 | - | - |
| **Mean2** | 98.91 | 0.05 | 0.02 | 6.11 | 110 | 120 | 2.91 | - | 0.3 | 6.9 | - | - |
| **Accuracy1** | - | - | - | - | - | - | - | - | - | 97 | - | - |
| **Accuracy2** | - | - | - | - | - | - | - | - | - | 111.29 | - | - |

| | **Ce** | **Co** | **Cr** | **Cs** | **Cu** | **Dy** | **Er** | **Eu** | **Ga** | **Gd** | **Ge** | **Hf** |
|---|---|---|---|---|---|---|---|---|---|---|---|---|
| **Certified Value** | 1.27 | 88.9 | 2460 | 0.184 | 43.5 | 1.61 | 1.041 | 0.3 | 8.79 | 1.17 | - | 0.551 |
| **X258634** | 1.4 | 87 | 2620 | 0.12 | 45 | 1.42 | 1.01 | 0.31 | 9.5 | 1.13 | <5 | 0.6 |
| **X259169** | 1.3 | 90 | 2480 | 0.2 | 46 | 1.54 | 0.97 | 0.3 | 11.7 | 1.14 | <5 | 0.5 |
| **Mean1** | 1.335 | 87.95 | 2540 | 0.152 | 44.25 | 1.515 | 1.026 | 0.305 | 9.145 | 1.15 | - | 0.5755 |
| **Mean2** | 1.285 | 89.45 | 2470 | 0.192 | 44.75 | 1.575 | 1.006 | 0.3 | 10.245 | 1.155 | - | 0.5255 |
| **Accuracy1** | 95 | 101 | 97 | 121 | 98 | 106 | 102 | 98 | 96 | 102 | - | 96 |
| **Accuracy2** | 101.18 | 100.62 | 100.41 | 104.35 | 102.87 | 97.83 | 96.59 | 100 | 116.55 | 98.72 | - | 95.37 |

| | **Hg** | **Ho** | **In** | **La** | **Li** | **Lu** | **Mo** | **Nb** | **Nd** | **Ni** | **Pb** | **Pr** |
|---|---|---|---|---|---|---|---|---|---|---|---|---|
| **Certified Value** | - | 0.355 | - | 0.412 | 4.4 | 0.148 | - | 0.37 | 1.494 | 886 | 0.26 | 0.235 |
| **X258634** | 0.005 | 0.31 | 0.01 | 0.5 | 9 | 0.14 | 1 | 0.3 | 1.4 | 923 | <2 | 0.23 |

| | | | | | | | | | | | | |
|---|---|---|---|---|---|---|---|---|---|---|---|---|
| **X259169** | <0.005 | 0.37 | 0.009 | 0.5 | 10 | 0.15 | <1 | 0.3 | 1.2 | 955 | <2 | 0.22 |
| **Mean1** | - | 0.3325 | 0.01 | 0.456 | 6.7 | 0.144 | - | 0.335 | 1.447 | 904.5 | 0.26 | 0.2325 |
| **Mean2** | - | 0.3625 | 0.009 | 0.456 | 7.2 | 0.149 | - | 0.335 | 1.347 | 920.5 | 0.26 | 0.2275 |
| **Accuracy1** | - | 107 | - | 90 | - | 103 | - | 110 | 103 | 98 | - | 101 |
| **Accuracy2** | - | 102.11 | - | 110.68 | 163.64 | 100.68 | - | 90.54 | 90.16 | 103.89 | - | 96.81 |

| | **Rb** | **Re** | **Sb** | **Sc** | **Se** | **Sm** | **Sn** | **Sr** | **Ta** | **Tb** | **Te** | **Th** |
|---|---|---|---|---|---|---|---|---|---|---|---|---|
| **Certified Value** | 0.96 | - | 0.079 | 27.9 | - | 0.715 | 0.25 | 16.1 | 0.0264 | 0.229 | - | 0.031 |
| **X258634** | 1 | <0.001 | 0.05 | 26 | 0.3 | 0.69 | <1 | 16.5 | <0.1 | 0.22 | 0.02 | <0.05 |
| **X259169** | 0.9 | <0.001 | 0.05 | 27 | <0.2 | 0.78 | <1 | 15.9 | <0.1 | 0.22 | 0.02 | <0.05 |
| **Mean1** | 0.98 | - | 0.0645 | 26.95 | 0.3 | 0.7025 | - | 16.3 | 0.0264 | 0.2245 | 0.02 | 0.031 |
| **Mean2** | 0.93 | - | 0.0645 | 27.45 | - | 0.7475 | - | 16 | 0.0264 | 0.2245 | 0.02 | 0.031 |
| **Accuracy1** | 98 | - | 122 | 104 | - | 102 | - | 99 | - | 102 | - | - |
| **Accuracy2** | 96.88 | - | 81.65 | 98.39 | - | 104.55 | - | 99.38 | - | 98.03 | - | - |

| | **Tl** | **Tm** | **U** | **V** | **W** | **Y** | **Yb** | **Zn** | **Zr** |
|---|---|---|---|---|---|---|---|---|---|
| **Certified Value** | - | 0.155 | 0.012 | 167.8 | - | 9.08 | 1.009 | 61.2 | 17 |
| **X258634** | 0.02 | 0.15 | <0.05 | 182 | 1 | 9.4 | 0.92 | 64 | 19 |
| **X259169** | <0.02 | 0.16 | <0.05 | 168 | <1 | 8.6 | 1.04 | 66 | 18 |
| **Mean1** | - | 0.1525 | 0.012 | 174.9 | - | 9.24 | 0.9645 | 62.6 | 18 |
| **Mean2** | - | 0.1575 | 0.012 | 167.9 | - | 8.84 | 1.0245 | 63.6 | 17.5 |
| **Accuracy1** | - | 102 | - | 96 | - | 98 | 105 | 98 | 94 |
| **Accuracy2** | - | 101.61 | - | 100.06 | - | 97.36 | 101.54 | 103.92 | 102.94 |